New Insights into Nucleophagy in *S. cerevisiae*

Dissertation
for the award of the degree
“Doctor rerum naturalium”
of the Georg-August-Universität Göttingen

within the doctoral program Molecular Medicine
of the Georg-August University School of Science (GAUSS)

submitted by
Stefanie Karnebeck
from Reutlingen

Göttingen, 2019

Members of the Thesis Committee

Prof. Dr. Michael Thumm
(First referee)

University Medical Centre Göttingen
Department of Cellular Biochemistry
Göttingen, Germany

Prof. Dr. Blanche Schwappach
(Second referee)

University Medical Centre Göttingen
Department of Molecular Biology
Göttingen, Germany

Prof. Dr. Stefan Jacobs

Structure and Dynamics of Mitochondria
Max Planck Institute for Biophysical Chemistry

Göttingen, Germany

Further members of the Examination Board

Prof. Dr. Detlef Doenecke

University Medical Centre Göttingen
Department of Molecular Biology
Göttingen, Germany

Prof. Dr. Michael Meinecke

University Medical Centre Göttingen
Department of Cellular Biochemistry
Göttingen, Germany

Dr. Roland Dosch

University Medical Centre Göttingen
Department of Developmental Biochemistry
Göttingen, Germany

Date of oral examination: 11.03.19

Affidavit:

Here I declare, that my doctoral thesis entitled “New Insights into Nucleophagy in *S. cerevisiae*” has been written independently and with no other sources and aids than quoted.

Stefanie Karnebeck

Göttingen, January 2019

„Freiheit bedeutet, dass man nicht unbedingt alles so machen muss wie andere Menschen.“

Astrid Lindgren

Content

List of Figures

List of Tables

List of Abbreviations

-	without
°C	Degree Celsius
Δ	Delta
A	Alanine
A	Ampere
AIM	Atg8-interacting motif
ANK	Ankyrin repeat domain
ApeI	Aminopeptidase I
APS	Ammonium persulfate
ARM	Armadillo repeat domains
Atg	Autophagy-related protein
cER	cortical ER
CBB	Coomassie brilliant blue
CM	Complete minimal medium
Cvt	Cytoplasm-to-Vacoule Targeting
cytoER	cytoplasmic ER
DDM	n-Dodecyl β-D-maltoside
DNA	Desoxyribonucleic acid
E	Glutamic acid
E. coli	*Escherichia coli*
EDTA	Ethylenediaminetetraacetic acid
ER	Endoplasmic Reticulum
g	gram
GFP	Green Fluorescent Protein
Glc	Glycogen
GOLD	Golgi dynamics
h	hour
HCl	Hydrogen Chloride
HRPO	Horsereddish peroxidase
KAN	Kanamycin
kb	kilobase
kDa	kilodalton

l	liter
M	Molar
m	meter
mCherry	monomeric Cherry
met	Methionine
min	minute
MIPA	Micropexophagic membrane apparatus
mTOR	mechanistic target of rapamycin
N	Nitrogen
n	nano
NaOH	Sodium hydroxide
NatNT2	Nourseotricine
NE	Nuclear envelope
Nop1	nucleolar protein 1
Nvj1	Nucleus-vacuole junction protein
NVJ	Nucleus-vacuole junction
OD_{600}	Optical Density (600 nm)
ORD	OSBP-related domain
ORPs	OSBP-related proteins
OSBP	Oxysterol-binding protein
Osh1	Oxysterol Binding Protein
P. pastoris	*Pichia pastoris*
PAGE	Polyacrylamide gel electrophoresis
PAS	Pre-autophagosomal structure
PCR	Polymerase Chain Reaction
pH	negative logarithm of H^+concentration
PH domain	Pleckstrin homology domain
Pho	Phosphate metabolism
PI4P	Phosphatidylinositol 4-phosphate
PMN	Piecemeal Microautophagy of the Nucleus
PMSF	Phenylmethylsulfonylfluoride
pnER	perinuclear ER
PpAtg	*P. pastoris* autophagy-related protein

PtdIns3P	Phosphatidylinositol 3-phosphate
PVS	Perivacuolar structure
prApeI	Precursor of ApeI
Q	Glutamine
rDNA	ribosomal DNA
RFP	Red fluorescent protein
rpm	Rounds per minute
RT	room temperature
S. cerevisiae	*Saccharomyces cerevisiae*
Scs	Suppressor of choline sensitivity
SD	Synthetic defined
SDS	Sodium dodecyl sulfate
SEM	Standard error of the mean
TCA	Trichloracetic acid
Tsc	Temperature-sensitive suppressors of Csg2 mutants
Ura	Uracil
V	Valine
V	Volt
Vac	Vacuolar Protein
VLCFA	very-long-chain fatty acid
VSM	Vacuolar sequestering membrane
v/v	volume per volume
w/o	without
wt	Wild type
w/v	weight per volume
YPD	Yeast Peptone Dextrose
µ	micro

1 Summary

Nucleophagy is a specific type of autophagy, a process for the degradation of non-essential parts of the nucleus under starvation conditions. Nucleophagy can be subdivided into Atg39 and Atg40 dependent macronucleophagy (Mochida *et al.*, 2015) and piecemeal microautophagy of the nucleus (PMN), also called micronucleophagy (Roberts *et al.*, 2003). PMN takes place at the contact site between nucleus and vacuole, the nucleus-vacuole junction (NVJ) (Roberts *et al.*, 2003). The backbone of the NVJs is formed by the interaction of Nvj1 and Vac8 (Pan *et al.*, 2000a). Furthermore, Osh1 and Tsc13 are part of this cellular contact site (Kohlwein *et al.*, 2001; Levine and Munro, 2001).

Surprisingly, within this study it was shown, that degradation of GFP-Osh1, a marker protein for PMN, can be degraded independent of Nvj1. Recently, the structure of Osh1 was partially solved and it was shown, that a mutated version of Osh1, Osh1_A159V, is impeded in its interaction with Nvj1 (Jeong *et al.*, 2017). Comparison of GFP-Osh1 and GFP-Osh1_A159V degradation showed equal results for both constructs in different deletion strains. This suggests, that impeded interaction of Osh1 and Nvj1 or the absence of NVJs results in an autophagic degradation of GFP-Osh1 different from PMN. Therefore, Nvj1-GFP is considered to be a better marker for PMN measurement. However, a genetic negative control for PMN isn't available at the moment. Also, a truncated version of Nvj1, Nvj1$^{\Delta 318\text{-}321}$, that is known to bind to Vac8 and impedes Vac8 dimerization, but still forms proper NVJs (Jeong *et al.*, 2017) can not serve as negative control for PMN measurement. This construct was shown to localize to the perinuclear ER and was degraded to a greater extent as Nvj1-GFP via Atg39 dependent macronucleophagy.

The N-terminus of Nvj1 is known to be essential for strict localization to the perinuclear ER (Millen *et al.*, 2008). In this study it was shown, that the hydrophobic core of the N-terminus is crucial for the degradation of Nvj1. Therewith, this marker protein can be used as negative control for PMN measurement. This suggests a role of the hydrophobic core of Nvj1 in the bulging of the NVJ into the vacuole and therewith PMN/ NVJ-phagy.

Degradation of Nvj1-GFP was completely blocked in *atg39*∆cells. Therewith, this study showed for the first time, that Atg39 is not only essential for

macronucleophagy (Mochida *et al.*, 2015), but also plays an important role in PMN.

Due to the lack of negative control for PMN measurement, several genes were tested in regard to their involvement in PMN. All tested genes, including *NVJ2*, *SCS2*, *GLC8* and *YMR310C* were shown to be dispensable for PMN. However, in *scs2*Δ cells the NVJs appeared to be affected.

Degradation of the nucleolar marker Nop1-GFP was shown to be independent of Nvj1 and therewith PMN. This means, that Nop1-GFP is mainly degraded via Atg39 dependent macronucleophagy (this study) (Mochida *et al.*, 2015). Based on these results is seemed to be reasonable that the main goal of PMN is not the degradation of nuclear material, but the degradation of the NVJ together with the associated protein machinery. Therefore, PMN should be renamed into NVJ-phagy.

Finally, the two marker proteins Nab-NLS-mCherry and Pho8-GFP were tested in regard to their ability for measuring of PMN/ NVJ-phagy or the differentiation between micro- and macroautophagy, respectively. Unfortunately, both marker proteins appeared not to be suitable for the intended purpose.

2 Introduction

2.1 Saccharomyces cerevisiae as a model organism

Saccharomyces cerevisiae (*S. cerevisiae*), also known as baker's yeast, is a budding yeast that belongs to the kingdom of Fungi and the class of *Saccharomycetes*. It is a round to oval shaped single-cell organism 5-10 µm in diameter with a short generation time under nutrient rich conditions (about 90 min at 30°C). The cell cycle of *S. cerevisiae* consists of three cell types: haploids of two isogamous mating types **a** and α, and **a**/α diploids (Figure 2.1). Mating can only take place between two mating types *MAT***a** (**a** cells) and *MAT*α (α cells) and results in an **a**/α diploid cell. The three cell types are all able to divide mitotically (Hanson and Wolfe, 2017). Under nitrogen-starving conditions diploid cells undergo meiosis and form four haploid spores. These can germinate into two *MAT***a** cells and two *MAT*α cells (Duina *et al.*, 2014).

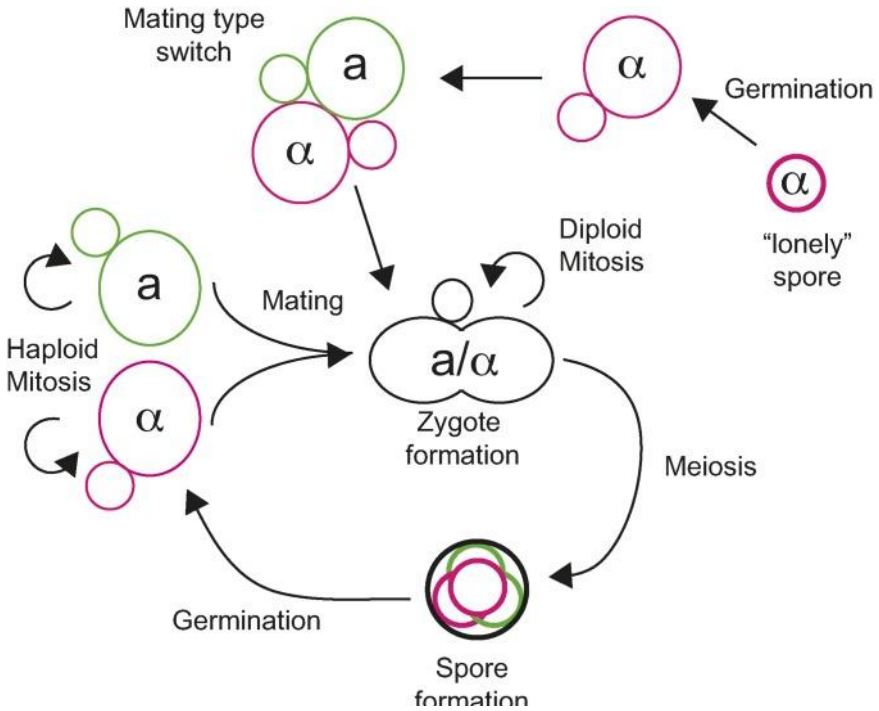

Figure 2.1: Schematic life cycle of *S. cerevisiae* (Hanson and Wolfe, 2017)

S. cerevisiae can exist in diploid or haploid cells. Haploid cells exist in two mating types: *MAT***a** (**a** cells) and *MAT*α (α cells). These three cell types can divide mitotically. Under starving conditions, diploid cells form four haploid spores.

Due to the fact, that handling as well as manipulation of *S. cerevisiae* is easy and it shows a great homology to the human genome, *S. cerevisiae* is widely used as a model organism in research. In 1996 *S. cerevisiae* was the first eukaryotic genome, that was completely sequenced and contains approximately 6 000 genes on 16 chromosomes (Goffeau *et al.*, 1996). Genetic manipulation of *S. cerevisiae* via homologous recombination is highly efficient and easy. Therefore, PCR-based strategies for deletion of genes and gene tagging, but also addition of genes via transformation in *S. cerevisiae* is widely used (Baudin *et al.*, 1993; Wach *et al.*, 1994; Schneider *et al.*, 1995; Wach *et al.*, 1997; Longtine *et al.*, 1998; Knop M *et al.*, 1999). Based on the great homology to the human genome, basic research for complex human diseases like Huntington's and Parkinson's disease can be performed in the model organism *S. cerevisiae* (Tenreiro *et al.*, 2017; Hofer *et al.*, 2018).

2.2 Autophagy

Autophagy is a catabolic process that is universal to all eukaryotic cells, e.g. yeast, worms, insects, plants and mammals (Reggiori and Klionsky, 2002; Delorme-Axford *et al.*, 2014). It serves as a stress response, for example during nutrient starvation, but also occurs under normal conditions at a basal level. During autophagy, cytoplasmic components as well as organelles are delivered to lysosomes/ vacuoles, where macromolecules are degraded and building blocks are recycled. Autophagy can be subdivided into three different forms: macroautophagy (Chapter 2.2.1), microautophagy (Chapter 2.2.2) and the Chaperone-mediated autophagy (CMA) (Chapter 2.2.3). During macroautophagic and the Cvt pathway cargo is engulfed by newly synthesized membranes. While in microautophagy cargo is directly engulfed by the vacuolar membrane. Autophagy holds homeostatic and biosynthetic functions, for example degradation of peroxisomes (pexophagy) (Chapter 2.4.2) when no longer needed (Hutchins *et al.*, 1999; Kim and Klionsky, 2000) or the Cvt pathway, where the hydrolase aminopeptidase I (ApeI) is delivered to the vacuole (Chapter 2.4.1). Autophagy depends on the so-called Atg-proteins of which until now 42 are known (Parzych *et al.*, 2018). For the biogenesis of autophagosomes the so-called core Atg-machinery, consisting of 18 genes, is

essential (Ariosa and Klionsky, 2016). This core Atg-machinery is needed for all kinds of autophagy (Suzuki and Ohsumi, 2010; Suzuki *et al.*, 2016).
Autophagy plays an important role during neurodegeneration, cancer, programmed cell death, ageing and removal of intracellular bacteria (Galluzzi *et al.*, 2017; Menzies *et al.*, 2017).

2.2.1 Macroautophagy

Macroautophagy (hereafter referred to as autophagy) starts with the formation of the phagophore (isolation membrane), a cup-shaped structure, that elongates and fuses into a cytosolic double membrane vesicle that sequesters parts of the cytoplasm. These vesicles are called autophagosomes (Klionsky and Ohsumi, 1999) (Figure 2.2). The biogenesis of the autophagosome takes place at the perivacuolar, phagophore assembly site (PAS) (Suzuki *et al.*, 2001; Noda *et al.*, 2002), where also the core Atg-machinery is localized. Autophagosomes reach sizes of 300-900 nm in diameter, these then fuse with the vacuole (lysosome) and the so-called autophagic body, a single membrane vesicle, is released into the vacuole. The autophagic body is lysed, its contents are degraded and finally recycled. Macroautophagy is activated by nutrient starvation or TORC1 inactivation, this leads to the dephosphorylation of Atg13 and subsequently the upregulation of Atg1 kinase activity (Nakatogawa *et al.*, 2009). TORC1 can be inhibited by the macrolide antibiotic Rapamycin, its effect mimics starvation in cells (Noda and Ohsumi, 1998; Abeliovich and Klionsky, 2001). Under starvation conditions, the TORC1 dependent repression the Nem1/ Spo7-Pah1 pathway is abolished. This pathway was found to be important for macroautophagy, since degradation of GFP-Atg8, a marker for macroautophagy, is severely reduced in the respective knockout strains (Rahman *et al.*, 2018).
Autophagy can be subdivided into bulk autophagy and selective autophagy, depending on how the cargoes are loaded into the autophagosomes. During selective autophagy receptor proteins bind to and thus recruit specific target proteins or organelles. These cargoes are then degraded via e.g. mitophagy (mitochondria), aggrephagy (protein aggregates) and pexophagy (peroxisomes) (Miller *et al.*, 2015; Wang and Subramani, 2017; Vigié *et al.*, 2019). The receptor proteins typically interact with Atg8 on the autophagosomal

membranes, which finally leads to the delivery of the respective cargo to the vacuole (Nakatogawa and Mochida, 2015). Selective autophagy is important for intracellular quality control. Cellular waste, e.g. superfluous or damaged organelles or invasive bacteria are degraded (Mizushima and Komatsu, 2011; Farré and Subramani, 2016).

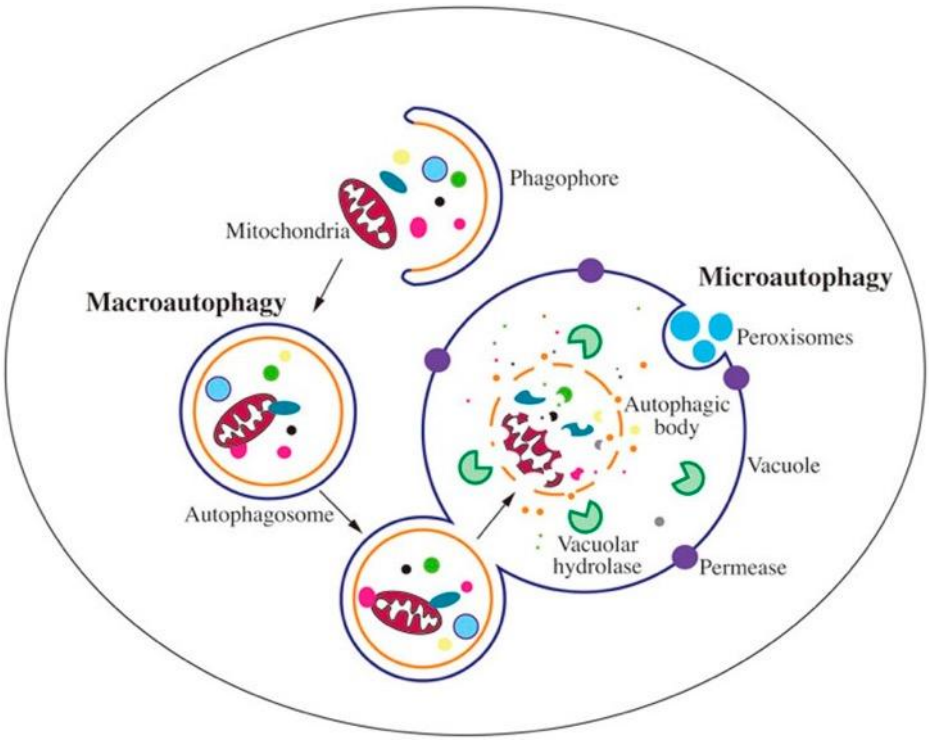

Figure 2.2: Macroautophagy and Microautophagy (Feng *et al.*, 2013)

Illustration of macro- and microautophagy in yeast. During macroautophagy cytoplasm and dysfunctional organelles are surrounded by the cup-shaped phagophore and finally by the autophagosome. The autophagosome fuses with the vacuole, the autophagic body is released and subsequently degraded via vacuolar hydrolases. During microautophagy, the cargo is directly taken up by invagination and scission of the vacuolar membrane. Finally, the cargo is degraded by vacuolar hydrolases.

2.2.2 Microautophagy

During microautophagy substrates are delivered to the vacuolar lumen by direct invagination and scission of the vacuole membrane. Finally, the cargoes are degraded via the vacuolar hydrolases (Figure 2.2) (Roberts *et al.*, 2003). Microautophagy can be induced by e.g. nitrogen starvation or rapamycin treatment. Piecemeal microautophagy of the nucleus (PMN) (Chapter 2.5.2)

and micropexophagy (Chapter 2.4.2.2) represent two typical forms of selective microautophagy (Krick *et al.*, 2008; Li *et al.*, 2012).

2.2.3 Chaperone-mediated autophagy

Chaperone-mediated autophagy (CMA) is a form of autophagy, that is almost exclusively described in mammalian cells. This process is based on chaperones, that recognize cargo proteins with a specific KFERQ motif. These proteins are then unfolded and transported into the lysosomes (Agarraberes and Dice, 2001; Bandyopadhyay *et al.*, 2008; Arias and Cuervo, 2011).

2.3 Biogenesis of autophagosomes

Non-selective autophagy is initiated at the pre-autophagosomal structure or phagophore assembly site (PAS), a punctate structure next to the vacuole (Suzuki *et al.*, 2001). For autophagosome formation 18 core Atg proteins are essential, the so-called core Atg-machinery (Suzuki *et al.*, 2016). The recruitment of the Atg-proteins to the PAS is carried out in a hierarchical manner (Suzuki *et al.*, 2007). Most Atg-proteins are at least transiently localized to the PAS (Mao *et al.*, 2013b).

Five main subcomplexes are involved in autophagy: the Atg1 complex (Chapter 2.3.1), the Atg9 cycling (Chapter 2.3.2), the phosphatidylinositol 3-kinase complex (Chapter 2.3.3) and two ubiquitin-like conjugation systems (Chapter 2.3.4).

2.3.1 The Atg1 complex

Atg1 is a serine/threonine protein kinase, that is essential for the initiation of autophagy and is up to now the only identified protein kinase in the autophagic machinery (Matsuura *et al.*, 1997). The induction of autophagy is triggered by the Atg1 kinase complex upon starvation and consists of the three components Atg1, Atg13 and the Atg17-Atg31-Atg29 scaffolding subcomplex (Cheong *et al.*, 2008; Mizushima, 2010). The proteins Atg17-Atg31-Atg29 form a ternary complex, that is constitutively located at the PAS (Kabeya *et al.*, 2009). Under nutrient rich conditions, this complex further recruits Atg11 to the PAS (Kawamata *et al.*, 2008; Mao *et al.*, 2013a). Upon induction of autophagy, the Atg17-Atg31-Atg29 subcomplex together with Atg11 are one of the first proteins

localized to the PAS and therefore are thought to promote the PAS assembly and autophagy progression (Kawamata *et al.*, 2008; Ragusa *et al.*, 2012; Mao *et al.*, 2013a). The target of rapamycin complex I (TORCI) kinase is a nutrient sensor and its inactivation through starvation induces autophagy (Davies *et al.*, 2015). Atg13 is a positive regulator of Atg1. Under nutrient rich conditions TORC1 phosphorylates Atg13 at different serine residues (Kamada *et al.*, 2000; Stephan *et al.*, 2009). Starvation leads to downregulation of TORC1 activity and dephosphorylation of Atg13. Then, Atg13 associates with Atg1, which activates its kinase activity (Kamada *et al.*, 2000; Fujioka *et al.*, 2014).

2.3.2 Atg9 cycling

So far, the origin of the membrane necessary for the autophagosome formation is unknown, even though different sources like mitochondria or the ER are under debate. After induction of autophagy, vesicles containing Atg9 are used for building the phagophore (Mari *et al.*, 2010). These vesicles are generated from the Golgi apparatus and probably endosomal pathways (Mari *et al.*, 2010; Ohashi and Munro, 2010; Yamamoto *et al.*, 2012). Atg9 is a transmembrane protein, that belongs to the core Atg-machinery (Noda *et al.*, 2000; Reggiori *et al.*, 2004). The expression levels of Atg9 are upregulated upon starvation (Mari *et al.*, 2010; Yamamoto *et al.*, 2012).

Atg9 is not only located at the PAS, but also at the ER, Golgi complex and adjacent to mitochondria. It is thought, that Atg9 might cycle between the PAS and the peripheral structures (Noda *et al.*, 2000; Reggiori *et al.*, 2004; Mari *et al.*, 2010). The cycling of Atg9 is mediated by Atg23 and Atg27, together with the scaffold protein Atg11 (He *et al.*, 2006; Yen *et al.*, 2007; Backues *et al.*, 2015). Also, Atg41 was found to interact with Atg9 and shows a comparable distribution pattern as Atg9. Atg41 plays a role in autophagosome formation (Yao *et al.*, 2015). Since Atg9 isn’t detected on the vacuolar membrane it is suggested, that the Atg9 vesicles, that are used for the autophagosome formation, are then recycled as new Atg9 vesicles (Yamamoto *et al.*, 2012). For this retrograde movement two complexes are necessary: one complex consisting of Atg9, Atg1-Atg13 and the other consisting of Atg2-Atg18 (Reggiori *et al.*, 2004; Suzuki *et al.*, 2013).

2.3.3 The phosphatidylinositol 3-kinase complex

S. cerevisiae has two similar phosphatidylinositol 3-kinase complexes, complexes I and II, that synthesize of phosphatidylinositol 3-phosphate (PI3P). During autophagy, PI3P acts as a platform for protein recruitment for phagophore assembly (Kihara *et al.*, 2001). Both complexes share three subunits, Vps34, Vps15 and Vps30/Atg6. Complex I is required for autophagy and contains Atg14 as a fourth subunit. The localization of complex I to the PAS is mediated by Atg14 (Obara *et al.*, 2006). Atg38, a further additional subunit of complex I, is important for PAS localization as well as for homodimerization (Ohashi *et al.*, 2016). Also the localization of Atg2, Atg5, Atg8 and Atg18 depends on Atg14 (Kihara *et al.*, 2001; Shintani *et al.*, 2001; Suzuki *et al.*, 2001; Krick *et al.*, 2006; Obara *et al.*, 2006). However, Jao *et al.* (2013) reported that a HORMA domain in Atg13 is required for the recruitment of Atg14 to the PAS.
Complex II contains Vps38 as a specific subunit and plays a role in the vacuolar protein sorting. In contrast to complex I, complex II isn't involved in autophagy and is localized to the endosomes (Obara *et al.*, 2006).

2.3.4 Two ubiquitin-like conjugation systems

For the phagophore expansion two ubiquitination systems, that mediate the conjugation of Atg8 and Atg12, are important (Ichimura *et al.*, 2000). Atg8 and Atg12 have structural similarities with ubiquitin (Geng and Klionsky, 2008).
The C-terminal glycine of Atg12 is conjugated to an internal lysine of Atg5 via an isopeptide bond. The enzymatic activation of Atg12 is mediated by Atg7, an E1-like enzyme (Figure 2.3). The conjugation of Atg12 to Atg5 is mediated by the E2-like enzyme Atg10 (Mizushima *et al.*, 1998; Shintani *et al.*, 1999). Atg16, is a coiled-coil protein, that is essential for autophagy. Atg16 interacts with the Atg12-Atg5 conjugate and mediates the formation of a multimeric complex, that finally leads to cross-linking of Atg5 and the formation of a stable protein complex (Mizushima *et al.*, 1999; Kuma *et al.*, 2002). Atg16 is crucial for autophagosome biogenesis, but is unnecessary for the enzymatic activity of the Atg12-Atg5 complex (Mizushima *et al.*, 1999; Hanada *et al.*, 2007). Dimerization of the Atg12-Atg5 complex leads to an increased affinity to negatively charged lipids. *In vitro* this leads to tethering of membranes (Romanov *et al.*, 2012). The Atg12-Atg5-Atg16 complex is only found on the convex site of the phagophore

and is set free before completion of the autophagosome (Mizushima *et al.*, 2001; 2003).

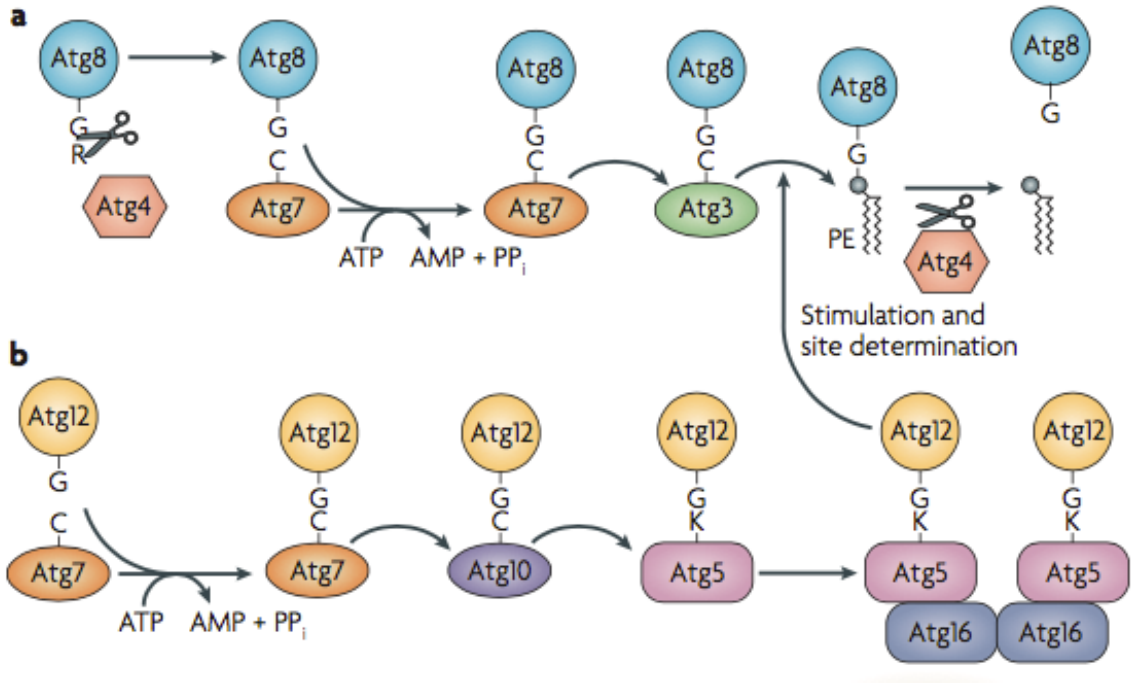

Figure 2.3: Two ubiquitin like conjugation systems (Nakatogawa *et al.*, 2009)

a) The Atg8 ubiquitin like conjugation system. Atg4 removes the C-terminal arginine residue of Atg8. Activation of Atg8 by the E1-like enzyme Atg7 and transfer to the E2-like enzyme Atg3. Finally, conjugation of phosphatidylethanolamine (PE) to Atg8. Recycling of Atg8 is also mediated by Atg4.
b) The Atg12 ubiquitin like conjugation system. Activation of Atg12 by the E1-like enzyme Atg7 and transfer to the E2-like enzyme Atg10. Formation of the Atg12-Atg5 complex and finally, interaction with Atg16 and formation of an oligomer. The Atg12-Atg5-Atg16 complex can act an E3-like enzyme function in the conjugation of Atg8 to PE. The Atg12-Atg5-Atg16 complex possibly determines the production site of Atg8-PE.

Atg8 is conjugated to the membrane lipid phosphatidylethanolamine (PE) (Figure 2.3). Therefore, the C-terminal arginine of Atg8 is removed by the cysteine protease Atg4, to expose the glycine that is needed for subsequent reactions (Kirisako *et al.*, 2000; Kim *et al.*, 2001a). Activation of Atg8 is mediated by the E1 enzyme Atg7. The activated protein is then transferred to the E2 enzyme Atg3, that conjugates Atg8 to PE (Ichimura *et al.*, 2000; Geng and Klionsky, 2008). The Atg12-Atg5/Atg16 complex acts as a ubiquitin-protein ligase (E3)-like enzyme during the conjugation of Atg8 to PE (Hanada *et al.*,

2007; Cao *et al.*, 2008). Atg8-PE associates together with Atg12-Atg5-Atg16 into a membrane coat, which is dissembled by Atg4 (Kaufmann *et al.*, 2014).
Atg8-PE is found on both sites of the autophagosome (Kirisako *et al.*, 2000; Xie *et al.*, 2008). Atg8 interacts with many proteins via the so called Atg8-interacting motifs (AIMs). On the concave site of the phagophore Atg8 recruits AIM-containing proteins (Yorimitsu and Klionsky, 2005; Kondo-Okamoto *et al.*, 2012). Therefore, Atg8 is delivered to the vacuole and degraded (Huang *et al.*, 2000).
Atg4 also acts as a deconjugation enzyme, that cleaves Atg8 off membranes. This cleavage is important for Atg8 recycling and controlling of Atg8 function (Kirisako *et al.*, 2000). Synthesis as well as lipidation of Atg8 are up-regulated under autophagy-inducing conditions (Kirisako *et al.*, 2000; Nakatogawa *et al.*, 2007) and since the amount of Atg8-PE correlates with the size of the autophagosomes, Atg8-PE is suggested to be directly involved in the expansion of the phagophore (Geng and Klionsky, 2008; Xie *et al.*, 2008).

2.3.5 Closure and delivery to vacuole

Before the content of the autophagosome can be degraded, the phagophore expansion has to be completed and form into a double membrane vesicle, the autophagosome. This vesicle can then be delivered to the vacuole and degraded.
The PI3P phosphatase Ymr1 was shown to be important in late steps of autophagosome formation. In *YMR1* deletion cells Atg proteins fail to dissociate from autophagosomal membranes and autophagosomes accumulate in the cytoplasm. This indicates that the Atg machinery has to be removed from the autophagosomes in order to allow fusion with the vacuole. This seems to be regulated by Ymr1 (Cebollero *et al.*, 2012).
Little is known about the very last steps of the closure and delivery of the autophagosome to the vacuole. It is possible, that the endosomal sorting complex required for transport (ESCRT) is involved in the membrane sealing (Hurley, 2010; Hurley and Hanson, 2010). For an *Arabidopsis* mutant defective for a component in the ESCRT-III complex arrested phagophores were reported, indicating an involvement in phagophore closure (Spitzer *et al.*, 2015).

Upon completion of the autophagosome, certain SNAREs are required for fusion with the vacuole: Ypt7 (a GTP-binding protein), Sec18, Vam7 and Ykt6 (Darsow *et al.*, 1997; Mayer and Wickner, 1997; Sato *et al.*, 1998; Dietrich *et al.*, 2004; Balderhaar *et al.*, 2010; Bas *et al.*, 2018).

After completion of the autophagosome, the outer membrane of the autophagosome fuses with the vacuolar membrane and leads to the release of a single membrane vesicle, the autophagic body. Following, the autophagic body is degraded via the lipase Atg15 and finally the cargo can be degraded with the help of vacuolar hydrolases (Epple *et al.*, 2001).

2.4 Selective forms of autophagy

2.4.1 The Cvt pathway

The cytoplasm-to vacuole targeting (Cvt) pathway in *S. cerevisiae* is a form of selective autophagy, that seems to exclude bulk cytoplasm. Selectively hydrolases, especially aminopeptidase I (ApeI) but also α-mannosidase (AmsI), are delivered to the vacuole under basal conditions (Xie and Klionsky, 2007). In comparison to normal autophagosomes (500 nm) the Cvt vesicles are rather small (150 nm) (Baba *et al.*, 1997; Scott *et al.*, 1997). Immediately after its synthesis prApeI (the precursor form of ApeI) folds into a homododecamer (Kim *et al.*, 1997). Subsequently, the homodecamers assemble to the so-called ApeI complexes, which is a main cargo for the Cvt vesicles. Dodecamer formation is essential for ApeI complex formation and its delivery to the vacuole via the Cvt pathway (Su *et al.*, 2015). The propeptide of ApeI is located at the N-termiuns of the protein and is important for the formation of the ApeI complex as well as the ApeI-Atg19 interaction (Oda *et al.*, 1996; Shintani *et al.*, 2002; Suzuki *et al.*, 2002). The ApeI complex is recognized by its receptor Atg19 (Scott *et al.*, 2001; Shintani *et al.*, 2002). Atg19 then recruits Atg11 and Atg8, what leads to the formation of the Cvt complex. The following recruitment of the core Atg machinery is initiated by Atg19 and Atg11, this then leads to the membrane formation around the Cvt complex, the Cvt vesicle (Shintani *et al.*, 2002; Suzuki *et al.*, 2002; Yorimitsu and Klionsky, 2005; He *et al.*, 2006). The double-membraned vesicle then finally fuses with the vacuole (Scott *et al.*, 1996; Baba *et al.*, 1997; Kim *et al.*, 1997; Klionsky and Ohsumi, 1999) and prApeI is processed into its mature form mApeI (Klionsky *et al.*, 1992).

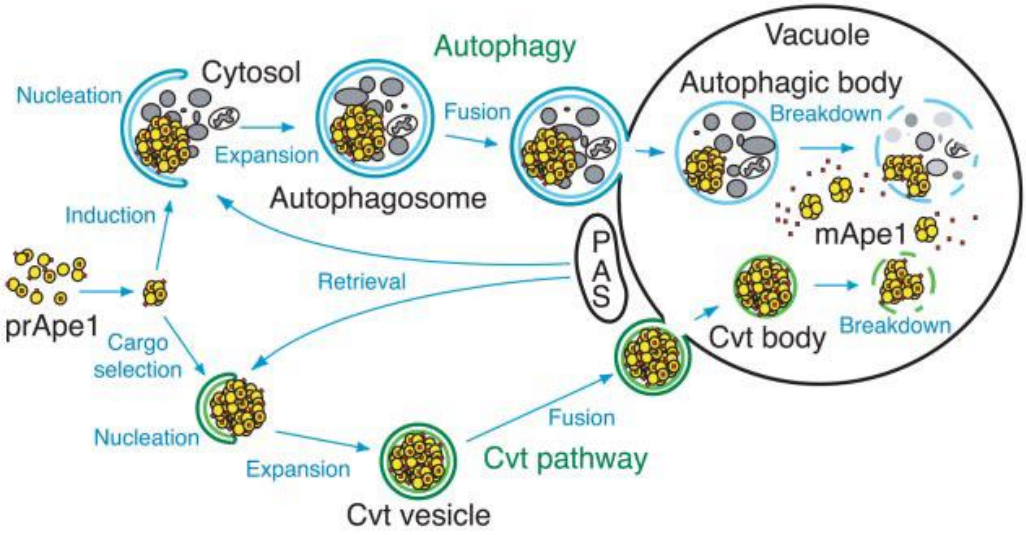

Figure 2.4: The Cvt pathway and macroautophagy in yeast (Nair *et al.*, 2010)

Under vegetative conditions, precursor ApeI (prApeI) is engulfed by double membrane vesicles and delivered to the vacuole via the Cvt pathway. There it is processed to its mature form mApeI. The Cvt pathway is a biosynthetic pathway, that uses the core Atg machinery. Upon starvation, ApeI is delivered to the vacuole via the macroautophagic pathway together with other cargo.

2.4.2 Pexophagy

Pexophagy is a selective form of autophagy, where superfluous or damaged peroxisomes are degraded. Peroxisomes are involved in many aspects of lipid metabolism and elimination of peroxides and depending on the cell status they are synthesized or degraded. Through the change of experimental conditions, from peroxisome biogenesis inducing conditions to peroxisome biogenesis repressing conditions, pexophagy can be triggered experimentally. Depending on the yeast species, pexophagy can be induced differently. In *S. cerevisiae* pexophagy can be triggered by the change from medium with oleic acid as sole carbon source to glucose-rich and nitrogen-limiting medium (Hutchins *et al.*, 1999). The methylotrophic yeast *Pichia pastoris* (*P. pastoris*), can use methanol as exclusive carbon source, what leads to the synthesis of high levels of peroxisomes. Peroxisomes contain enzymes that are necessary for the metabolism of methanol (Fukui *et al.*, 1975a; 1975b). Two forms of autophagy are known in methylotrophic yeast: macropexophagy (Chapter 2.4.2.1) and micropexophagy (Chapter 2.4.2.2) (Veenhuis *et al.*, 1992; Dunn *et al.*, 2005). In *P. pastoris* a shift from methanol to ethanol induces macropexophagy (Nazarko

et al., 2009), whereas a shift from methanol to glucose induces micropexophagy (Tuttle and Dunn, 1995). For pexophagy most of the core Atg-machinery and some additional components, like Atg30 are required (Farré *et al.*, 2009). In contrast to *S. cerevisiae*, *P. pastoris* (or alternatively *Hansenula polymorpha*) exhibit giant methanol induced peroxisome clusters, thus, the structures of interest can be visualized more clearly. Therefore, these two yeast species are mainly used for pexophagy studies (Farré *et al.*, 2009).
Macropexophagy and micropexophagy are analogous to macroautophagy and microautophagy (Veenhuis *et al.*, 1983; Tuttle and Dunn, 1995; Sakai *et al.*, 1998).

2.4.2.1 Macropexophagy

Transfer of the methylotrophic yeast *P. pastoris* from methanol containing medium to ethanol-containing medium leads to macropexophagy. Here, single peroxisomes are enclosed in autophagosomes (pexophagosomes), that arise from the PAS. The peroxisomes are then individually delivered to the vacuole (Tuttle and Dunn, 1995; Sakai *et al.*, 1998). The process of macropexophagy is similar to that of autophagy. After selection of the cargo, the isolation membrane forms and expands and finally engulfs the peroxisomes in pexophagosomes. Then, the autophagic machinery is removed, the pexophagosome fuses with the vacuole and finally, the cargo can be degraded and recycled (Farré *et al.*, 2009). The same core Atg-machinery as during autophagy is required with a few adaptions to obtain specificity for pexophagy. This specificity is mainly obtained by PpAtg30, a receptor that interacts with peroxisomes via Pex3 and Pex14 (Farré *et al.*, 2008). PpAtg30 also interacts with PpAtg11 and PpAtg17, proteins that organize PAS assembly (Farré *et al.*, 2008).

2.4.2.2 Micropexophagy

Micropexophagy is induced in *P. pastoris* after a switch from methanol-containing medium to glucose-containing medium. Methanol-containing medium leads to development and clustering of peroxisomes juxtaposed to the vacuole. In order to engulf the peroxisome cluster, the vacuolar membrane invaginates along the peroxisomes after shift to glucose-containing medium (Figure 2.5).

The so-called vacuolar sequestering membrane (VSM) protrudes along the peroxisomes. Additionally, the micropexophagic membrane apparatus (MIPA), a cup-shaped double-membrane structure develops on the surface of the peroxisome cluster. The heterotypic fusion of the MIPA and VSM tips is dependent on Atg24 (Ano *et al.*, 2005) and leads to the transport of the peroxisome cluster into the vacuole (Mukaiyama *et al.*, 2004). The MIPA possibly originates from the Golgi (Yamashita *et al.*, 2006). The complete core Atg machinery is needed for the assembly of the MIPA and pexophagosome formation, as well as the pexophagy-specific Atg proteins Atg11, Atg26 and Atg30 (in *H. polymorpha* also Atg25 is a specific factor) (Monastyrska *et al.*, 2005). Like in *S. cerevisiae*, Atg8 is localized to the isolation membrane (Mukaiyama *et al.*, 2004). Under peroxisome proliferation conditions, the Atg8 levels increase, but mainly remain localized to the cytosol. Under pexophagy conditions the Atg8 levels remain consistent, but Atg8-PE levels increase, now localized to the PAS, a perivacuolar structure, where the MIPA and herewith the pexophagosome will develop (Farré and Subramani, 2004).

Atg11 is the scaffold in yeast, in *S. cerevisiae* Atg36 is the corresponding cargo receptor for pexophagy, in *P. pastoris* PpAtg30 is used as cargo receptor for pexophagy. Atg36 (PpAtg30) is essential for selective autophagy of peroxisomes. Binding to Atg36 (PpAtg30) is mediated via Pex3 (PpPex3) (Farré *et al.*, 2008; Motley *et al.*, 2012). Atg11 initiates the attachment of Atg8-PE to the peroxisomes and following the engulfment of the peroxisomes with the phagophore. Localization of PpAtg11 to the vacuole is dependent on PpVac8 (Kim *et al.*, 2001b; Fry *et al.*, 2006).

Atg26 is a sterol glucosyltransferase, that is specific for micro-and macropexophagy in *P. pastoris* (Nazarko *et al.*, 2007) and is not involved in autophagy in *S. cerevisiae* (Cao and Klionsky, 2007). For the localization to the MIPA and the pexophagosome phosphatidylinositol 4-phosphate (PI4P) is required. This localization is mediated by Atg26, since this protein binds PI4P (Oku *et al.*, 2003; Yamashita *et al.*, 2006).

The formation of complete VSM is inhibited in several mutants (*atg2*Δ, *atg9*Δ, *atg11*Δ, *atg18*Δ, *atg28*Δ, *vac8*Δ and *vps15*Δ) (Kim *et al.*, 2001b; Mukaiyama *et al.*, 2002; Chang *et al.*, 2005; Dunn *et al.*, 2005; Fry *et al.*, 2006).

In *P. pastoris* PpAtg9 is essential for formation of the sequestering membranes and assembly of the MIPA. During peroxisome biogenesis conditions PpAtg9 is localized to a peripheral compartment, localized near the plasma membrane. Upon induction of micropexophagy, PpAtg9 relocates together with PpAtg11 to unique perivacuolar structures (PVS). PVS are located next to VSMs and are distinct from the PAS (Chang *et al.*, 2005). Subsequently, PpAtg9 can be found on the sequestering membranes and on the vacuolar surface (Chang *et al.*, 2005). Cycling of PpAtg9 from the peripheral compartment to the PVS is based on PpAtg11 and PpVps15. Movement of PpAtg9 from the PVS to the VSM and the vacuolar surface requires PpAtg2 and PpAtg7 (Chang *et al.*, 2005).

During micropexophagy PpAtg28 and its interaction partner PpAtg35 are required for MIPA formation. PpAtg35 is specific for micropexophagy, but not required for macropexophagy, in contrast to PpAtg28, that is at least partially required for autophagy and the Cvt pathway (Nazarko *et al.*, 2011). PpAtg35 interacts with PpAtg17, a scaffold protein that is involved in the pexophagy-specific PAS assembly together with PpAtg30 and PpAtg11 (Farré *et al.*, 2008; Nazarko *et al.*, 2009). The interaction of PpAtg35 and PpAtg17 is mediated by PpAtg28 (Nazarko *et al.*, 2011). Overexpression of PpAtg35 specifically leads to an inhibition of micropexophagy (Nazarko *et al.*, 2011).

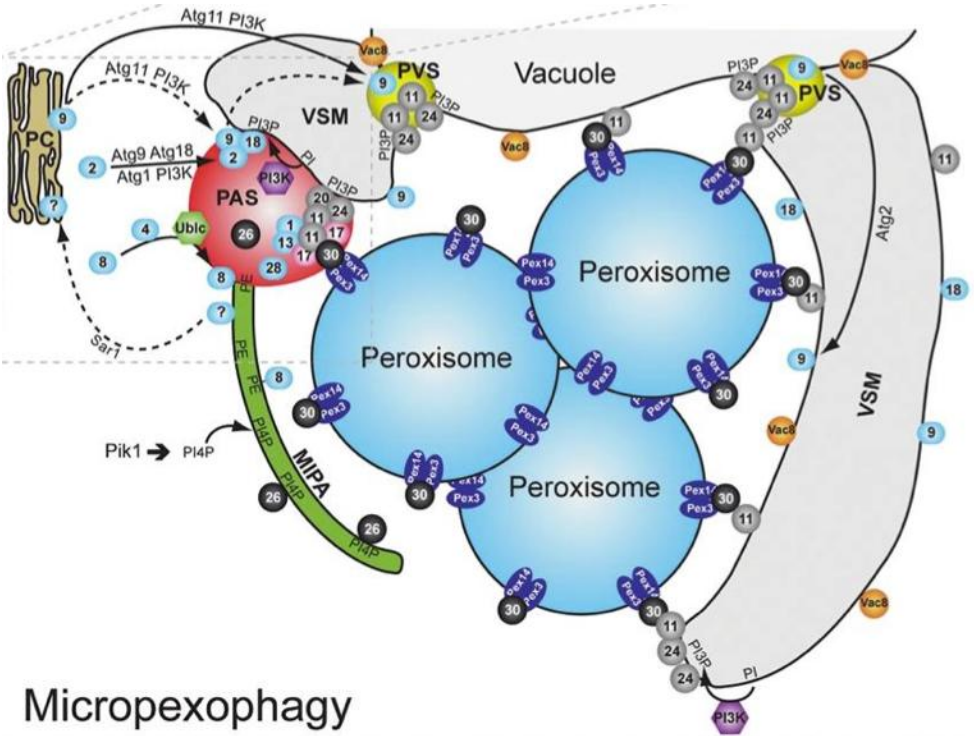

Figure 2.5: Micropexophagy in *P. pastoris* (Farré *et al.*, 2009)

In *P. pastoris* micropexophagy is induced through the shift of methanol-containing medium to glucose-containing medium. The vacuolar membrane invaginates to so called vacuolar sequestering membranes (VSM) and engulfs peroxisome clusters. On the surface of the peroxisomes, the micropexophagic membrane apparatus (MIPA) is formed and finally mediates the heterotypic fusion of VSM and MIPA.

2.5 Nucleophagy: the autophagic degradation of the nucleus

Nucleophagy is the autophagic degradation of superfluous or damaged parts of the nucleus. This process is important to maintain cellular integrity in yeast, as well as in mammalian cells (Roberts *et al.*, 2003; Park *et al.*, 2009; Mijaljica *et al.*, 2012). Until now nucleophagy in mammalian cells is only mentioned in the context of pathological conditions (Park *et al.*, 2009). Since nucleophagy targets specifically the nucleus, it is a selective form of autophagy. This selective degradation of the nucleus can be differentiated into two forms of nucleophagy: macronucleophagy (Chapter 2.5.1) and micronucleophagy (also referred to as PMN; Chapter 2.5.2). It was recently shown, that macronucleophagy as well as micronucleophagy are dependent on the Nem1/ Spo7-Pah1 pathway after inactivation of TORC1 (Rahman *et al.*, 2018). Unfortunately, both processes are poorly described.

2.5.1 Macronucleophagy and ER-Phagy

During macronucleophagy non-essential or damaged parts of the nucleus are sequestered by autophagosomes in a Atg39 dependent manner (Mochida *et al.*, 2015). These then fuse with the vacuole and the content is released into the vacuole and is finally degraded

Atg39 and Atg40 are two proteins involved in ER-phagy and nucleophagy and are localized to different ER domains. Atg39 is localized to the perinuclear ER (pnER)/ nuclear envelope (NE) and is needed for pnER-phagy and nucleophagy. It is under debate, if proper localization of Atg39 is dependent on the Nem1/ Spo7-Pah1 pathway (Rahman *et al.*, 2018). The cytoER-phagy is dependent on Atg40, which is localized to the cytoplasmic ER (cytoER)/ cortical ER (cER) (Mochida *et al.*, 2015). Both proteins contain Atg8-family-interacting motifs (AIM) and probably bind to Atg8 on forming autophagosomal membranes (Mochida *et al.*, 2015).

Atg39 is a single membrane-spanning protein with its C-terminus located in the pnER lumen. Therefore it is speculated, that Atg39 might interact as a receptor with nuclear proteins and/or lipids in the inner nuclear membrane with its C-terminal region. This interaction might lead to the formation double-membrane vesicles (Nakatogawa and Mochida, 2015). Atg40 preferably localizes to highly curved ER regions and its putative transmembrane region contains a reticulon-like domain (Mochida *et al.*, 2015).

Endoplasmic reticulum (ER) is further degraded by the so-called ER-phagy (or reticulophagy). In *S. cerevisiae*, ER stress leads to massive ER expansion, what results in the formation of large ER whorls. During ER-phagy these whorls are selectively taken up into the vacuole. This event is independent of the core autophagic machinery and it involves the invagination of vacuolar membrane (Schuck *et al.*, 2014).
It is under debate how the ER is fragmented and sequestered by a phagophore. Either the ER fragments before autophagosome formation or the fragmentation and autophagosome formation are coupled (Figure 2.6) (Nakatogawa and Mochida, 2015).
Both Atg39 and Atg40 are upregulated under nitrogen starvation or inhibition of TORCI, suggesting a role of these two proteins in the regulation of nucleophagy and ER-phagy (Mochida *et al.*, 2015). ER-phagy is reduced in knockout of either *ATG39* or *ATG40* and almost completely blocked in the double knockout. The deletion of *ATG39* leads to decreased cell survival under starving conditions, indicating, that nucleophagy is important for cell survival under these conditions (Mochida *et al.*, 2015).

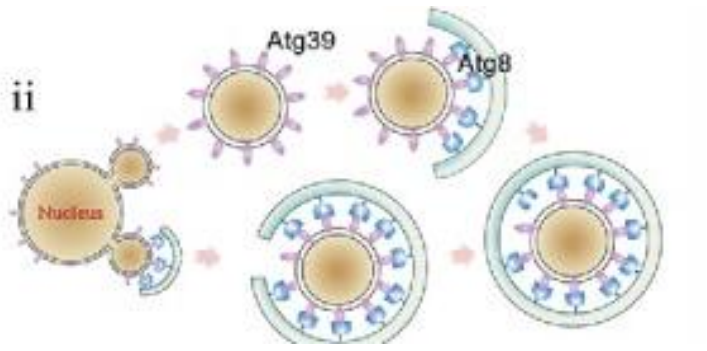

Figure 2.6: Macronucleophagy is dependent on Atg39 in *S. cerevisiae* (modified from Luo *et al.*, 2016)

Macronucleophagy is dependent on Atg39. The formation of the autophagosomal membrane is induced upon binding of Atg39 to Atg8. Parts of the nucleus are engulfed by autophagosomes and finally degraded in the vacuole.

2.5.2 Piecemeal Microautophagy of the Nucleus (PMN) (Micronucleophagy)

Piecemeal microautophagy of the nucleus (PMN) is a selective autophagic process (Roberts *et al.*, 2003) that occurs upon nitrogen or carbon starvation. PMN can also be induced by rapamycin, an inhibitor of the TORC1 kinase (Roberts *et al.*, 2003). During PMN only non-essential parts of the nucleus are removed, chromosomal DNA, nuclear pore complexes and spindle pole bodies are excluded from PMN (Roberts *et al.*, 2003; Kvam and Goldfarb, 2007; Farré *et al.*, 2009; Kraft *et al.*, 2009; Millen *et al.*, 2009). Therefore this process is not linked to cell death (Roberts *et al.*, 2003). PMN occurs at the so-called nucleus-vacuole junction (NVJ), the membrane contact site between nucleus and vacuole (Roberts *et al.*, 2003), that is formed by the interaction of Nvj1 and Vac8 (Pan *et al.*, 2000b). Stress induces enlargement of the NVJ (Pan *et al.*, 2000a). Upon starvation, the NVJs bulge into the vacuole, to form a teardrop-like nuclear bleb, that finally is pinched off and degraded in the vacuole (Roberts *et al.*, 2003). PMN doesn’t require the components of the homotypic fusion machinery (Krick *et al.*, 2008; 2009a; Millen *et al.*, 2009). Using GFP-Osh1 as a marker for PMN, the core Atg-machinery was described to be essential for PMN together with some macroautophagic- and Cvt-specific Atg-proteins like Atg11 and Atg24 (Krick *et al.*, 2008). However, this is under debate, as by that time, macronucleophagy was unknown and a differentiation between micro- and macronucleophagy wasn’t possible (Mostofa *et al.*, 2018).

Lately it was shown, that inactivation of TORC1 results in the separation and repositioning of nucleolar proteins and ribosomal DNA (rDNA) depending on the CLIP-cohibin system (Mostofa *et al.*, 2018). This system is required for the anchoring of rDNA to the inner nuclear membrane (Mekhail *et al.*, 2008). Both, CLIP and cohibin were tested to be essential for the degradation of nucleolar proteins, but not for macro- or microautophagy (Mostofa *et al.*, 2018). Micronucleophagy seems to be a very specific process, since the lack of CLIP or cohibin does not lead to aberrant nucleophagy of rDNA, in the meantime,

micronucleophagy still occurs. Furthermore, micronucleophagy was shown to be the driving force for repositioning of rDNA and nucleolar proteins after TORC1 inactivation (Mostofa *et al.*, 2018).

2.5.2.1 Structure and function of the Nucleus-vacuole junction

The crucial backbone of the NVJ is formed by the interaction of Nvj1 and Vac8 (Figure 2.7). These two interaction partners cluster into velcro-like patches. Deletion of either *NVJ1* or *VAC8* leads to the disruption of the NVJ (Pan *et al.*, 2000a). Nutritional limitation leads to an expansion and proliferation of the NVJs (Roberts *et al.*, 2003). In addition to the two backbone proteins Nvj1 and Vac8, also Osh1 and Tsc13 are part of the NVJ, which play roles in lipid biosynthesis and trafficking (Kohlwein *et al.*, 2001; Levine and Munro, 2001). Both, Osh1 and Tsc13 are interacting with Nvj1, also in the absence of Vac8 (Kvam and Goldfarb, 2004; Kvam *et al.*, 2005).

In addition to the just mentioned proteins, further components of the NVJ have been described: e.g. Nvj2, Nvj3, Lam5, Lam6, Mdm1, Vps13 (Toulmay and Prinz, 2011; Elbaz-Alon *et al.*, 2015a; Gatta *et al.*, 2015; Henne *et al.*, 2015; Murley *et al.*, 2015; Lang *et al.*, 2015a).

In *S. cerevisiae* Lam6 can be found in several contact sites: ERMES (ER/mitochondria encounter structure), vCLAMP (vacuole and mitochondria patch) and in NVJs. The formation of NVJs is not dependent on Lam6 (Elbaz-Alon *et al.*, 2015a), but Lam6 is able to enlarge the ERMES, vCLAMP and NVJs, when it is overexpressed (Elbaz-Alon *et al.*, 2015a). Lam6 is considered to be a regulatory protein and to regulate cross-talk between different contact sites (Elbaz-Alon *et al.*, 2015a).

Mdm1 is localised to the ER-vacuole/ lysosome membrane contact site (NVJ) and is therefore a interorganelle tethering protein (Henne *et al.*, 2015).

Overexpression of Mdm1 leads to an elongated vacuole- nER interphase, similar to what Pan *et al.* (2000a) observed for Nvj1. Nvj3 is a paralog to Mdm1 and was also found to be localised to the NVJ. However, this localisation is dependent on Mdm1, since in *mdm1*Δ cells Nvj3 is located in the cytoplasm (Henne *et al.*, 2015). The localisation of Mdm1 and Nvj3 to the ER-vacuole contact site is independent of the presence or absence of Nvj1 and vice versa, Mdm1 has no impact on the formation of the NVJs (Henne *et al.*, 2015).

A clear role for the NVJs is so far unknown. However Osh1 and Tsc13 are two proteins that are located at the NVJs and are involved in lipid biosynthesis and trafficking (Elbaz and Schuldiner, 2011). Osh1 is a oxysterol-binding protein (Levine and Munro, 2001) and is involved in non-vesicular lipid trafficking (Kvam and Goldfarb, 2004). Deletion of the seven-membered yeast Osh family leads to inhibition of PMN at a late stage (Kvam and Goldfarb, 2004). Osh1 is known to bind PI4P and ergosterol in a competitive manner and is therefore considered to transport ergosterol in exchange for PI4P in a non-vesicular manner between lipid bilayers (Manik *et al.*, 2017). Tsc13 is an essential enoyl-CoA reductase that is involved in the biosynthesis of very-long-chain fatty acid synthesis (VLCFAs) (Kohlwein *et al.*, 2001), that are important for structure and fluidity of membranes (Elbaz and Schuldiner, 2011). A decrease in the size of PMN blebs is observed in the absence of Tsc13 (Kvam *et al.*, 2005).

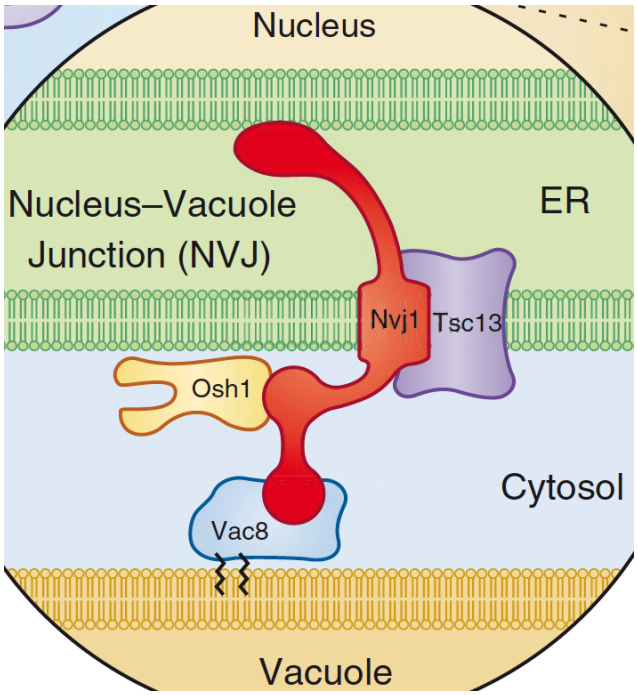

Figure 2.7: Structure of the nucleus-vacuole junction (modified from Elbaz and Schuldiner, 2011)

The nucleus-vacuole junction (NVJ) consist of four proteins: Nvj1, Osh1, Tsc13 and Osh1, whereat the backbone of this membrane contact site is formed by the interaction of Nvj1 and Vac8.

2.5.2.1.1 The integral ER-membrane protein Nvj1

Nvj1 is an integral ER-membrane protein, that contains a single transmembrane domain and clamps together inner and outer nuclear membrane (Millen *et al.*, 2008). At the lumenal N-terminus Nvj1 contains an inner nuclear membrane anchor, that strictly retains Nvj1 in the perinuclear ER and furthermore bisects the width of the perinuclear lumen. Reduction of hydrophobicity or introduction of charged residues to the inner nuclear membrane anchor leads to disrupted localization of Nvj1 (Millen *et al.*, 2008). Also the Nem1/ Spo7-Pah1 axis, a pathway involved in the synthesis of triacylglycerol, is reported to be crucial for correct Nvj1 localisation (Rahman *et al.*, 2018). The C-terminus of Nvj1 is located in the cytoplasm, where it interacts with Vac8 (Pan and Goldfarb, 1998; Wang *et al.*, 1998). Binding of Nvj1 and Vac8 is crucial for formation of NVJs (Pan *et al.*, 2000a), since Nvj1 induces Vac8 dimerization, what is essential for normal formation of NVJs (Jeong *et al.*, 2017). Nvj1 also interacts with Osh1 and Tsc13 (Kvam and Goldfarb, 2004; Kvam *et al.*, 2005). The Osh1 binding was localized to the cytosolic segment (residues 130-177), next to the membrane-spanning region (Kvam and Goldfarb, 2006). Independent of interaction with Vac8 or NVJ formation, Nvj1 binds targets Tsc13 to the perinuclear ER (Kvam *et al.*, 2005).

2.5.2.1.2 The vacuolar protein Vac8

Vac8 is a vacuolar protein, that forms through its interaction with Nvj1 the crucial backbone for the NVJ (Pan *et al.*, 2000a). Vac8 is dimerized by binding of Nvj1, what is necessary for normal formation of NVJs (Jeong *et al.*, 2017). The N-terminus of Vac8 is palmitoylated and myristoylated and these lipid modifications are anchored into the vacuolar membrane (Wang *et al.*, 1998). Additionally, Vac8 contains several ARM domains (Tewari *et al.*, 2010). These are partially required for proper localization of Nvj1 to the NVJs (Tang *et al.*, 2006). Due to its ARM domains, Vac8 serves as an adapter protein, that is involved in different vacuolar processes, e.g. vacuole inheritance and homotypic fusion (Fleckenstein *et al.*, 1998; Pan and Goldfarb, 1998). Through its interaction with Atg13, Vac8 also plays an important role in the import of aminopeptidase I during the CVT pathway (Wang *et al.*, 1998; Scott *et al.*,

2000). Jeong *et al.* (2017) recently reported that Vac8 either can interact with Nvj1 or Atg13, what is in agreement with their physiological role.

2.5.2.1.3 The oxysterol-binding protein Osh1

Osh1 is an oxysterol-binding protein (OSBP), similar to those in mammalian cells (Schmalix and Bandlow, 1994). OSBP-related proteins (ORPs) are reported to be involved in intracellular lipid transfer and facilitate the transport of sterols and other phospholipids between intracellular membranes (Mesmin and Antonny, 2016). Osh1 contains three targeting domains: Ankyrin repeat domain (ANK), PH and the FFAT motif additionally, it contains the OSBP-related domain (ORD) (Levine and Munro, 2001; Tong and Boone, 2006). Osh1 interacts via the ANK domain with Nvj1 in an Vac8 independent manner (Levine and Munro, 2001; Kvam and Goldfarb, 2004). The Osh1 ANK displays a bi-lobed structure, with an Nvj1-binding cleft between the two subdomains, and recognizes the small cytosolic segment of Nvj1 (Manik *et al.*, 2017). The recruitment of Osh1 from cytoplasmic and Golgi pools into the NVJs depends on the cellular level of Nvj1 (Kvam and Goldfarb, 2004). Osh1 also interacts with the ER anchor protein Scs2 at the NVJ (Loewen *et al.*, 2003).
Furthermore, GFP-Osh1 was postulated to be a marker for PMN measurement (Krick *et al.*, 2008; Millen *et al.*, 2009).

2.5.2.1.4 The enoyl reductase Tsc13

Tsc13 is a enoyl reductase that is involved in last step in very-long-chain fatty acid synthesis (VLCFAs) (Kohlwein *et al.*, 2001; Gable *et al.*, 2004). Through its physical interaction with Nvj1, which is independent of Vac8, Tsc13 is enriched in NVJs (Kvam *et al.*, 2005). During PMN Tsc13 is degraded in a Nvj1 dependent manner (Kvam *et al.*, 2005).

2.5.2.2 Different stages of PMN

PMN can be divided into five different stages (Figure 2.8). The NVJs are formed by the interaction of Nvj1 and Vac8 (Pan *et al.*, 2000a). Then, the NVJs bulge into the vacuole and form bleb-like structures, followed by partial nuclear bud off. The vacuolar extensions then fuse and now the vesicle is surrounded by three membranes: two from the nucleus and one from the vacuole. Finally, the

PMN vesicle is released into the vacuole and is degraded by the vacuolar proteinase A (Kvam and Goldfarb, 2007). No PMN occurs in *VAC8* or *NVJ1* deletion strains (Roberts *et al.*, 2003).

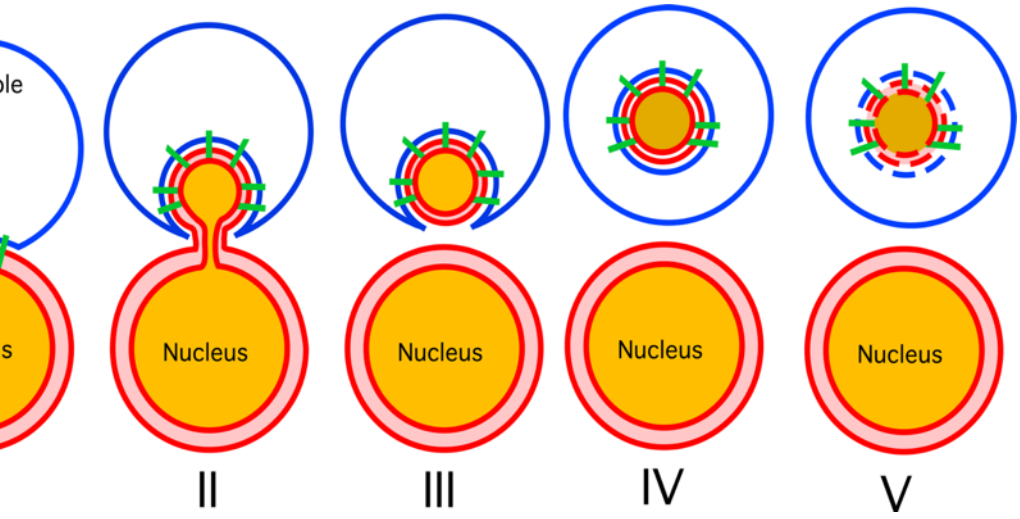

Figure 2.8: Five Stages of PMN (Krick *et al.*, 2009a)

I. NVJs are formed
II. NVJs bulge into the vacuole
III. Part of the nucleus buds off
IV. Fusion of the vacuolar extensions
V. PMN vesicle is released in the vacuole and is degraded

2.6 Aim of the thesis

PMN is a selective type of autophagy, during which non-essential parts of the nucleus are degraded in a Nvj1-dependent manner. This takes place at the NVJ, a contact site of nucleus and vacuole. The backbone of the NVJ is caused by the interaction of Nvj1 and the Vac8 (Pan *et al.*, 2000a). Knowledge about this process is limited.

Recently, two new Atg-proteins that are involved in ER-phagy were described: Atg39 and Atg40. Atg39 is localized to the perinuclear ER and is involved in autophagic degradation of the perinuclear ER and parts of the nucleus. In contrast to that, Atg40 is localized to the cortical and cytoplasmic ER and is important for the degradation of these ER subdomains (Mochida *et al.*, 2015). One aim of this thesis was to determine the role of Atg39 and Atg40 in PMN.

Based on results obtained initially during this study, the first question to be answered was, if Nvj1 is essential for the degradation of GFP-Osh1, the marker protein for PMN, and Nop1-GFP, a nucleolar marker protein. Subsequently, the potential involvement of Nvj2, Scs2, Glc8 and Ymr310c in PMN was analysed. In this context, the role of Nvj1 during PMN was analysed using two different Nvj1 mutants Nvj1_V20E_V23E (Millen *et al.*, 2008) and Nvj1$^{\Delta 318\text{-}321}$ (Jeong *et al.*, 2017).

Jeong *et al.* (2017) were able to partially solve the structure of Osh1 and showed that Osh1_A159V is impeded in its interaction with Nvj1. Within this study, it was one aim to investigate, how this Osh1 mutation influences its degradation during PMN.

Finally, two marker proteins, Pho8-GFP and Nab-NLS-mCherry were to be tested in regard of their suitability for differentiation of micro- and macroautophagy and PMN measurement, respectively.

3 Material and Methods

3.1 Material

3.1.1 Yeast Strains

Table 1: Yeast Strains used in this study

Yeast Strain	Genotype	Reference
WCG4	WCG4a MAT α *his 2-11,15 leu2-3,112 ura3*	Thumm *et al.*, 1994
*atg1*Δ	WCG4a MAT α *his 2-11,15 leu2-3,112 ura3 atg1*Δ::*KAN*	Straub *et al.*, 1997
*atg39*Δ	WCG4a MAT α *his 2-11,15 leu2-3,112 ura3 atg39*Δ::*natNT2*	AG Thumm
atg40Δ	WCG4a MAT α *his 2-11,15 leu2-3,112 ura3 atg40*Δ::*hphNT2*	AG Thumm
*atg39*Δ *atg40*Δ	WCG4a MAT *α his 2-11,15 leu2-3,112 ura3 atg39*Δ::*natNT2 atg40*Δ::*hphNT2*	This study
*atg39*Δ *atg40*Δ *nvj1*Δ	WCG4a MAT α *his 2-11,15 leu2-3,112 ura3 atg39*Δ::*natNT2 atg40*Δ::hphNT2 *nvj1*Δ::*HIS3*	This study
*glc8*Δ	WCG4a MAT *α his 2-11,15 leu2-3,112 ura3 glc8*Δ::*NatNT2*	This study
*osh1*Δ	WCG4a MAT α *his 2-11,15 leu2-3,112 ura3 osh1*Δ::*NatNT2*	This study
nvj1-6xHA	WCG4a MAT α *his 2-11,15 leu2-3,112 ura3 Nvj1*-6xHA::*KanMX6*	This study
*nvj1*Δ	WCG4a MAT α *his 2-11,15 leu2-3,112 ura3 nvj1*Δ::*HIS3*	Krick *et al.*, 2008
*nvj1*Δ	WCG4a MAT α his *2-11,15 leu2-3,112 ura3 nvj1*Δ::NatNT2	This study
nvj1Δ scs2Δ	WCG4a MAT α *his 2-11,15 leu2-3,112 ura3 nvj1*Δ::*NatNT2 scs2*Δ::*hphNT1*	This study

*nvj2*Δ	WCG4a MAT α *his 2-11,15 leu2-3,112 ura3 nvj2*Δ::*hphNT1*	This study
*nvj1*Δ *nvj2*Δ	WCG4a MAT α *his 2-11,15 leu2-3,112 ura3 nvj1*Δ::*NatNT2 nvj2*Δ::*hphNT1*	This study
*Scs2*Δ	WCG4a MAT α *his 2-11,15 leu2-3,112 ura3 scs2*Δ::*hphNT1*	This study
*vac8*Δ	WCG4a MAT α *his 2-11,15 leu2-3,112 ura3 vac8*Δ::*HIS3*	Krick *et al.*, 2008
*ymr310c*Δ	WCG4a MAT α *his 2-11,15 leu2-3,112 ura3 ymr310c*Δ::*hphNT1*	This study

3.1.2 *E. coli* Strains

Table 2: *E. coli* strains used in this study

E. coli strains	Genotype	Reference
DH5α	F' (Φ 80 (ΔlacZ) M15) Δ(lacZYAargF) U169 recA1 endA1 hsdR17 rK- mK + supE44 thi-1 gyrA relA	Hanahan, 1983
XL1 blue	endA1 gyrA96(nalR) thi-1 recA1 relA1 lac glnV44 F'[::Tn10 proAB+ lacIq Δ(lacZ)M15] hsdR17(rK- mK+)	Stratagene

3.1.3 Plasmids

Table 3: Plasmids used/ generated for this study

Name/ Insert	**Genotype**	**Reference**
GFP-Osh1	pRS416 CEN6 URA3 TEF1 GFP-OSH1	AG Thumm (Göttingen)
GFP-Osh1_A159V	pRS416 CEN6 URA3 TEF1 GFP-OSH1_A159V	This study
mRFP1-Nop1	pUN100 CEN6 LEU2 mRFP1-Nop1	AG Bohnsack (Göttingen)
Nab2NLS-mCherry	pYX242 2µ LEU2 TPI1 Nab2NLS-2mCherry	D. Goldfarb (University of Rochester)

Nop1-GFP	pUG35 CEN6 URA3 MET25 Nop1-GFP	AG Thumm (Göttingen)
Nvj1-GFP	pUG35 CEN6 URA3 MET25 Nvj1-GFP	Millen et al., 2009
Nvj1-GFP_V20E_V23E	pUG35 CEN6 URA3 MET25 Nvj1-GFP_V20E_V23E	This study
Nvj1-GFP$^{\Delta 318\text{-}321}$	pUG35 CEN6 URA3 MET25 Nvj1-GFP$^{\Delta 318\text{-}321}$	This study
Pho8-GFP	pUG35 CEN6 URA3 Pho8-yEGFP3	This study
pFA6a-natNT2	pFA6a-natNT2	Euroscarf, (Janke et al., 2004)
pFA6a-hphNT1	pFA6a-hphNT1	Euroscarf, (Janke et al., 2004)
pFA6a-kanMX6	pFA6a-kanMX6	Longtine et al., 1998
pFA6a-HIS3MX6	pFA6a-HIS3MX6	Longtine et al., 1998
pUG35	pUG35 CEN6 URA3 MET25 yEGFP3 C-FUS	AG Thumm (Göttingen)
pYM17	pYM17-6xHA	Euroscarf, (Janke et al., 2004)

3.1.4 Oligonucleotides

Table 4: Oligonucleotides used in this study

Name	Sequence (5' to 3')
MCS-KPN1	aatacgactcactatagggcg
NatNT2 rev	CGATTCGTCGTCCGATTCGTC
ATG16 seq 3 for	GGCCAACACTTGTCACTAC
Glc8 KO_S1	ATCAGTACAACGAGTTCGTATCATCAAGAACGCACATCAGCAGAA TAATGCGTACGCTGCAGGTCGAC
Glc8 KO_S2	AAATAAGATATATTTAGTATAGGTAAACGTTATGGAGGTGTCATGT TTCAatcgatgaattcgagctcg
Glc8_Prom	CACCACTACAACTTAAAGTCC
Glc8_rev	GTCGTACTATCATCTTCGTC
HIS-2	CATCTGGGCAGATGATGTC
hphNT1 r	CAATCGCGCATATGAAATCAC
kanMX-r	GTAATGAAGGAGAAAACTCACC

NatNT2 rev	CGATTCGTCGTCCGATTCGTC
NVJ1 KO S1	TGTGCATAATATCAAAAAAGCTACAAATATAATTGTAAAATATAA TAAGCATGCGTACGCTGCAGGTCGAC
NVJ1 KO S2	CACCTCGTTGTAAGTGACGATGATAACCGAGATGACGGAAATATA GTACATTAATCGATGAATTCGAGCTCG
S2_Nvj1-HA	CGTTGTAAGTGACGATGATAACCGAGATGACGGAAATATAGTACA TTAATCGATGAATTCGAGCTCG
S3_Nvj1-HA	GCACAAGTGAACACTGAACAAGCATACTCTCAACCATTTAGATAC CGTACGCTGCAGGTCGAC
PromNvj1_Contro	GGAACCAACAACTGTTGCGTTTGCG
Nvj2 KO S1	CATCGAAGAGCAGAACAGCAAGAGAAAAGTAGCATTAAAAGACC ATAATGCGTACGCTGCAGGTCGAC
Nvj2 KO S2	TATAGCTTCAAGTGATATTTATTTATTTTTAATATAGTACCGTGGA CTCAatcgatgaa ttcgagctcg
Nvj2rev	GGGCTCTCGCTGTTCTTCAAATTCT
Prom Nvj2	GGGTTTTGAACACATCGAAGAGCAG
Nvj1_L20E_V23E_forw	GTCTTTCTGTAGCCGTTGAGAAAGGTGAAGAAAAAACAGTTCGTA AG
Nvj1_L20E_V23E_rev	CTTACGAACTGTTTTTTCTTCACCTTTCTCAACGGCTACAGAAAGA C
Nvj1_BamHI_forw	AGTCAAGGATCCAGCATGACTCGTCCCCCATTGGTTCGTGGAAT CTTTTC
Nvj1_EcoRI_rev	TTGACTTTAGTATCTAAATGGGAATTCTTGAGAGTATGCTTGTTCA GTGTTCACTTGTGCATC
Osh1_KO_S1	GAAAAGTTTAAACATCAAAGTACACCTTTCACCCCTCCACACACC ATGCGTACGCTGCAGGTCGA
Osh1_KO_S2	CAATGGATACAAATGAACGAGTGTTATTGTGACTACATTGCACAG CTTAGatcgatgaattcgagctcg
Osh1_fw	GCTGAGTTTTTGCGCATCAATATTATTTTTACTACTAC
Osh1 forw 3	CTACAAATTGCGTTGGTTC
Osh1 forw 4	AGGAGACTCCAGCTAATG
Osh1_rev	GTTGGTCCATTTTTTCAGGTAGCCTTTGTAAG
Osh1 rev 2	GGAGATCTTGTAGGTTGG
Osh1 rev 4	TTCTCACTGGGTCTTCATATC
Osh1_A159V_forw	CCACATACGTTGCAGAGACCGTCCAGGAATTCAGAACAGCTTTTA AC
Osh1_A159V_rev	GTTAAAAGCTGTTCTGAATTCCTGGACGGTCTCTGCAACGTATGT GG

Osh1 forw 2	GGAACAACCTGATCTATCG
Osh1 rev Osh1 rev 3	CAGCACAATCTTTAAAGTCATG GAATTTCAACTTTTCAGACG
Pho8-GFP_ BamHI_rev	TTGACTGGATCCGTTGGTCAACTCATGGTAGTATTCGTC
Pho8-GFP_ BspEI_forw	AGTCAATCCGGATTCTACTGTTGGAATTCAATGTTAGGAGGAGAA C
Pho8_seq forw (1)	GAGACTCATATGGAGAAACG
Pho8_seq forw (2)	CACCAGTTAGGCGAATATC
Pho8_seq rev (1)	GCAAAGAGACCCAAGAAAG
Scs2 KO S1	TTAATAGTGTAGCAGAAGGGTATTCTACAATCTCCGCGAACCTAA GTATGCGTACGCTGCAGGTCGAC
Scs2 KO S2	CACACATATATAAATATATATTTAGAATACAGCTATATCCTCAATC TCCCTATTAatcgatgaattcgagctcg
Scs2 Prom	TCAGCACACCTGATCTAATAC
Scs2 rev	GCAACCAATATGAATATACCCATG
Seq2r Nvj1	CCCTTCCAAAACGTTCATGTC
Seq 3f Nvj1	CCTTAAGTCGTTAAACCAGC
Sec3r Nvj1	GCTGGTTTAACGACTTAAGG

3.1.5 Antibodies

Table 5: Primary Antibodies used in this study

Antibody	**Dilution** (in TBST containing 10% skim milk powder (w/v))	**Source**
Mouse-anti-GFP	1:1 000	Roche, Mannheim
Mouse-anti-HA	1: 10 000	Santa Cruz Biotechnology, Heidelberg
Mouse-anti-PGK1	1: 10 000	Molecular Probes, Leiden, NL
Mouse-anti Red	1:1 000	ChromoTek, Planegg-Martinsried

Table 6: Secondary Antibodies used in this study

Antibody	Dilution (in TBST containing 1% skim milk powder (w/v))	Source
anti-mouse-HRPO-conjugate	1:10 000	Dianova, Hamburg

3.1.6 Commercial available Kits

Table 7: Commercial available Kits used in this study

Name of the Kit	Source
Clarity Western ECL Substrate	BIO RAD, München
CloneJET PCR Cloning Kit	ThermoFisher Scientific™
ECL Western Blotting Detection	Amershan Bioscience, GB
Instant Sticky-end Ligase Master Mix	NEB, Frankfurt
NucleoSpin®Microbial DNA	Macherey-Nagel, Düren
QIAGEN Plasmid Maxi Kit	Qiagen, Hilden
QIAquick Gel Extraction Kit	Qiagen, Hilden
QIAquick PCR Purification Kit	Qiagen, Hilden
QuickChange Lightning Sit-Directed Mutagensis Kit	Agilent Technologies
Wizard Plus SV Miniprep Kit	Promega, Mannheim

3.1.7 Chemicals, supplements, enzymes and protein purification systems

Table 8: Chemicals, supplements, enzymes and protein purification systems

Name	Source
Acetone	Carl Roth, Karlsruhe
Ammoniumperoxodisulfat	Carl Roth, Karlsruhe
Acrylamid	Carl Roth, Karlsruhe
Bacto Agar	Becton Dickinson, Heidelberg
Bacto Peptone	Becton Dickinson, Heidelberg

Bacto Tryptone	Becton Dickinson, Heidelberg
Bacto Yeast Extract	Becton Dickinson, Heidelberg
β-mercaptoethanol	Carl Roth, Karsruhe
clon NAT (nourseotricine)	Werner BioAgents, Jena
CompleteTM protease inhibitor (EDTA-free)	Roche, Mannheim
Deosyadenosin-triphosphate (dATP)	NEB, Frankfurt
Deoxycytidin-triphosphate (dCTG)	NEB, Frankfurt
Deoxyguanosin-triphosphate (dGTP)	NEB, Frankfurt
Deoxythymidin-triphosphate (dTTP)	NEB, Frankfurt
Difco Yeast nitrogen base w/o amino acids and ammonium	Becton Dickinson, Heidelberg
Difco Yeast nitrogen base w/o amino acids	Becton Dickinson, Heidelberg
DDM	SIGMA-ALDRICH
DNA polymerase (FideliTaq)	USB, Santa Clara, USA
DNA polylmerase (KOD)	Novagen, Darmstadt
DNA polymerase (Taq)	NEB, Frankfurt
DNA polymerase (Vent)	NEB, Frankfurt
DNA-marker (1 kb DNA-ladder)	NEB, Frankfurt
DreamTaq™ Hot Start Green PCR Master Mix	ThermoFisher Scientific™
Gel Loading Dye, Purple (6x)	NEB, Frankfurt
FM4-64	ThermoFisher Scientific™
GFP-Trap	Chromotek, München
Glass Beads	Schütt, Göttingen
Glucose	Carl Roth, Karlsruhe
Glycerin	Carl Roth, Karlsruhe
Glycin	Merck, Munich
Herring-sperm-DNA	Promega, Madison, USA
Hydrochloric acid	Carl Roth, Karlsruhe
Isopropanol	Carl Roth, Karlsruhe
2x Laemmli Sample Buffer	BIO RAD, München
PMSF	Carl Roth, Karlsruhe
Sodium hydroxide	Carl Roth, Karlsruhe
Precision Plus Protein All Blue Standard	BIO RAD, München

Protease inhibitor cocktail (bacteria)	Sigma, Deisenhofen
Protogel	National Diagnostics, fisher scientific
Restriction enzymes	NEB, Frankfurt
SDS	Carl Roth, Karlsruhe
Skim milk powder	Granovita, Lüneburg
Sodium chloride	Carl Roth, Karlsruhe
Supplements for yeast media	Becton Dickinson, Heidelberg
T4-Ligase	NEB, Frankfurt
TEMED	Carl Roth, Karlsruhe
TritonX-100	Carl Roth, Karlsruhe
Tris	Carl Roth, Karlsruhe

3.1.8 Equipment

Table 9: Equipment used in this study

Name	**Source**
Agarose gel equipment	BioRad Laboratores GmbH, München
Autoclave	Adolt Wolf, SANOclav, Bad Überkingen-Hausen
Autoclave DX200	Systec, Wettenberg
Bench	BDK Luft- und Reinraumtechnik GmbH, Sonnenbühl
Blot shaker GFL 3019	GFL, Burgwedel
Centrifuge 5804	Eppendorf, Hamburg
Centrifuge 5404R	Eppendorf, Hamburg
Centrifuge 5415D	Eppendorf, Hamburg
Centrifuge 5415R	Eppendorf, Hamburg
Chemical balance	Sartorius, Göttingen
Cuvettes no. 67.742	Sarstedt, Nümbrecht
Freezer (-20°C)	Liebherr, Bulle, CH
Freezer (-80°C)	Heareus, Hanau
Incubator (37°C)	Heraeus, Hanau
Incubator 4200	Innova, USA
Incubator Thermomixer comfort	Eppendorf, Hamburg
Labshaker for diverse culture sizes	A. Kühner, Birsfelden, CH
LAS 3000 Intelligent Dark Box	Fuji/ Raytest, Benelux

Magnetic stirrer MR 3001	Heidolph, Kelheim
Microscope cover slides	Menzel-Gläser, Braunschweig
Microscope DeltaVision, Olympus IX71	Applied Precision, USA
Microscope slides (76x26 mm)	Menzel-Gläser, Braunschweig
Microwave R-939	Sharp, Hamburg
Mini centrifuge M6	Allsheng, China
Multivortex IKA vibray VXR basic	IKA, Staufen
Over head shaker Roto-Shake Genie	Scientific Industries Inc, USA
PCR Mastercycler gradient	Eppendorf, Hamburg
pH meter pH537	WTW, Weilheim
Photometer	Eppendorf
Pipette tips, petri dishes,…	Sarstedt, Nümbrecht/ Eppendorf, Hamburg
Pipettes	Gilson, USA/ Eppendorf, Hamburg
PowerPac Basic Power Supply	BioRad Laboratories GmbH, München
PowerPac HC Power Supply	BioRad Laboratories GmbH, München
PVDF membrane Hybond-P	Amersham; GE healthcare, Freiburg
Refrigerator	Bosch, Stuttgart/ Liebherr, Bulle CH
SDS-PAGE equipment BioRAD Mini Protean cell	BioRad Laboratories GmbH, München
Sterile filter	Whatman, GE healthcare, München
Thermomixer Comfort	Eppendorf, Hamburg
Transilluminator TI1	Whatman Biometra, Göttingen
Vacuum pump	Vacuubrand, Wertheim
Water bath SWB25	Thermo Electron, Karlsruhe
Western Blot equipment Trans Blot Cell	BioRad Laboratories GmbH, München

3.1.9 Software

Table 10: Software used in this study

Name	Source
Adobe Illustrator CS6, Version 16.0.0	Adobe
Aida Version 4.06.116	Raytest Isotopenmessgeräte GmbH, Straubenhardt
FileMakerPro 12.Ov1	FileMaker, Inc.

Graphpad Prism 7.0d	GraphPad Software, Inc.
ImageJ 1.48	National Institutes of Health, USA
MATLAB	MathWorks®
Microsoft Office	Microsoft
Papers[3], Version 3.4.19	Digital Science & Research Solutions Inc.
SnapGene® 4.0.8	GSL Biotech LLC

3.1.10 Media

The media used in this study, was prepared with deionized water (H_2O_{dd}). The pH of the media was adjusted by using HCl or NaOH. For sterilization, the media was autoclaved at 121°C for 20 min. This chapter indicates percent values in weight per volume (w/v). The addition of 2% of liquid sterile agar to the respective 2x medium was used for the generation of plates.

Table 11: Yeast Media used in this study

Name	Supplements
YPD medium, pH 5.5	1% Bacto Yeast Extract, 2% Bacto Pepton, 2% D-glucose
CM medium, pH 5.6*	0.67% Yeast Nitrogen Base w/o amino acids, 2% D-glucose and dropout-mix: 0.0117% of each of L-alanine, L-methionine, L-arginine, L-phenylalanine, L-asparagine, L-proline, L-aspartic acid, L-serine, L-cysteine, L-threonine, L-glutamine, L-tyrosine, L-glutamic acid, L-valine, L-glycine, myo-inositol, L-isoleucine and p-aminobenzoic-acid
CM medium w/o methionine, pH 5.6*	See CM-medium, pH 5.6 w/o methionine
SD(-N) medium	0,67 Yeast Nitrogen Base w/o amino acids and w/o ammonium sulfate, 2% D-glucose

*Following supplements were added depending on selection of genetic markers: 0.4 mM L-tryptophan, 0.3 mM adenine, 1 mM L-lysine, 0.2 mM uracil, 0.3 mM L-histidine and 1.7 mM L-leucine

Table 12: *E. coli* media used in this study

Name	Supplements
LB-medium, pH 7.5	1% Bacto Trypton, 0.5% Bacto Yeast extract, 0.5% sodium chloride For plasmid selection: 75 µg/ml ampicillin
SOC-medium, pH 7.5	2% Bacto Trypton, 0.5% Bacto Yeast extract, 0.4% D-glucose, 10 mM sodium chloride, 10 mM magnesium sulfate, 10 mM magnesium chloride, 2.5 mM potassium chloride

3.2 Methods

3.2.1 Cultivation and storage of *E. coli*

The *E. coli* cell lines XL1 blue and DH5α were used for all described methods. The *E. coli* cells were grown in LB medium containing the respective antibiotic for plasmid selection. The liquid cultures were inoculated from an agar plate or a long-term storage and grown at 37°C at 220 rpm overnight. The *E. coli* cells were on agar plates for 3-5 weeks at 4°C. For long time storage, a liquid cell culture was mixed with 60 % sterile glycerol in a 1:2 ratio and was stored at -80°C.

3.2.2 Cultivation and storage of *S. cerevisiae*

As nutrient rich medium YPD medium containing 2% glucose was used. Synthetic selection medium CM supplemented with the essential compounds and lacking the selection compounds was used for the selection of genetic markers in liquid yeast cell cultures. The liquid cell cultures were grown at 30°C with an agitation of 220 rpm overnight. The cell density was measured at OD_{600}. 1 OD_{600} of the yeast cell culture corresponds with $3x10^7$ cells per millilitre. A preculture was inoculated from an agar plate for the main culture for the experiment. For the main culture the preculture was diluted depending on the growth strain of the respective strain.

Yeast was stored for up to six weeks on agar plates. For long-term storage, a liquid cell culture was mixed with 30% glycerol in a 1:2 ratio and was stored at -80°C.

3.2.3 Molecular biologic methods

3.2.3.1 Determination of cell density

The cell density in liquid cell cultures was determined via photometry. The liquid cell culture was diluted by a factor of 10 and the OD_{600} (optical density measured at a wavelength of 600 nm) was determined. As a reference a sample of the respective medium was used. 1 OD_{600} corresponds to $3x10^7$ cells per millilitre.

3.2.3.2 Determination of DNA concentration

DNA concentration was determined by using the UV spectrometer (GE Healthcare).

3.2.3.3 Restriction of DNA

For DNA analysis and the generation of defined DNA fragments for cloning, restriction enzymes were used. For the restriction of DNA enzymes from NEB were used according to the manufacturer's recommendations. For the digestion 0.5-1.0 µg DNA was used. The reaction was incubated at the indicated optimal enzyme temperature for 1-2 h. Following, the restricted DNA was analysed by DNA electrophoresis (chapter 3.2.3.4).

3.2.3.4 DNA agarose gel electrophoresis

DNA agarose gel electrophoresis was used for analysing DNA fragments in regard to their size. The negatively charged DNA moves along the electric field to the anode, what leads to a separation of DNA fragments by size, since smaller fragments move faster than larger fragments. Before loading of the samples, the DNA was mixed with 6x loading dye (NEB). The samples were separated in 0.8% agarose gels (w/v) in TAE buffer (40 mM Tris/acetate pH 8.2, 2 mM EDTA, 0.144% acidic acid) and 1 µg/ml ethidium bromide for visualization of DNA by UV light. For size determination, the DNA ladder Tri Dye 1 kb (NEB) was used as a reference.

3.2.3.5 DNA gel extraction

The "Qiagen Gel Extraction Kit" was used to purify DNA after agarose gel electrophoresis and to purify PCR reactions. The kit was used according to the manufacturers recommendations.

3.2.3.6 Polymerase chain reaction (PCR)

The polymerase chain reaction (PCR) was used to amplify DNA fragments for different purposes: e.g. homologous recombination in yeast, control of knockout strains and molecular cloning. Two primers (DNA oligomers) that correspond to the complementary target region and flank the region of interest were created. The PCR can be subdivided into four repetitive steps: initialization, denaturation, annealing and elongation. The DNA was amplified by a DNA

polymerase during repeated cycles of heating and cooling. Depending on the purpose of the PCR and the length of the PCR product, different polymerases were used. Normally, the KOD Hot Start DNA Polymerase (NEB) was used for PCRs and for control PCRs the DreamTaq Mastermix (Thermo Fisher Scientific) was used. As a template, genomic yeast DNA or plasmid DNA was used. Standard PCRs were done according to the manufacturers recommendations. The cycle of the thermocycler was adapted to the size of the DNA product (elongation time) and the annealing temperature of the primers.

3.2.3.7 Molecular cloning

Molecular cloning is the integration of DNA fragments into vectors for replication of this DNA in large quantities. The DNA fragments (inserts) with two flanking restriction sites were generated via PCR (chapter 3.2.3.6). The therefore designed primers contained the respective restriction sites. DNA gel electrophoresis (chapter 3.2.3.4) was used to determine if the PCR product had the predicted size and was then purified using the gel extraction kit (Qiagen, chapter 3.2.3.5). According to manufacturer's advice (NEB) the target plasmid and the PCR product was digested in a 50 µl reaction using the respective enzymes. The reaction was incubated at the recommended temperature for 2-4 hours. To avoid religation, the vector was incubated with 1 µl CIP (alkaline phosphatase, calf intestinal, NEB) for the dephosphorylation of the 5' and 3' ends of the vector DNA. The reaction was purified using the gel extraction kit from Qiagen (protocol for purification of PCR products). The ligation of DNA fragments and the vector DNA was done in a 20 µl overall reaction volume according to the manufacturers recommendation (NEB, chapter 3.2.3.8). The ligated vector was then transformed into chemically competent *E. coli* cells (chapter 3.2.3.10).

3.2.3.8 Ligation of DNA fragments

For the ligation of DNA fragments into a linearized vector the T4-DNA-ligase (NEB) was used. DNA fragments and vector were prepared by DNA restriction (chapter 3.2.3.3) and DNA gel extraction (chapter 3.2.3.5). In a total volume of 20 µl, 2 µl T4-DNA-ligase, 10 µl DNA and 2 µl vector were incubated for 2 h at 25°C or at 16°C overnight. The ligated vector was used for transformation in

E. coli cells (chapter 3.2.3.10). The insert/vector ration was calculated by following equation:

$$\text{mass insert (ng)} = \frac{\text{5x mass plasmid (ng) x length insert (bp)}}{\text{length plasmid (bp)}}$$

Alternatively, the Sticky-end Ligase Master Mix (NEB) was used according to the manufacturers recommendations.

3.2.3.9 Preparation of chemically competent *E. coli* (XL1 blue)

In order to generate chemically competent *E. coli*, XL1 blue cells were used. Therefore, a 400 ml cell culture of OD_{600}~0.6 (growing in LB medium) was pelleted (3000 g, 10 min, 4°C). The pellet was resuspended in 150 ml buffer I (100 mM rubidium chloride, 50 mM manganese(II) chloride, 30 mM potassium acetate pH 5.8, 10 mM calcium chloride, 15% glycerol) and was incubated for 15 min on ice. The cells were harvested (3000 g, 10 min, 4°C) and the pellet was resuspended in 15 ml buffer II (75 mM calcium chloride, 10 mM MOPS pH 6.8, 10 mM rubidium chloride, 15% glycerine). Aliquots of 100 µl were stored at -80°C.

3.2.3.10 Transformation of plasmid DNA in chemically competent *E. coli*

For transformation, chemically competent XL1 blue cells were thawed on ice and the complete ligation reaction or 1 µl of the respective plasmid-DNA was added to 50 µl *E. coli* aliquots (chapter 3.2.3.8). The cells were incubated on ice for 30 min and then incubated at 42°C for 90 seconds. The cells were then chilled on ice for 2 min. Afterwards the *E. coli* resuspended in 1 ml SOC medium and were incubated for 40 min at 37°C while shaking. Finally, the cells were harvested and plated on LB agar plates containing the respective antibiotic for plasmid selection. The plates were incubated overnight at 37°C. Finally, clones were picked and were prepared for plasmid isolation (chapter 3.2.3.12), checked for correct insertion by restriction enzyme digestion and sequencing (chapter 3.2.3.3 and 3.2.3.13).

3.2.3.11 Site directed mutagenesis of plasmids

For the site directed mutagenesis of plasmids the QuickChange Lightning Site-directed Mutagenesis Kit (Agilent) was used. For the introduction of the desired point mutations in a DNA sequence, two complementary primers with the exchanged nucleotides were designed and used according to the manufacturer's recommendations. Via sequencing, the introduced (point) mutations were tested (chapter 3.2.3.13).

3.2.3.12 Purification of plasmids from *E. coli*

For small-scale plasmid purification, the Wizard Plus SV Minipreps DNA Purification System (Promega) was used according to the manufacturer's recommendations.

For large-scale plasmid purification, the Plasmid Maxi Kit (Qiagen) was used according to the manufacturer's recommendations.

3.2.3.13 Sequencing of DNA

All cloned plasmids were verified by sequencing. The sequencing was done by Microsynth Seqlab (Göttingen). For the sequencing the samples, including the plasmid DNA and the primers, were prepared according to the manufacturer's recommendations.

3.2.3.14 Plasmid constructs

3.2.3.14.1 GFP-Osh1_A159V construct

For construction of pRS416-GFP-Osh1_A159V, plasmid DNA was amplified using the primers Osh1_A159V_forw and Osh1_A159V_rev. The PCR was performed according to the QuickChange Lightning Site-Directed Mutagenesis protocol (chapter 3.2.3.11). This construction was made according to Manik *et al.* (2017)

3.2.3.14.2 Nvj1_V20E_V23E-GFP construct

For construction of pUG35-Nvj1_V20E_V23E-GFP, plasmid DNA was amplified using the primers Nvj1_L20E_V23E_forw and Nvj1_L20E_V23E_rev. The PCR was performed according to the QuickChange Lightning Site-Directed

Mutagenesis protocol (chapter 3.2.3.11). This construction was made according to Millen *et al.* (2008).

3.2.3.14.3 Nvj1$^{\Delta 318\text{-}321}$-GFP construct

Nvj1 was amplified from wild type chromosomal DNA using the primers Nvj1_BamHI_forw and Nvj1_EcoRI_rev. The PCR was performed according to the molecular cloning protocol (chapter 3.2.3.7). The vector pUG35 and the PCR product were digested using the enzymes EcoRI and BamHI and were then ligated. This construction was made according to Jeong *et al.* (2017).

3.2.3.14.4 Pho8-GFP

Pho8 was amplified from wild type chromosomal DNA using the primers Pho8-GFP_BspEI_forw and Pho8-GFP_BamHI_rev. The PCR was performed according to the molecular cloning protocol (chapter 3.2.3.7). The vector pUG35 and the PCR product were digested using the enzymes BspEI and BamHI and were then ligated.

3.2.3.15 Isolation of chromosomal DNA from yeast cells

For the isolation of chromosomal DNA from yeast cells, the Nucleo Spin®Microbial DNA Kit (Macherey-Nagel) was used according to the manufacturer's recommendations.

3.2.3.16 High efficiency yeast cell transformation

The high efficiency yeast cell transformation was used for gene knockout or chromosomal tagging of genes. A 50 ml liquid cell culture was grown to a OD_{600}~0.5 and were harvested by centrifugation (2 000 rpm, 5 min, RT). The cells were washed twice with 20 ml H_2O_{dd} and once with 2,5 ml LiOAc-Sorb (1 M D-sorbitol, 100 mM lithium acetate, 10 mM Tris/acetate pH 8.0). Then the cells were resuspended in 250 µl LiOAc-Sorb and were incubated at 30°C for 15 min. Subsequently, 50 µl of the cell suspension was mixed with 5 µl herring sperm DNA (10 mg/ ml), 5 µl of DNA and 300 µl PEG in Li-TE (1 mM EDTA, 100 mM lithium acetate, 10 mM Tris/acetate pH 8.0, 40% (v/v) PEG 3350). The cells were incubated at 30°C for 30 min and then heat-shocked at 42°C for 15 min. The cells were harvested (2 000 rpm, 5 min, RT) and were

resuspended in 2 ml YPD for recovery (2 h, 30°C, 220 rpm agitation). In the last step, the cells were harvested (2 000 rpm, 5 min, RT), resuspended in 50 µl H_2O_{dd} and were plated on the corresponding agar plates containing the respective antibiotics for selection of genetic markers. After 2-3 days of incubation at 30°C, colonies were picked, tested for the correct transformation and then used for further analyses.

3.2.3.17 "Quick and Dirty" variant of yeast cell transformation

For plasmid transformation into yeast cells a „quick and dirty" variant of the transformation protocol (chapter 3.2.3.16) was used. Yeast cells were directly picked from agar plates and incubated with 5 µl of herring sperm DNA (10 mg/ml), 300 µl of PEG in Li-TE (10 mM Tris/acetate pH 8.0, 100 mM lithium acetate, 1 mM EDTA, 40% (v/v) PEG 3350) and 5 µl of the respective plasmids for 30 min at 30°C. The cells then were heat-shocked at 42°C for 15 min, harvested by centrifugation (5 min, 2 000 rpm), resuspended in 50 µl H_2O_{dd} and plated on CM agar plates containing the respective selection markers. The plates were incubated at 30°C for two to three days.

3.2.3.18 Knockout and chromosomal tagging of genes by homologous recombination

Deletion strains and chromosomal tagging of genes were done by homologous recombination according to the protocol of Janke *et al.* (2004). For this purpose, primers consisting of a ~ 45 bp region homologous to the flanking region of the target gene and a 20 bp region homologous to the selection gene were designed. As a template for the PCR reaction the plasmid containing the respective selection gene, e.g. pFA6a-NatNT2 (a nourseothricin cassette) was used (chapter 3.2.3.6). The PCR product was purified using the DNA extraction kit (Qiagen, chapter 3.2.3.5) and then integrated via homologous recombination (chapter 3.2.3.16). So, the target gene was either replaced with the selection gene or the chromosomal tag was integrated. After growth on selection plates, the obtained clones were verified by PCR.

3.2.3.19 Direct fluorescence microscopy

Via direct fluorescence microscopy fluorescence labelled proteins or plasmids were visualized in the cell. The protein of interest was tagged on a plasmid with a protein, that fluoresces when it is exposed to light in a defined range, e.g. GFP or mCherry. The yeast strains were grown overnight in the respective selection medium and depending on the experiment setup, starved for 2-4 h in SD(-N) medium. The yeast strain of interest was dropped on a glass slide and was covered by a cover slip. The microscopy was performed using the DeltaVision Spectris fluorescence microscope (Olympus IX71, Applied Precision). Pictures were taken by a CoolSNAP HQ camera with the respective filter set for each fluorescent tag (Table 13) and an 100x objective. Image stacks were taken, so that 20 stacks with a distance of 20 µm covered the yeast cells from top to bottom. For each stack one image was taken for each fluorescent marker and one reference image from the middle of the sample. Deconvolution of the obtained pictures was done using the SoftWoRx software (Applied Science). Analyses and editing of the images were performed using Fiji and Illustrator software.

Table 13: Filter sets for living cell imaging

Filter set	Excitation wavelength (nm)	Emission wavelength (nm)
GFP	475/28	525/50
mCherry	575/25	632/60
Pol	-50/28	-50/0

3.2.3.20 Vacuolar staining using FM4-64

For visualization of vacuolar membranes during microscopy, the FM4-64 staining was used. Cells were grown to stationary phase, harvested and resuspended in 2 ml of the respective selection medium. 2 µl of a FM4-64 solution (1 mg/ 200 µl H_20, Thermo Fisher Scientific) was added. The cells were incubated at 30°C for 30 min, then starved in SD(-N) medium and finally microscoped.

3.2.3.21 Induction and monitoring of autophagy

For the induction of autophagy in yeast cells nitrogen free medium (SD(-N)) or rapamycin was used. As the measurement of the breakdown of an overexpressed marker is difficult, therefore the breakdown of GFP-tagged proteins was determined. Free GFP is proteolysis resistant and the accumulation of GFP can be used as a readout marker.

Free GFP was either detected by immunoblotting (chapter 3.2.4.4) or by direct fluorescence microscopy (chapter 3.2.3.19). For alkaline lysis (chapter 3.2.4.1) and following immunoblotting (chapter 3.2.4.4) up to 40 OD_{600} of yeast cell culture with a cell density of 5-9 OD_{600} was harvested, washed twice in SD(-N) medium and resuspended to a cell density of 10 OD_{600} per millilitre. Samples of 2 OD_{600} were collected after different time points (e.g. 0 h, 2 h, 4 h, 6 h and 24 h starvation). The obtained signals were quantified and evaluated statistically using the AIDA and PRISM software.

For microscopic analysis 5 OD_{600} of a yeast cell culture with a cell density of 3-4 OD_{600} were harvested, washed twice in SD(-N) medium and resuspended to a cell density of 2 OD_{600} per millilitre. Microscopic imaging was done after 2-4 h starvation. The images were analysed as described in chapter 3.2.3.19.

3.2.4 Biochemical Methods

3.2.4.1 Alkaline lysis of yeast cells

Yeast cells (up to 40 OD_{600}) were harvested by centrifugation (2 000 rpm, 5 min, RT). The supernatant was discarded and the pellet was resuspended in 1 ml ice-cold H_2O_{dd}. 150 µl of lysis solution (7,5% β-Mercaptoethanol, 1,85 M NaOH) was added, the samples were mixed, incubated on ice for 10 min and 150 µl of 50% TCA (w/v) was added. The samples were vortexed and incubated on ice for 10 min. After centrifugation (13 200 rpm, 10 min, 4°C) the supernatant was discarded and the pellet was washed twice with 200 µl ice-cold acetone (storage at -20°C). After the last washing step, the supernatant was discarded and the pellet was dried at 37°C. Then the pellet was dissolved in 50 µl 2x laemmli-buffer (116 mM Tris/HCl pH 6.8, 3.42% (w/v) SDS, 12% (w/v) glycerol, 2% β-mercaptoethanol, 0.004% bromphenolblue).

3.2.4.1.1 PMN-Assay (measurement of e.g. GFP-Osh1 breakdown)

The deletion strains were transformed with pRS416-GFP-OSH. In order to improve the signal intensity of the free GFP, the plasmids were prepared by a Maxi-Preparation Kit (Qiagen). A pre-culture of the transformed cells was made in the respective selective medium (usually CM-Ura) and was cultured overnight at 30°C. The main culture was inoculated 1:100 in the same selective medium, or in selective medium containing 0,3 mM methionine and grown over night (depending on the respective promotor) at 30°C. The next morning 40 OD_{600} were harvested at an OD_{600} of 5-9. The cells were washed twice in SD(-N) starvation medium, resuspended in 4 ml SD(-N) medium and incubated at 30°C. 200 µl samples (2 OD_{600} cells) were collected at the different time points (usually 0, 2, 4, 6, and 24 h) and alkaline lysed (chapter 3.2.4.1). The samples were applied on 10% SDS gels and analysed using a wet blot (chapter 3.2.4.4). The signals were detected with *ECL (BioRad).*

The degradation of Nop1-GFP, Nab-NLS-mCherry, Pho8-GFP, GFP-Osh1_A159V, Nvj1_V20E_V23E-GFP, Nvj1$^{\Delta 318\text{-}321}$-GFP was measured accordingly.

3.2.4.2 GFP-Trap

For protein-protein interactions *in vivo* the GFP-Trap approach was used. This method is based on the idea, that the bait protein, expressed with a GFP tag, can attach to GFP beads via GFP binding proteins on the surface of the GFP beads. In the end, the bound bait protein as well as the interacting proteins or protein complexes can be purified from the cell extracts.

250 OD_{600} were harvested by centrifugation (2000 rpm, 5 min, 4°C), were washed once with 15 ml cold PBS and were resuspended in GFP-Trap buffer *(*250 OD_{600}/ ml buffer; 1x PBS pH 7.4, 5 mM $MgCl_2$, 0.2 M sorbitol, 1x Complete (w/o EDTA) (Roche), 1x protease inhibitors, 1 mM PMSF, DDM,). For cell disruption, the cells were incubated with 200 µl glass beads (Schütt, Göttingen, Germany) on a shaker (Disruptor Genie® digital 230 V, Schütt Labortechnik, Göttingen, Germany) for 30 min. During that time, the GFP-beads were equilibrated, 8 µl of the GFP-beads were resuspended in 500 µl GFP-Trap buffer and sedimented (2000 g, 2 min, 4°C). The cells were then centrifuged (5 min, 2700 g, 4°C) for the removement of glass beads and cell debris. The

supernatant (Input sample) was incubated with GFP-Trap beads (GFP-Trap A, ChromoTek, Planegg-Martinsried, Germany) on an overhead shaker at 4°C for 2 h (Roto-Shake Genie, Scientific Industries Inc, USA). The GFP-Trap beads were then washed 4 times using 1,4 ml GFP-Trap buffer (centrifugation 2000 g, 2 min) (Non bound sample). Finally, the proteins were eluted in 25 µl GFP-Trap buffer and 25 µl 4xLaemmli at 95°C for 5 min. The samples were loaded to a polyacrylamide gel (chapter 3.2.4.3) and were analysed by immunoblotting (chapter 3.2.4.4).

3.2.4.3 Discontinuous SDS-Polyacrylamid-Gel-Electrophoresis (SDS-PAGE)

Discontinuous SDS-PAGE is a biochemical method to separate proteins according to their molecular weight in an electric field. SDS masks the intrinsic charge of the proteins and at the same time negatively charges the proteins proportionally to their weight. Therefore, the proteins can be separated according to their molecular weight. For SDS-PAGE a Mini-Protean III electrophoresis chamber from BioRad was used according to the manufacturer's recommendations. The contents of the SDS-polyacrylamid-gels are described in Table 14.

Table 14: Mixture of one SDS Polyacrylamid gel for a Mini-Protean III electrophoresis chamber from BioRad

Components	10% Separating Gel	5% Collecting Gel
H_2O_{dd}	1.9 ml	3.0 ml
1.5 M Tris, pH8.8	1.25 ml	-
0.5 M Tris, pH 6.8	-	1.25 ml
Protogel	1.8 ml	1.8 ml
10% (w/v) SDS	50 µl	50 µl
10% (w/v) APS	50 µl	50 µl
TEMED	2.5 µl	5 µl

The SDS chamber was filled with SDS running buffer (25 mM Tris, 200 mM glycerol, 0.1% SDS). For the estimation of the molecular weight of the separated proteins, the protein marker Precision Plus Protein All Blue Standard (BioRad) was used. The samples for SDS-PAGE were dissolved in laemmli buffer (0.35 M Tris/HCl (pH 6.8), 36% glycerin, 10.28% SDS, 5% β-

mercaptoehanol 0.012% bromphenolblue,). Normally, 15 µl of the protein sample were loaded per lane. The electrophoresis was performed at 150 V and was stopped when the bromphenolblue of the laemmli buffer left the gel. The SDS-gels then were used for immunoblotting (chapter 3.2.4.4).

3.2.4.4 Immunoblotting (Wet Blot)

Immunoblotting was used to visualize proteins that were separated by SDS-Page (chapter 3.2.4.3). The proteins were transferred from a polyacrylamide gel to a PVDF membrane by immunoblotting (Western blot). The protein transfer was performed using a blotting chamber from BioRad, filled with wet blot buffer (25 mM tris, 192 mM glycine and 20% ethanol). Each gel was blotted with 75 mA (1.2 mA per cm^2) for 5 to 6 h at 4°C. The SDS gel and the PVDF membrane were placed between 2x2 Whatman papers and two fiber pads, that were soaked with wet blot buffer. The gel holder cassette was closed and placed into the wet blot chamber (Figure 3.1).

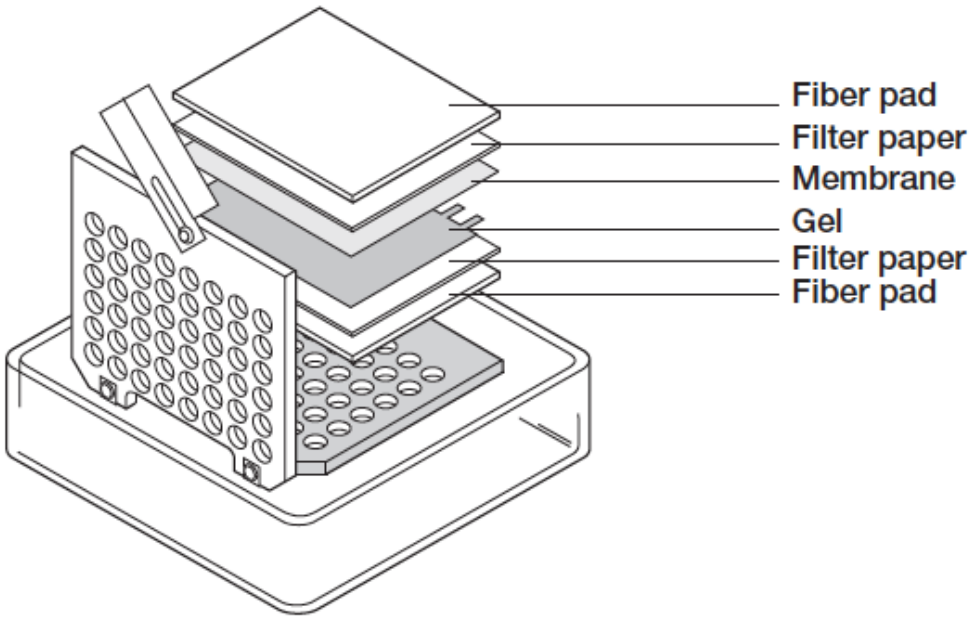

Figure 3.1: Setup for immunoblotting

(adapted from Mini Trans-Blot® Electrophoretic Transfer Cell Instruction Manual, BioRad). Immunoblotting was used for the protein transfer from a polyacrylamide gel to a PVDF membrane, followed by a staining of the membrane with the respective antibodies.

After the protein transfer, the membrane was incubated in blocking solution (10% (w/v) skim milk powder in TBST (20 mM Tris/HCl pH7.6, 137 mM NaCl, 0.1% (w/v) Tween20)) for at least 1 h at room temperature or overnight at 4°C. Unspecific binding sites are masked by the proteins in the milk powder. The membrane was then washed three times with TBST for 10 min. Following, the membrane was incubated in the primary antibody for 2-4 h at room temperature or overnight at 4°C (table Table 5). The membrane was washed three times with TBST, was then incubated in the secondary antibody for 45 min to 1 h and was washed then again with TBST. For development of the western blot, the membrane was incubated in ECL solution from BioRad for 5 min. Signals were visualized using the LAS-3000 (Fujifilm). The AIDA software (version 4.06.116) was used for further analyses and quantification of the obtained signals.

For further analyses the membrane was stripped using 10% acetic acid for 10 min and then could be incubated with another primary antibody.

3.2.4.5 Statistical Analysis

The Graph Pad Prism 6 software was used for statistical analysis of western blots. The standard error of the mean (SEM) is indicated by the error bars. The statistical significance as follows: not significant for $P > 0.05$ (ns), * for $P < 0.05$, ** for $P < 0.01$, *** for $P < 0.001$ and **** for $P < 0.0001$.

The AIDA software was used for quantification of the Western blots. For the PMN-Assay the amount of free GFP was determined and the wild type was set to 100%. Subsequently, the different samples were tested in regard of their statistical significance. For this purpose, a one sample t-test was used.

4 Results

4.1 Nvj1 isn't essential for degradation of nucleolar proteins

Nvj1 together with Vac8 forms the backbone of the NVJ (Pan *et al.*, 2000a). Deletion of one of these two proteins is considered to block the degradation of GFP-Osh1, a marker protein for PMN (Krick *et al.*, 2008; Millen *et al.*, 2009). Also nucleolar proteins were shown to be putative marker proteins for the measurement of PMN, however degradation of these proteins wasn't blocked in *NVJ1* deletion strains (Dawaliby and Mayer, 2010; Mochida *et al.*, 2015).

4.1.1 Relevance of Nvj1 for the degradation of GFP-Osh1

In order to be more flexible in the usage of plasmids, within this study a new *NVJ1* knockout strain was made using nourseothricin (*NatNT2*) as a knockout marker. The new *nvj1*Δ::*NatNT2* knockout strain was then compared to the already existing *nvj1*Δ::*HIS3* knockout stain in regard of the PMN rate.

As previously shown (Krick *et al.*, 2008), the PMN rate in different knockout strains was measured by the breakdown of GFP-Osh1 in SD(-N) starvation medium (Chapter 3.2.4.1.1). Under these conditions, GFP-Osh1 is transported to the vacuole and degraded. The degradation of GFP-Osh1 results in a rather proteolysis resistant GFP that can be used for the measurement of the PMN rate. GFP-Osh1 was expressed from a pRS416 plasmid. Cells were grown to late stationary phase and were starved for 0 h, 2 h, 4 h, 6 h and 24 h in SD(-N) starvation medium. Then, the cells were alkaline lysed and free GFP was detected on western blots using an anti-GFP antibody.

As expected deletion of *VAC8* completely blocked the degradation of GFP-Osh1. For that reason, the *vac8*Δ strain was used here as a negative control. The amount of free GFP in the wild type strain after 24 h starvation in SD(-N) starvation medium in the wild type strain was set to 100%.

Degradation of GFP-Osh1 was blocked in *vac8*Δ cells, the negative control (8,97% ± 3,45%), as well as in *nvj1*Δ::*HIS3* cells (7,82% ± 0,83%) (Figure 4.1 A, B). In contrast, PMN wasn't blocked in the new knockout strain *nvj1*Δ::*NatNT2*, that showed wild type like behaviour (104,1% ± 4,81%).

Since the PMN rate in both tested *NVJ1* deletion strains was contradicting, the

degradation of Nop1-GFP, a nucleolar marker, was measured in the respective knockout strains.

4.1.2 Relevance of Nvj1 for the degradation of Nop1-GFP

Knockout of NVJ1 was shown not to affect degradation of Nop1-GFP (Mochida *et al.*, 2015). Therefore, *nvj1*Δ::*HIS3* and *nvj1*Δ::*NatNT2* were analysed in regard to their ability to degrade Nop1-GFP. Nop1-GFP was expressed from a plasmid under a *MET25* promotor. Cells were grown over night to late stationary phase in CM medium containing 0,3 mM methionine. The cells were then starved for 0 h, 2 h, 4 h, 6 h and 24 h in SD(-N) medium. Following, the cells were alkaline lysed and free GFP was detected on western blots using an anti-GFP antibody.

No free GFP was detected in *vac8*Δ and nvj1Δ::*HIS3*, whereas in *nvj1*Δ::NatNT2 free GFP was visible (Figure 4.1 C). Quantification showed, that degradation of Nop1-GFP was blocked in *vac8*Δ (3,12% ± 1,28%) and in *nvj1*Δ::*HIS3* (13,1% ± 1,69%), but again was only slightly reduced in *nvj1*Δ::NatNT2 (56,36% ± 13,61%) compared to the wild type (Figure 4.1 D).

This indicates, that both degradation of GFP-Osh1 (Chapter 4.1.1), and of Nop1-GFP results in contradicting phenotypes in the two tested *NVJ1* knockouts.

However, Mochida *et al.* (2015) found, that degradation of Nop1-GFP wasn't blocked in *nvj1*Δ cells. But they used a slightly different experimental setup, so it couldn't be completely ruled out, that varying results were based on these differences. Thus, both experimental setups were compared (Chapter 4.1.3).

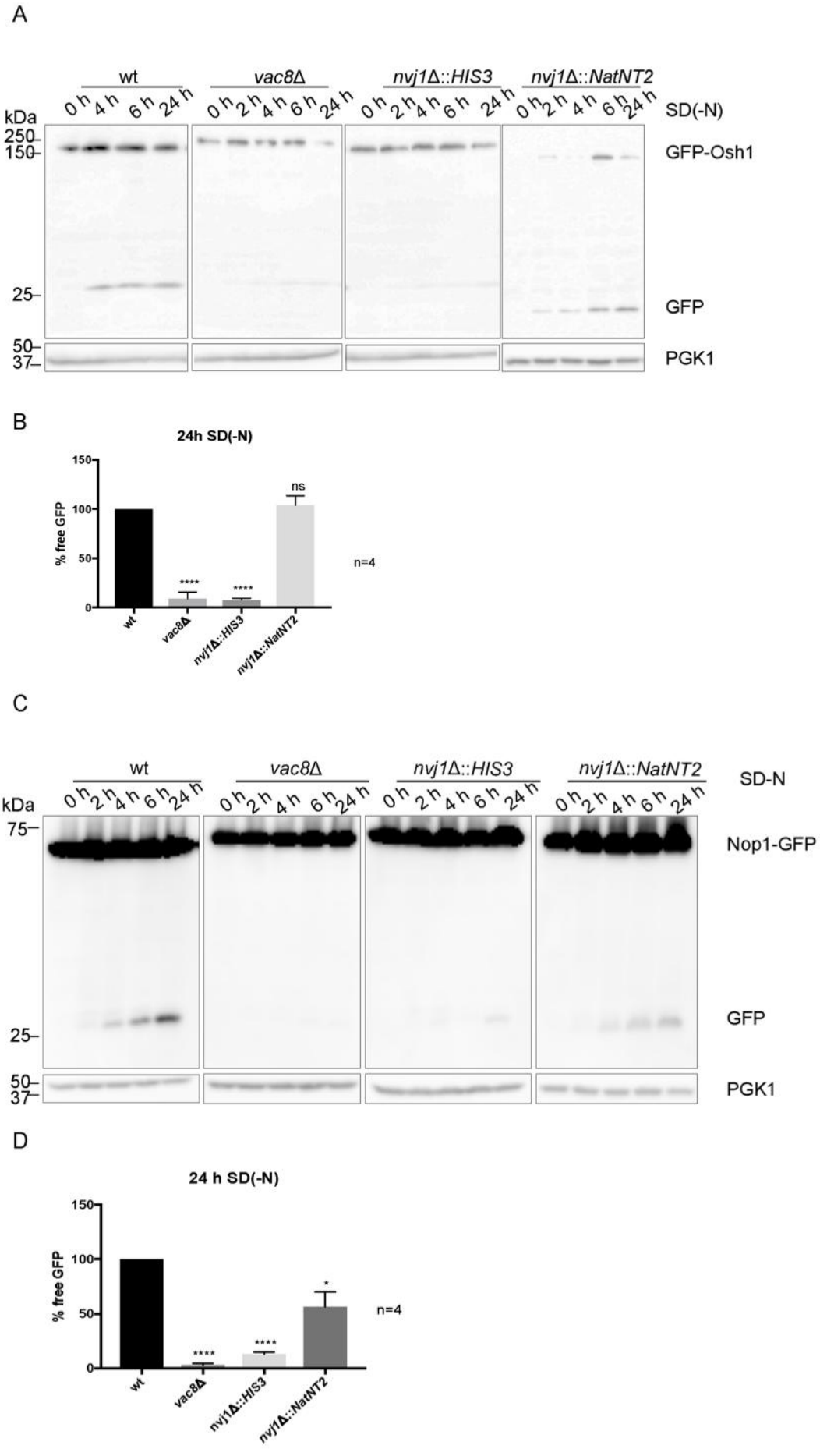
A
wt
vac8Δ
nvj1Δ::HIS3
nvj1Δ::NatNT2
0 h
2 h
4 h
6 h
24 h
SD(-N)
kDa
250
150
25
50
37
GFP-Osh1
GFP
PGK1
B
24h SD(-N)
% free GFP
150
100
50
0
ns
****
****
n=4
wt
vac8Δ
nvj1Δ::HIS3
nvj1Δ::NatNT2
C
SD-N
75
Nop1-GFP
GFP
PGK1
D
24 h SD(-N)
*
n=4

Figure 4.1: Degradation of GFP-Osh1 and Nop1-GFP is blocked in different *nvj1*Δ strains

(A) PMN was measured through the expression of GFP-Osh1 and analysis via western blot. Degradation of GFP-Osh1 in the vacuole leads to the release of free GFP and therefore corresponds with the PMN rate. Cells were starved in SD(-N) medium and samples were taken at 0 h, 2 h, 4 h, 6 h, 24 h and were alkaline lysed. Free GFP was detected with an anti-GFP antibody. PGK1, used as a loading control, was detected with an anti-PGK1 antibody.
(B) Quantification of four independent experiments showed, that the degradation of GFP-Osh1 was blocked in *nvj1*Δ::*HIS3* but not in *nvj1*Δ::*NatNT2* cells. Statistics were performed using the one sample t-test. Error bars represent SEM and asterisks represent p-values.
(C) Degradation of Nop1-GFP was measured in different knockouts and was analysed via western blot. Cells were starved in SD(-N) medium and samples were taken at the indicated time points. Free GFP and was detected with an anti-GFP antibody. PGK1, used as a loading control, was detected by an anti-PGK1 antibody.
(D) Quantification of four independent experiments showed, that the degradation of Nop1-GFP was blocked in *nvj1*Δ::*HIS3* but not in *nvj1*Δ::*NatNT2* cells. Statistics were performed using the one sample t-test. Error bars represent SEM and asterisks represent p-values

4.1.3 Degradation of Nop1-GFP is similar in SD(-N) medium or after rapamycin treatment

Mochida *et al.* (2015) were able to show that degradation of Nop1-GFP isn't blocked in *NVJ1* knockout cells. However, they had a different experiment setup, as they used rapamycin for starvation of the cells. To clarify the reason for the contradicting results in two different *NVJ1* knockout strains (Chapter 4.1.2), both starvation conditions were compared. Cells expressing Nop1-GFP from a plasmid under a *MET25* promotor were grown to late stationary phase in CM medium containing 0,3 mM methionine. The cells were then starved in either SD(-N) medium or CM medium containing rapamycin (0,2 µg/ml). Samples were collected after 0 h, 2 h, 4 h, 6 h and 24 h starvation in the respective starvation medium. Following, the cells were alkaline lysed and free GFP was detected on western blots using an anti-GFP antibody.

The type of starvation induction had no impact on the outcome of the experiment. While degradation of Nop1-GFP was blocked in *nvj1*Δ::*HIS3* cells, as it was the case in the negative controls *atg1*Δ and *vac8*Δ cells under both starving conditions, *nvj1*Δ::*NatNT2* cells showed wild type like amounts of free GFP (Figure 4.2). This was to be expected, since starvation of cells with SD(-N)

medium or treatment of cells with rapamycin, leads both to inhibition of TORC1, what results in a hypophosphorylation of Atg13 and finally to the induction of autophagy (Noda and Ohsumi, 1998). Together the data suggest, that unknown differences between the both *nvj1*Δ strains might be responsible for the contradictory outcomes and not the experimental setup. Thus, these strains were next analysed microscopically (Chapter 4.1.4).

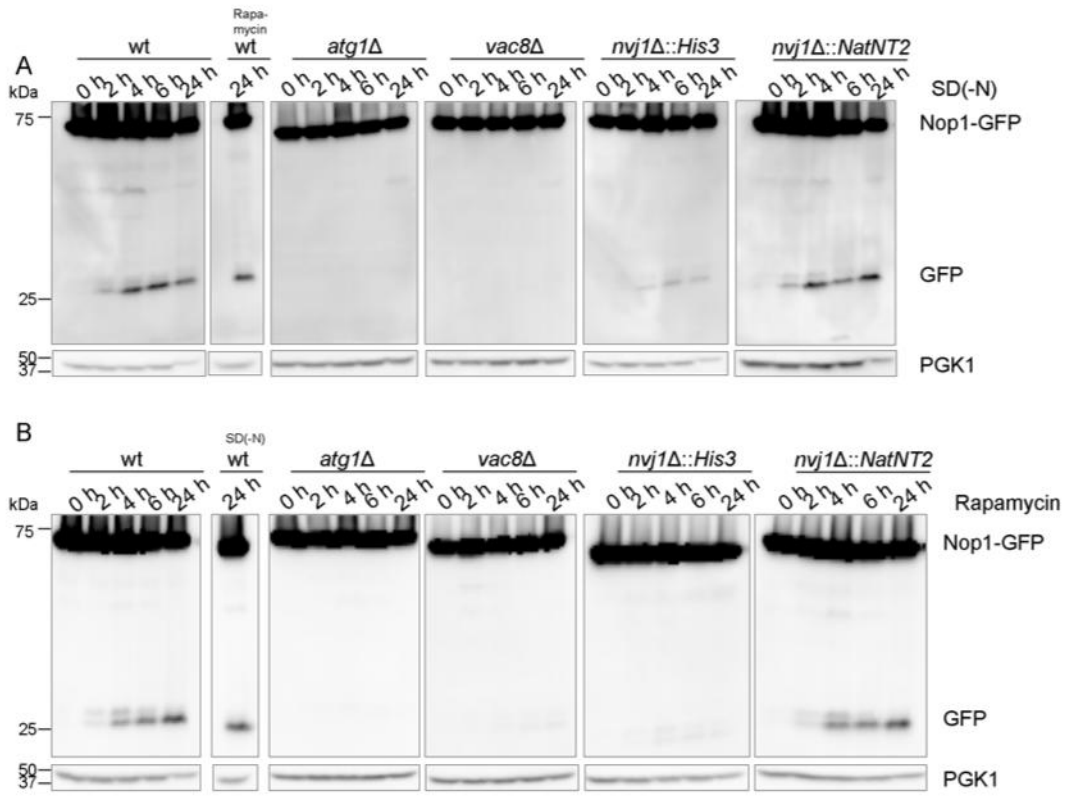

Figure 4.2: Nop1-GFP degradation in cells starved with either SD(-N) or rapamycin containing medium

Degradation of Nop1-GFP was measured in different knockouts and was analysed via western blot. Cells were starved in SD(-N) medium (upper western blots) or with 0,2 µg/ml rapamycin (lower western blots), samples were taken after different time points (0 h, 2 h, 4 h, 6 h, 24 h) and were alkaline lysed. Free GFP and Nop1-GFP was detected with an anti-GFP antibody. PGK1, used as a loading control, was detected by an anti-PGK1 antibody.

4.1.4 The nucleus-vacuole junction is intact in *nvj1*Δ::*HIS3* cells but not in *nvj1*Δ::*NatNT2* cells

To further analyse the discrepancy between *nvj1*Δ::*HIS3* and *nvj1*Δ::*NatNT2* cells (Chapter 4.1.1 and 4.1.2 and), the NVJs were visualized microscopically. Pan *et al.* (2000a) showed, that absence of either Nvj1 or Vac8 affects NVJs.

For visualization of the NVJs GFP-Osh1 was expressed from a plasmid under a *TEF1* promotor. Nop1-RFP was further expressed from a pUN100 plasmid as nucleolus marker. Nop1-RFP was included, since it was observed, that the NVJ is mostly localized adjacent to the nucleolus (data not shown).

The cells were grown to stationary phase and starved for 2 h in SD(-N) medium and then microscopically evaluated using the Delta Vision microscope. The NVJ in *nvj1*Δ::*HIS3* was localized next to Nop1 and appeared wild type like (Figure 4.3). In contrast to that, the new knockout strain *nvj1*Δ::*NatNT2* showed only residuals of the NVJ, comparable to the negative control, the *vac8*Δ strain.

Taken together, these results indicate, that one of the *NVJ1* knockout strains might carry additional mutations. However, it was unclear which strain was potentially incorrect. *nvj1*Δ::*HIS3* was blocked in the degradation of the respective marker proteins, but showed intact NVJs, while *nvj1*Δ::*NatNT2* showed disrupted NVJs, but wild type like degradation of the tested marker proteins.

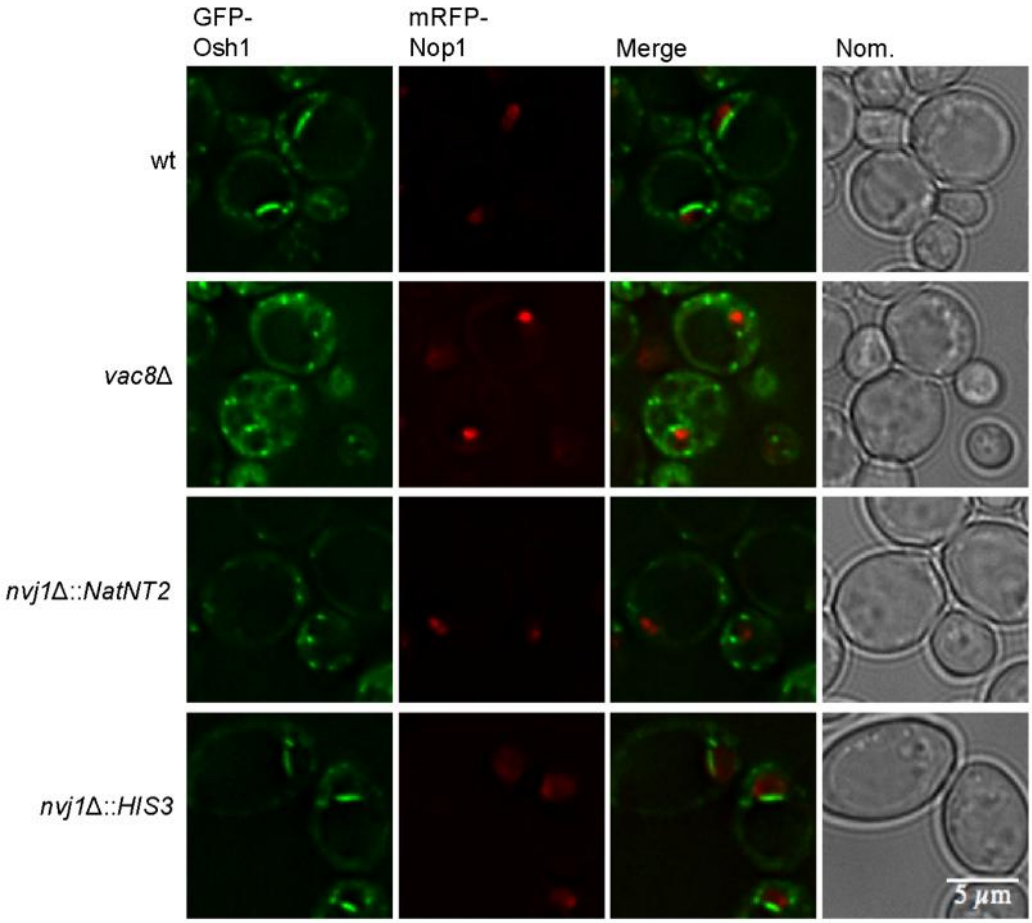

Figure 4.3: Nucleus-vacuole junctions are intact in *nvj1*Δ::*HIS3* cells but not in *nvj1*Δ::*NatNT2* cells

The NVJs were visualized using GFP-Osh1 as a marker in the indicated strains. The nucleolar marker Nop1-RFP was expressed as an additional marker. The cells were grown to late stationary phase and starved for 2 h in SD(-N) medium. Finally, the cells were analysed using the Delta Vision microscope.

4.1.5 Degradation of Nab-NLS-mCherry is only blocked in *atg1*Δ cells

The results obtained previously (Chapter 4.1.1, 4.1.2, and 4.1.4), suggested that one of the *NVJ1* knockout strains, either *nvj1*Δ::*HIS3* or *nvj1*Δ::*NatNT2*, might be wrong. In order to clarify, which one of the *NVJ1* knockout strains was correct, the breakdown of Nab-NLS-mCherry was measured. Nab-NLS-mCherry is localized to the nucleus and, according to the current literature, shouldn't be degraded in the correct *NVJ1* knockout, since PMN is blocked in the respective strain.

Different deletion strains expressing Nab-NLS-mCherry were grown to late stationary phase and were starved in SD-(N) medium. Samples were taken after 0 h, 2 h, 4 h, 6 h and 24 h. Following, the cells were alkaline lysed and free

mCherry was detected on western blots using an anti-RFP antibody.

The measurement of free mCherry showed, that the breakdown was blocked only in *atg1*Δ cells, but was wild type like in all other tested strains. This suggested that there was an alternative mechanism for the breakdown of Nab-NLS-mCherry than PMN and that this marker wasn't suitable to solve the problem or to measure PMN (Figure 4.4).

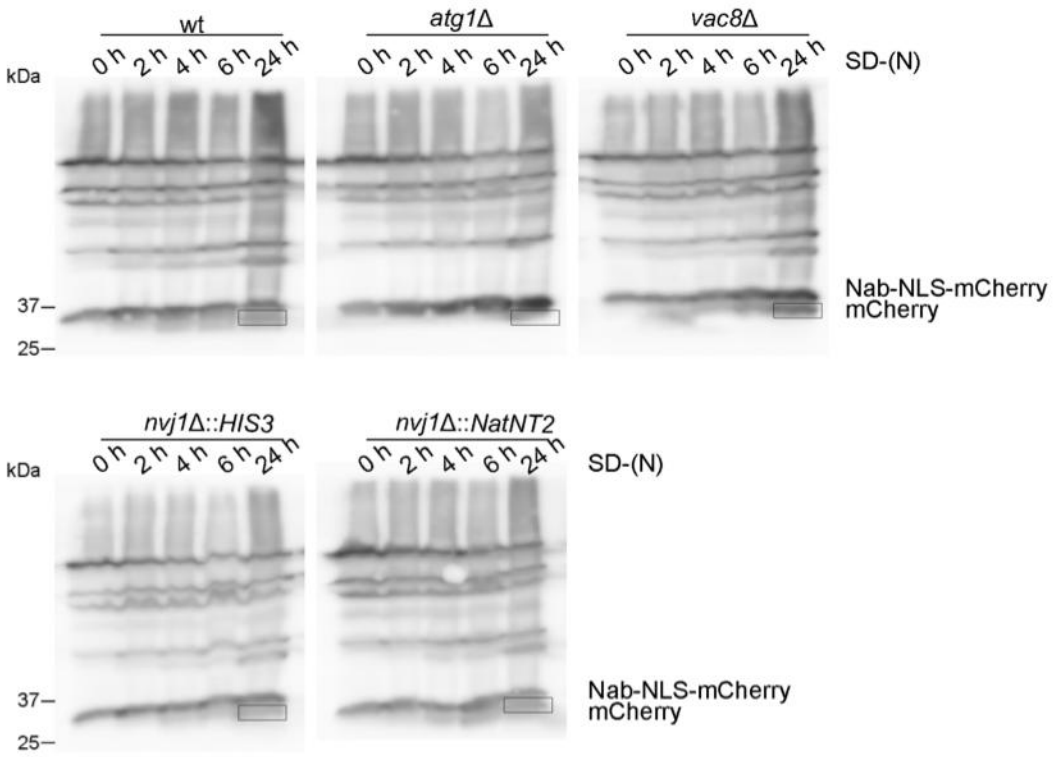

Figure 4.4: Degradation of Nab-NLS-mCherry isn't blocked in *nvj1*Δ::*HIS3* and *nvj1*Δ::*NatNT2* cells.

Different deletion strains expressing Nab-NLS-mCherry were starved in SD(-N) medium. Samples were taken at 0 h, 2 h, 4 h, 6 h and 24 h, were alkaline lysed and immunoblotted. Degradation of Nab-NLS-mCherry results in free mCherry in the vacuole, therefore mCherry signals were detected using an anti-RFP antibody.

4.1.6 Degradation of GFP-Osh1 and Nop1-GFP isn't blocked in different *nvj1*Δ deletion strains

Not being able to explain the different phenotypes between *nvj1*Δ::*HIS3* and *nvj1*Δ::*NatNT2* cells in regard of the breakdown of GFP-Osh1 (Chapter 4.1.1) or Nop1-GFP (Chapter 4.1.2) and the intactness of the NVJs (Chapter 4.1.4), new *NVJ1* knockout strains using *NatNT2* or *HIS3* as a knockout marker were

generated. Cells expressing either GFP-Osh1 from a plasmid under a *TEF1* promotor or Nop1-GFP from a plasmid under a *MET25* promotor were grown to late stationary phase overnight in CM medium or CM medium containing 0,3 mM methionine, and were starved in SD(-N) medium. Samples were taken after 0 h and 24 h starvation. Following, the cells were alkaline lysed and free GFP was detected on western blots using an anti-GFP antibody. Surprisingly, all newly generated knockouts weren't blocked in the degradation of GFP-Osh1 or Nop1-GFP, respectively (Figure 4.5). Meaning, that the already existing *nvj1*Δ::*HIS3* is wrong, even though it showed the expected degradation defects of GFP-Osh1.

Therefore, for all following experiments, the correct *nvj1*Δ::*NatNT2* strain was used.

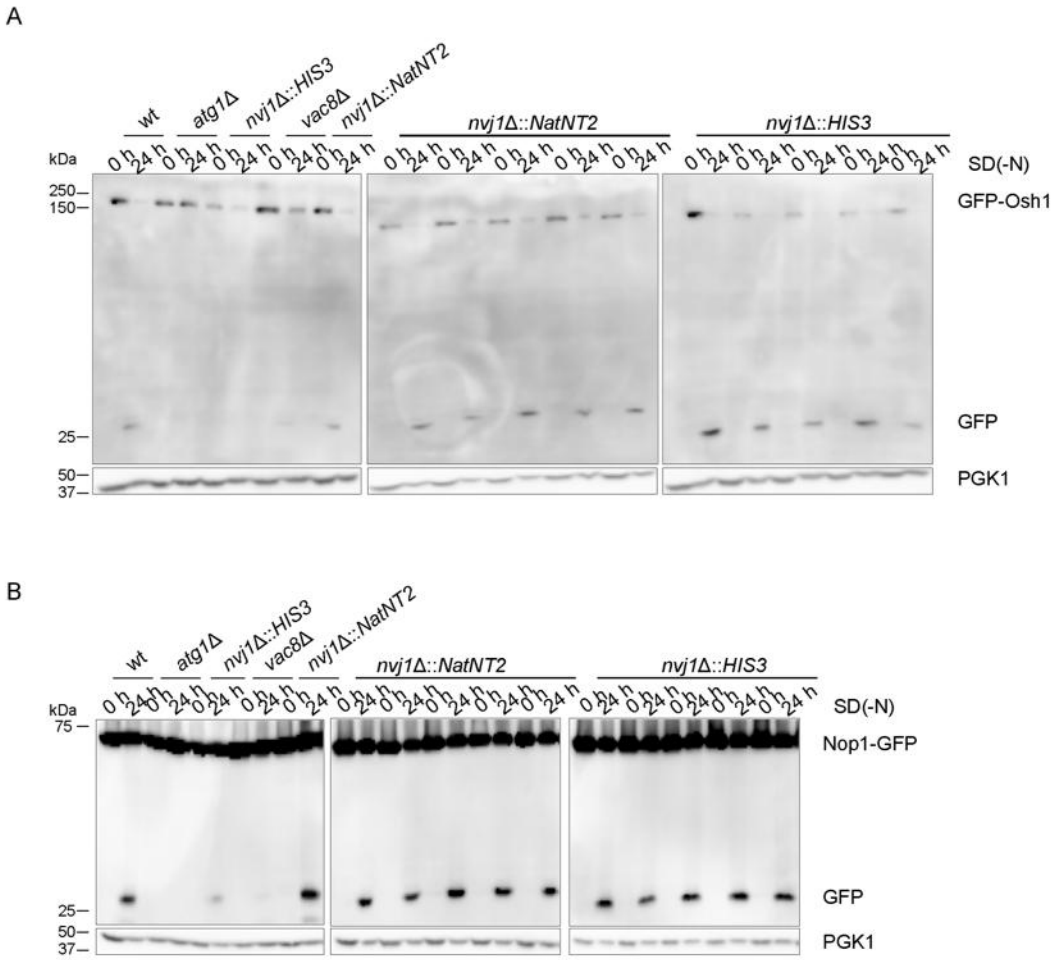

Figure 4.5: Further newly generated *NVJ1* knockouts were tested in regard of their ability to degrade GFP-Osh1 or Nop1-GFP.

New *nvj1*Δ::*HIS3* or *nvj1*Δ::*NatNT2* knockout strains expressing GFP-Osh1 or Nop1-GFP were starved for 0 h and 24 h in SD(-N) medium. The samples were alkaline lysed and immunoblotted. Free GFP was visualized using anti-GFP

antibody. PGK1, used as a loading control, was detected by an anti-PGK1 antibody.

4.2 Screen for potential novel components of the nucleus-vacuole junction

In contrast to the current view, Nvj1 seems not to be essential for the degradation of GFP-Osh1 or Nop1-GFP (Chapter 4.1.1 and 4.1.2). But since the *nvj1*Δ::*HIS3* knockout was proven to be wrong, the question came up, what gene was further affected in this strain and caused the observed phenotypes. Therefore, this study focused among other things on the question, which further proteins might play an essential role in PMN in addition to what was already known. Different proteins were tested for their potential involvement in PMN: Nvj2 (Chapter 4.2.1), Scs2 (Chapter 4.2.2), as well as Glc8 and Ymr310c (Chapter 4.2.3)

4.2.1 Nvj2 as an additional essential component of the nucleus-vacuole junction

An additional essential component for PMN was thought to be Nvj2. Nvj2 is enriched at the NVJ and is a lipid-binding ER protein (Toulmay and Prinz, 2012). Therefore, it was thought to play a role in PMN, possibly in combination with Nvj1.

4.2.1.1 Nvj2 is not essential for degradation of GFP-Osh1 or Nop1-GFP

To answer the question, if Nvj2 might play a role in PMN, the respective knockouts were tested in regard of the degradation rate of GFP-Osh1. The cells expressing GFP-Osh1 from a plasmid under a *TEF1* promotor, were grown to late stationary phase and starved in SD(-N) medium. Samples were taken after 0 h, 2 h, 4 h, 6 h and 24 h starvation, were alkaline lysed and free GFP was detected on western blots using anti-GFP antibody.

Degradation of GFP-Osh1 wasn't blocked in *nvj2*Δ (124,8% ± 31,9%) or *nvj1*Δ *nvj2*Δ cells (151,5% ± 53,98%) (Figure 4.6 A, B).

To further analyse the respective *NVJ2* deletion strains, cells expressing Nop1-GFP from a plasmid under a *MET25* promotor were grown to late stationary phase in CM medium containing 0,3 mM methionine. Samples were prepared as described above. Also, degradation of Nop1-GFP wasn't blocked in *nvj2*Δ or

*nvj1*Δ *nvj2*Δ cells (Figure 4.6 C). Quantification of the experiment showed significantly increased levels of free GFP in *nvj2*Δ (248,8% ± 28,48%) and *nvj1*Δ (167% ± 8,89%) when compared to wild type (Figure 4.6 D). The amount of free GFP was wild type like in *nvj1*Δ *nvj2*Δ (189,8% ± 43,82%).

These results indicated, that Nvj2 wasn't necessary for the degradation of GFP-Osh1 or Nop1-GFP and therefore wasn't essential for PMN. Despite these results, the diverse *nvj2*Δ cells were evaluated microscopically (Chapter 4.2.1.2).

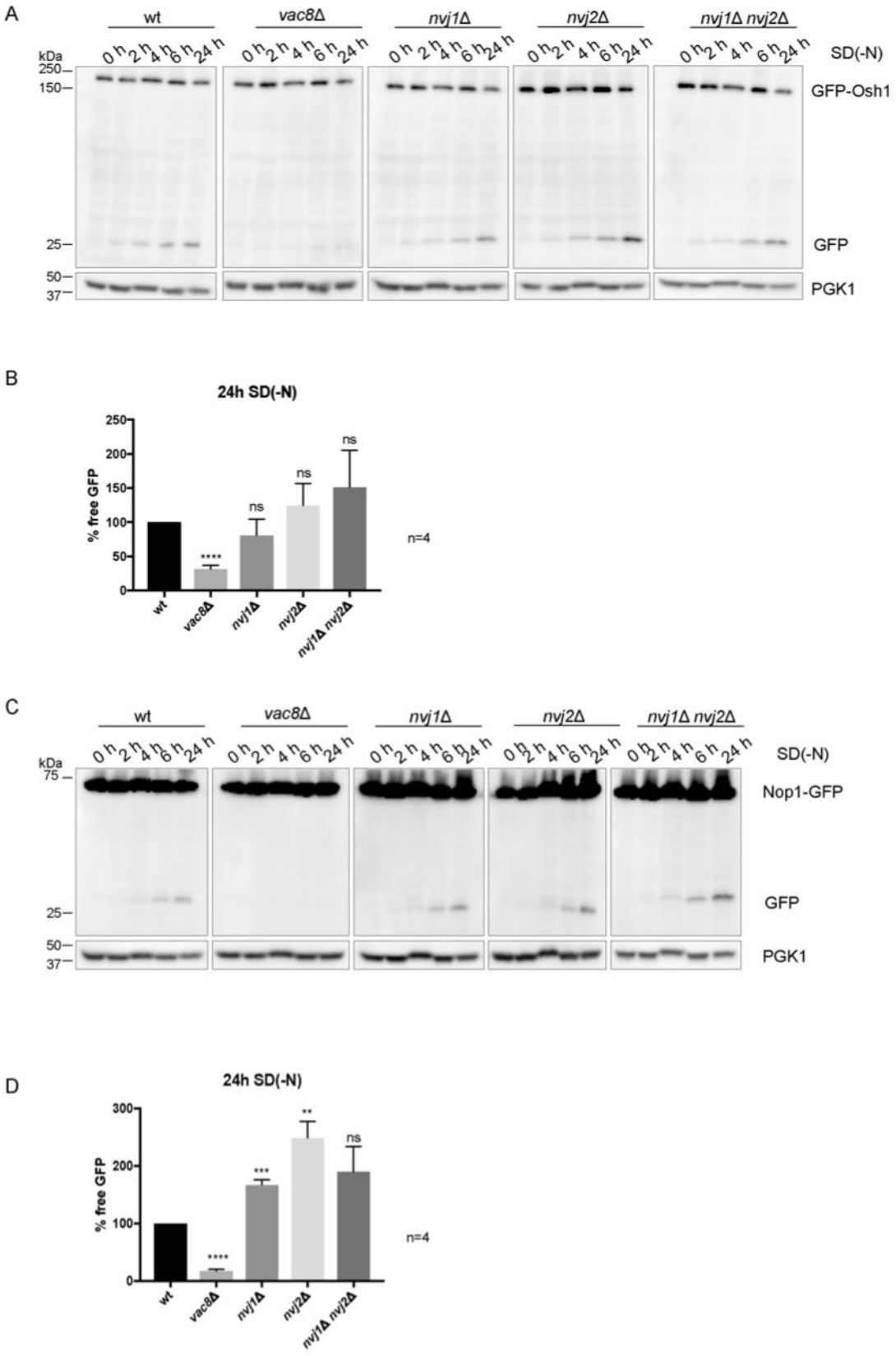

Figure 4.6: Degradation of GFP-Osh1 and Nop1-GFP isn't blocked in *NVJ2* knockouts.

(A) Different deletion strains expressing GFP-Osh1 were starved in SD(-N) medium. Samples were taken at 0 h, 2 h, 4 h, 6 h and 24 h, were alkaline

lysed and immunoblotted. Free GFP was detected using an anti-GFP antibody. Pgk1 was used as a loading control and was stained with anti-Pgk1 antibody.
(B) Quantification of four independent experiments showed that degradation of GFP-Osh1 wasn't blocked in *nvj2*Δ and *nvj1*Δ *nvj2*Δ. Statistics were performed using the one sample t-test. Error bars represent SEM and asterisks represent p-values
(C) Nop1-GFP degradation was measured as described in (A).
(D) Degradation of Nop1-GFP was wild type like in the *nvj1*Δ *nvj2*Δ deletion strain. Significantly increased free GFP levels were measured in *nvj1*Δ and *nvj2*Δ deletion strains. Statistics were performed as described in (B).

4.2.1.2 Nucleus-vacuole junctions are intact in Nvj2 deletion strains

Even though degradation of GFP-Osh1 and Nop1-GFP wasn't affected in *NVJ2* deletion strains, the NVJs were analysed using the Delta Vision microscope. Cells expressing GFP-Osh1 and mRFP-Nop1 from plasmids were grown to stationary phase and starved for 2 h in SD(-N) medium.

The *nvj2*Δ cells showed intact NVJs, comparable to those seen in the wild type strain (Figure 4.7), what also was seen by others (Toulmay and Prinz, 2012). However, the *nvj1*Δ *nvj2*Δ strain showed disrupted NVJs. This was expected, since knockout of *NVJ1* leads to the disruption of the NVJs (Pan *et al.*, 2000a).

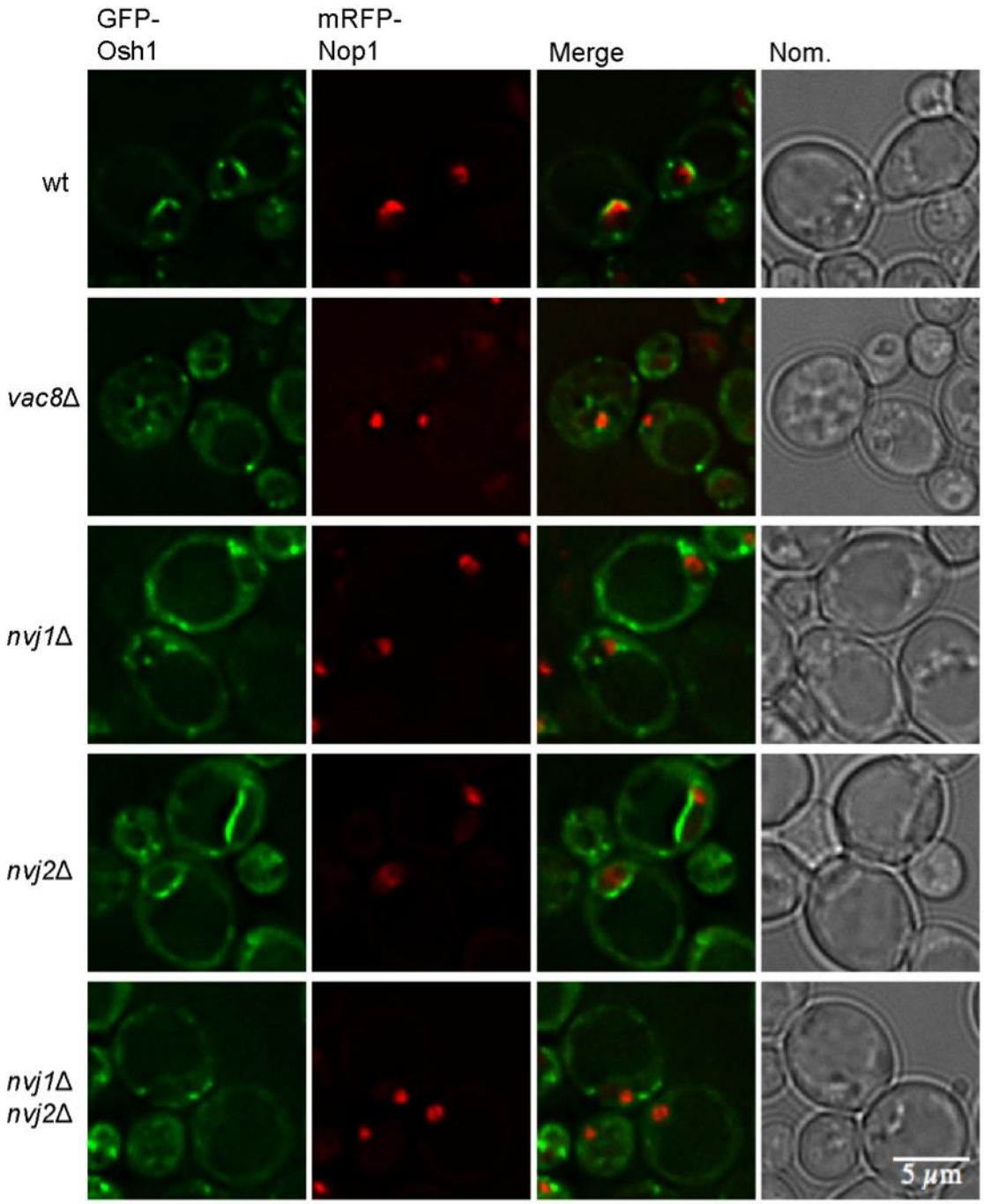

Figure 4.7: Evaluation of nucleus-vacuole junctions in *nvj2*Δ strains

In the indicated strains the intactness of the NVJ was visualized using GFP-Osh1 and mRFP-Nop1 as marker proteins. Cells were grown to stationary phase and starved for 2 h in SD(-N) medium. Finally, the cells were analysed using the Delta Vision microscope.

4.2.2 Scs2 as an additional essential component of the nucleus-vacuole junction

Scs2 is an integral ER anchor protein (Kagiwada *et al.*, 1998) and interacts with Osh1 at the NVJ (Loewen *et al.*, 2003). Based on this interaction, Scs2 was thought to be a possible essential component of the NVJs.

4.2.2.1 Scs2 isn't essential for degradation of GFP-Osh1 or Nop1-GFP

In order to test, if Scs2 was essential for PMN, different deletion strains expressing GFP-Osh1 from a plasmid under a *TEF1* promotor were grown to late stationary phase. The yeast strains were then starved in SD(-N) medium for 0 h, 2 h, 4 h, 6 h and 24 h. Samples were taken at the respective time points, were alkaline lysed and free GFP was detected on western blots using an anti-GFP antibody.

Degradation of GFP-Osh1 was significantly increased in *scs2*Δ cells in comparison to the wild type (173,8% ± 21,8%) (Figure 4.8 A, B). The double knockout of *NVJ1* and *SCS2* showed wild type like behaviour (145,5% ± 22,7%).

For further analysis, degradation of Nop1-GFP was also measured in the respective deletion strains. Cells expressing Nop1-GFP from a plasmid under a *MET25* promotor were grown in medium containing 0,3 mM methionine to late stationary phase. Samples were taken as outlined above. Degradation of Nop1-GFP was wild type like in *scs2*Δ cells (57,5% ± 22,33%), as well as in the double knockout cells *nvj1*Δ *scs2*Δ (127% ± 27,36%) (Figure 4.8 C, D).

Taken together, these results show that Scs2 is not essential for the degradation of GFP-Osh1 or Nop1-GFP. Anyhow, the *SCS2* deletion strains were analysed in respect to the intactness of the NVJs (Chapter 4.2.2.2).

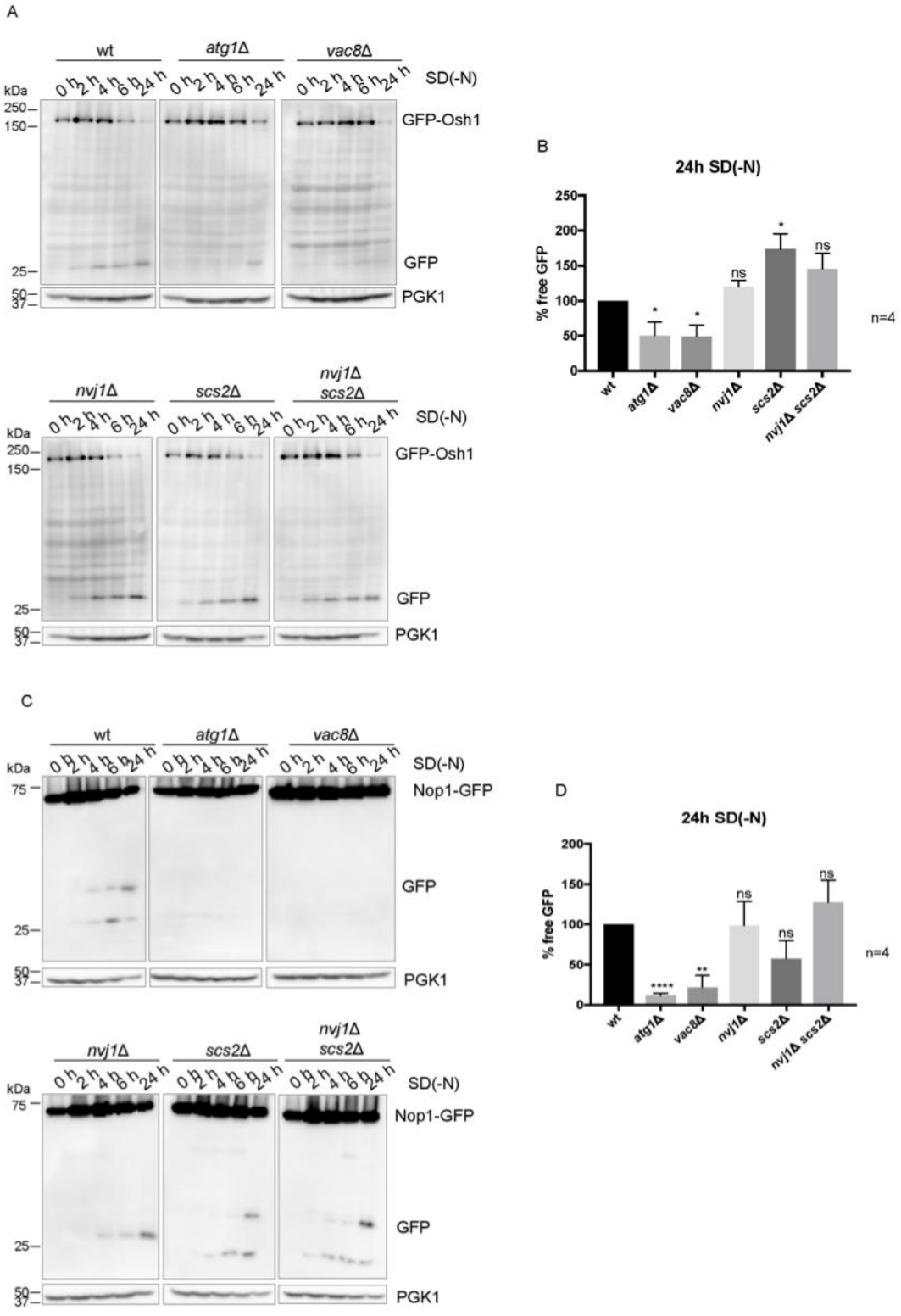

Figure 4.8: PMN isn't blocked in *scs2*Δ strains

(A) The indicated deletion strains expressing GFP-Osh1 were starved in SD(-N) medium. Samples were taken at 0 h, 2 h, 4 h, 6 h and 24 h, were alkaline lysed and immunoblotted. Free GFP was detected using an anti-GFP antibody. Pgk1 was used as a loading control and was stained with anti Pgk1-antibody.

(B) Quantification of four independent experiments showed, that degradation of GFP-Osh1 was slightly increased in *scs2*Δ cells and was wild type like in *nvj1*Δ *scs2*Δ cells. Statistics were performed using the one sample t-test. Error bars represent SEM and asterisks represent p-values
(C) Nop1-GFP degradation was measured as described in (A).
(D) Degradation of Nop1-GFP was wild type like in *scs2*Δ and *nvj1*Δ *scs2*Δ cells. Statistics were performed as described in (B).

4.2.2.2 Scs2 is necessary for the intactness of the nucleus-vacuole junction

The NVJs in *scs2*Δ and *nvj1*Δ *scs2*Δ cells were analysed using the Delta Vision microscope. The NVJ was visualized with GFP-Osh1 as a marker, additionally the nucleolus marker Nop1-RFP was expressed in the respective deletion strains. The cells were grown to late stationary phase and then starved for 2 h in SD(-N) medium.

Like the negative controls *vac8*Δ and *nvj1*Δ cells, also *scs2*Δ cells showed disrupted NVJs (Figure 4.9). Accordingly, also *nvj1*Δ *scs2*Δ cells had no intact NVJs. This was expected, as knockout of *NVJ1* disrupts NVJs (Pan *et al.*, 2000a). These results indicate, that Scs2 is necessary for the intactness of the NVJs. This further shows, that the NVJs don't necessarily have to be intact for wild type like degradation of GFP-Osh1 or Nop1-GFP (Chapter 4.2.2.1). However, it can't be ruled out, that the usage Nvj1-GFP as a marker for the NVJ, might lead to a different result, as Nvj1 does not directly interact with Scs2.

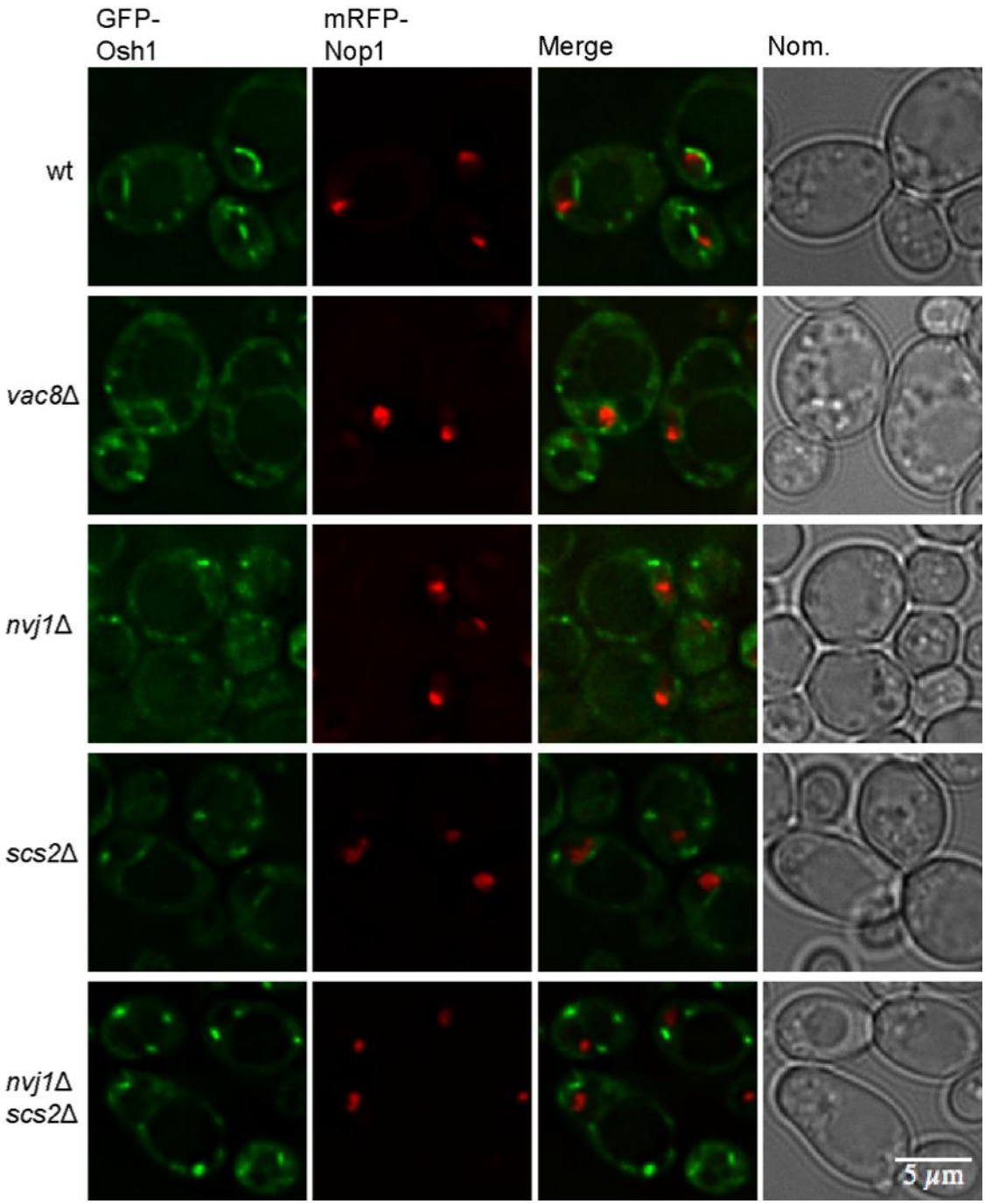

Figure 4.9: Microscopic evaluation of *scs2Δ* cells

GFP-Osh1 and mRFP-Nop1 were expressed in the indicated yeast strains. Cells were grown to late stationary phase, starved for 2 h in SD(-N) medium and evaluated via fluorescence microscopy.

4.2.3 Glc8 as an additional essential component of the nucleus-vacuole junction

As previously shown (Chapter 4.1.6), the *nvj1*Δ::*HIS3* knockout strain might contain further mutations. PCR analysis showed, that this strain contained the *HIS3* knockout cassette, but also the whole *NVJ1* gene (data not shown). Sequencing of the PCR product of the *NVJ1* gene showed no mutations (data not shown). Therefore, it was assumed, that the knockout cassette might have integrated additionally at another wrong site. Nevertheless, this strain showed an interesting phenotype for the understanding of PMN, since the degradation of the two marker proteins GFP-Osh1 and Nop1-GFP was blocked. To identify which gene might have been affected by chance, a PCR approach was used. Using primers that bound in the *HIS3*-cassette and random primers, a PCR product was received and cloned into the pJET vector. Sequencing of the vector led to two possible gene regions, where the knockout cassette might have been integrated: *GLC8* and *YMR310C*. Thus, these two genes were tested in regard of their involvement in PMN.

4.2.3.1 Degradation of GFP-Osh1 and Nop1-GFP isn't blocked in *glc8*Δ or *ymr310c*Δ strains

To verify, that the *HIS3* knockout cassette was integrated at regions that encode either Glc8 or YMR310C, different deletion strains expressing GFP-Osh1 from a plasmid under a *TEF1* promotor were grown to late stationary phase and were starved in SD(-N) medium. Samples were collected after 0 h, 2 h, 4 h, 6 h and 24 h starvation and were alkaline lysed. Free GFP was detected on western blots using anti-GFP antibody.

Degradation of GFP-Osh1 wasn't blocked in either *glc8*Δ or *ymr310c*Δ cells (Figure 4.10 A). Quantification of the experiment showed wild type like amounts of free GFP in *glc8*Δ cells (97,75% ± 11,01%) and a slight reduction in *YMR310C*Δ cells (70,25% ± 7,76%) (Figure 4.10 B).

In addition, the respective deletion strains expressing Nop1-GFP from a plasmid under a *MET25* promotor were grown to late stationary phase in CM medium containing 0,3 mM methionine. Samples were collected as described above. The *glc8*Δ cells as well as the *ymr310c*Δ cells weren't blocked in degradation of Nop1-GFP (Figure 4.10 C). Quantification showed wild type like

degradation of Nop1-GFP in *glc8*Δ (115% ± 21,08%) and *ymr310c*Δ cells (102% ± 20,36%) (Figure 4.10 D).

Measurement of the degradation of GFP-Osh1 and Nop1-GFP showed that the degradation of these two marker proteins wasn't blocked as it was the case for the "wrong" *nvj1*Δ::*HIS3* deletion strain. This indicates, that the obtained PCR product might have been a result of unspecific binding of the two primers and that the so obtained genes weren't involved in PMN. Nevertheless, both deletion strains were examined using the Delta Vision microscope (Chapter 4.2.3.2).

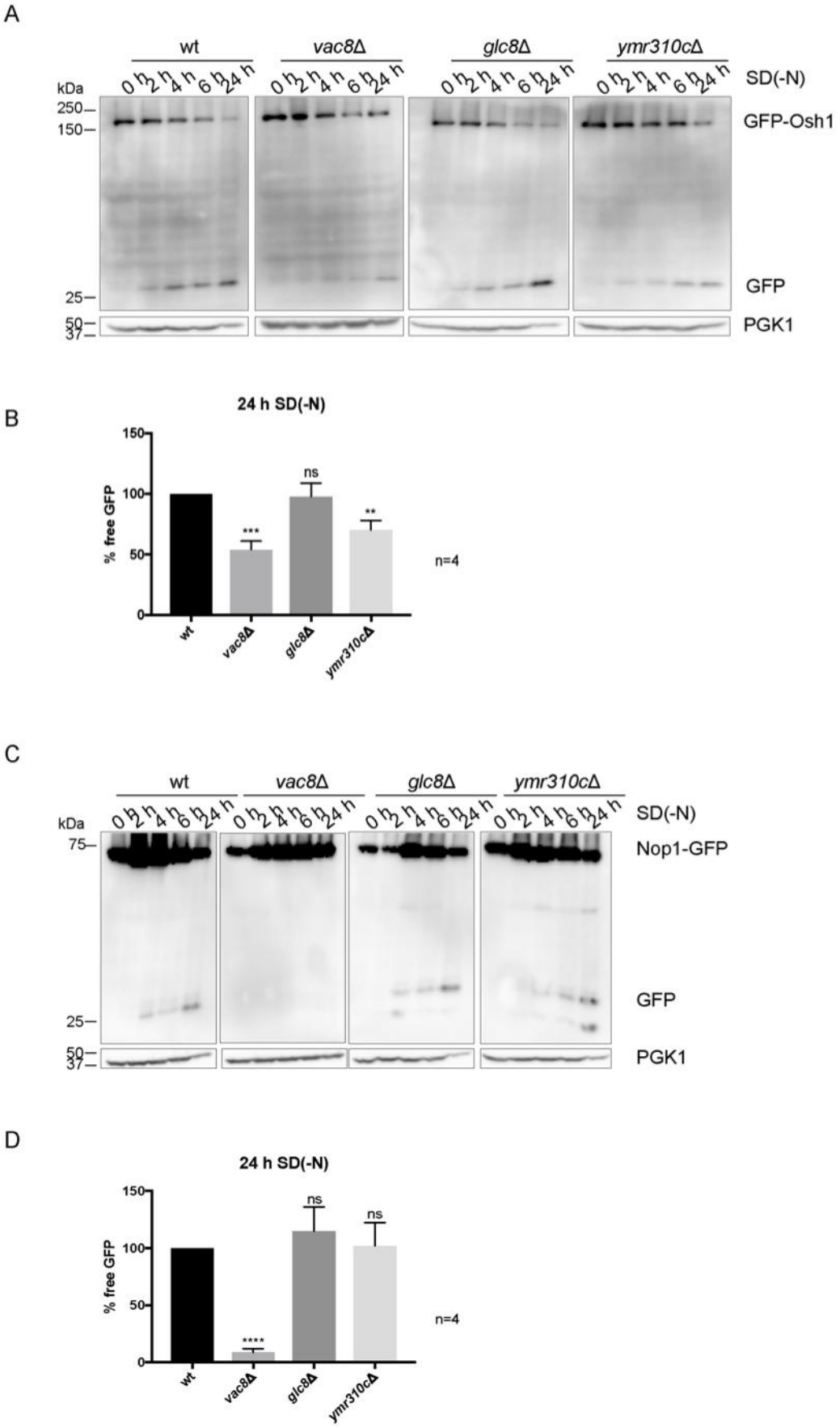

Figure 4.10: Degradation of GFP-Osh1 and Nop1-GFP in *glc8*Δ or *ymr310c*Δ cells.

(A) The indicated deletion strains expressing GFP-Osh1 were starved in SD(-N) medium. Samples were taken at 0 h, 2 h, 4 h, 6 h and 24 h, were alkaline lysed and immunoblotted. Free GFP was detected using an anti-GFP antibody. Pgk1 was used as a loading control and was stained with anti-Pgk1 antibody.
(B) Quantification of four independent experiments showed, that degradation of GFP-Osh1 was wild type like in *glc8*Δ cells and was slightly reduced in *ymr310c*Δ cells. Statistics were performed using the one sample t-test. Error bars represent SEM and asterisks represent p-values.
(C) Nop1-GFP degradation was measured as described in (A).
(D) Degradation of Nop1-GFP was wild type like in *glc8*Δ and *ymr310c*Δ cells. Statistics were performed as described in (B).

4.2.3.2 The nucleus-vacuole junction is intact in *GLC8* or *YMR310C* deletion strains

For further evaluation, the NVJs in *GLC8* and *YMR310C* deletion strains were analysed using GFP-Osh1 and mRFP-Nop1 as marker proteins. Cells expressing the respective marker proteins from plasmids were grown to stationary phase and starved for 2 h in SD(-N) medium. The yeast strains were evaluated using the Delta Vision microscope. Both deletion strains of interest, *GLC8* and*YMR310C*, showed intact NVJs (Figure 4.11).

If either *GLC8* or *YMR310C* would have been the gene knocked out accidentally in the “wrong” *nvj1*Δ::*HIS3* knockout strain, intact NVJs would have been expected, as it was the case in this strain of interest. But measurement of the degradation of GFP-Osh1 and Nop1-GFP (Chapter 4.2.3.1) have already shown, that neither *GLC8* nor *YMR310C* had been knocked out by chance.

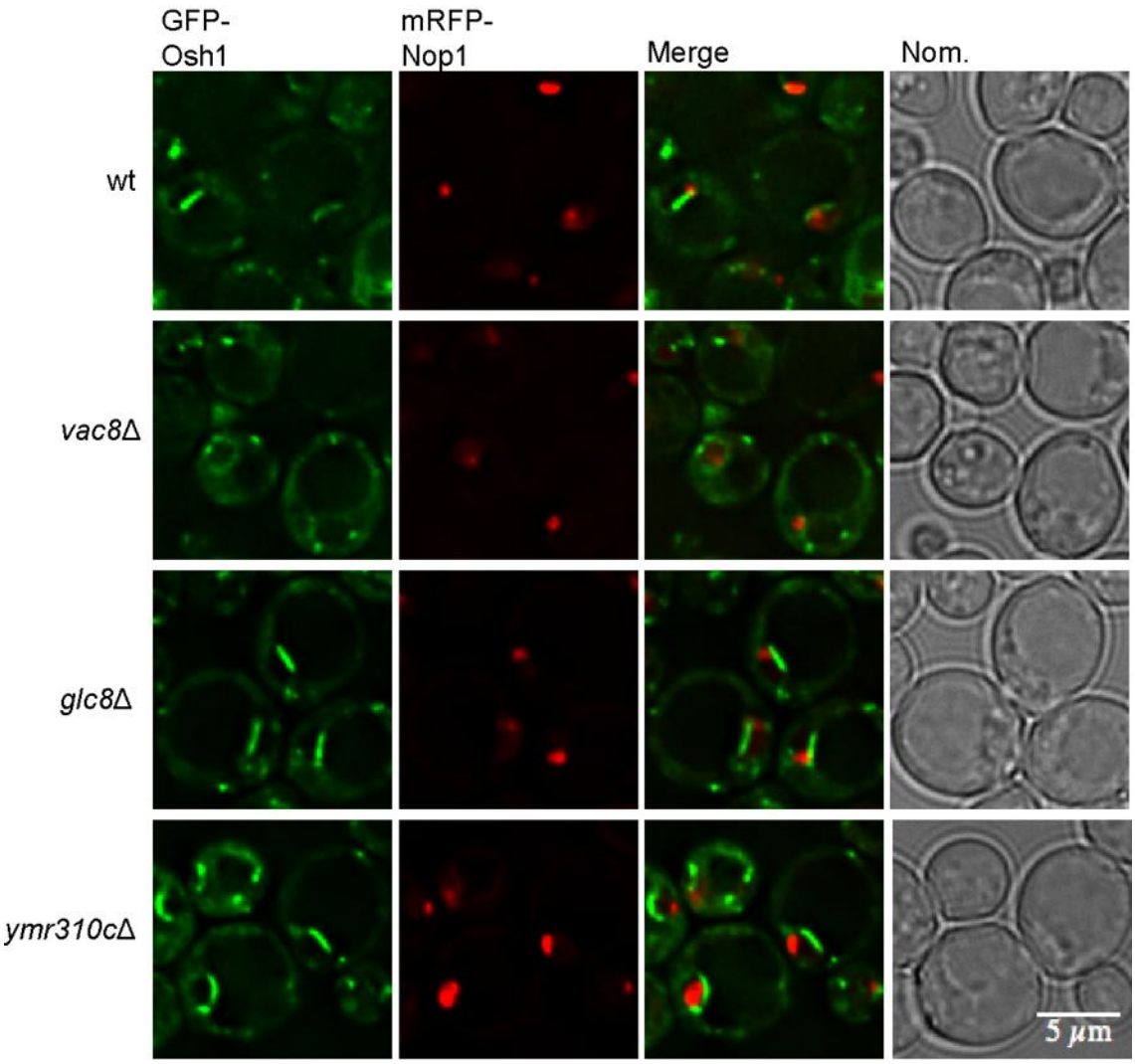

Figure 4.11: Evaluation of nucleus-vacuole junctions in *GLC8* and *YMR310C* deletion strains.

The indicated yeast strains expressing GFP-Osh1 and mRFP-Nop1 as marker proteins were grown to stationary phase and starved for 2 h in SD(-N) medium. The NVJ was analysed using fluorescence microscopy.

4.3 Osh1 is not exclusively degraded via PMN

It was shown, that mutation of either A159Q or A159V in the binding pocket of Osh1 ANK impedes its interaction with Nvj1 (Manik *et al.*, 2017). The targeting of Osh1 to the NVJs is dependent on the ANK domain of Osh1 (Levine and Munro, 2001). Since GFP-Osh1 was reported to be a suitable marker for the measurement of PMN (Krick *et al.*, 2008), it was of great interest, if the mutated version of this marker protein, GFP-Osh1_A159V, was degraded differently than the non-mutated version.

4.3.1 Mutation of Osh1 impedes interaction with Nvj1

It was reported, that mutation of Osh1 to Osh1_A159V prevents interaction with Nvj1 (Manik *et al.*, 2017). First of all, the lack of interaction between Osh1_A159V and Nvj1 was confirmed *in vivo* using the GFP-Trap approach. GFP-Osh1_A159V was expressed from a plasmid under a *TEF1* promotor in cells with chromosomally HA-tagged *NVJ1*. GFP-Osh1 and GFP were used as controls. The cells were grown to late stationary phase before cell lysis and protein co-precipitation. The proteins were detected in western blot analysis using anti-GFP and anti-HA antibodies.

The interaction between GFP-Osh1_A159V and Nvj1-6xHA was very week when compared to the interaction of GFP-Osh1 and Nvj1-6xHA (Figure 4.12 A). Nvj1-6xHA didn't bind to GFP alone. This confirmed, that the described mutation of Osh1 prevents its interaction with Nvj1 and that this mutant could be used to examine localization as well as degradation of Osh1_A159V.

4.3.2 GFP-Osh1_A159V is not localized to nucleus-vacuole junctions

To see the impact of the mutation A159V in GFP-Osh1 in regard to its localization, GFP-Osh1_A159V was analysed using the Delta Vision microscope. GFP-Osh1_A159V and the respective controls GFP-Osh1 and GFP together with the nucleolar marker mRFP-Nop1 were expressed from plasmids in *osh1*Δ cells. The cells were grown to stationary phase, were starved for 2 h in SD(-N) medium and then analysed via fluorescence microscopy (Figure 4.12 B).

GFP-Osh1 was exclusively localized to the NVJs next to mRFP-Nop1. In contrast to that, GFP-Osh1_A159V wasn't localized to the NVJs, but appeared

in patches all over the cells. Therefore, the NVJ weren't visible in cells expressing the mutated Osh1. This can be explained by the fact, that the GFP-Osh1_A159V mutant wasn't localizing to the NVJ since its Nvj1-binding site wasn't functional.

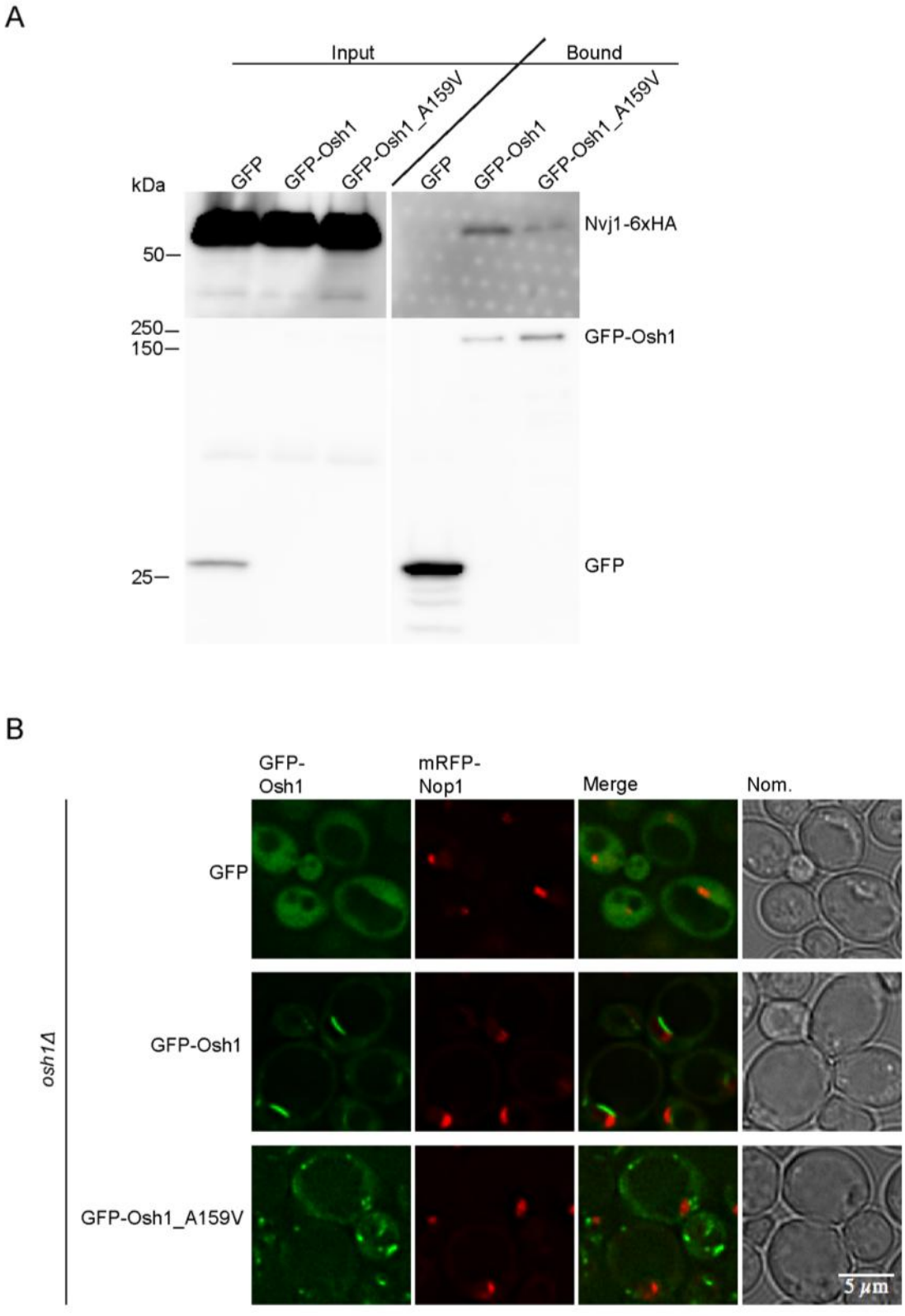

Figure 4.12: Binding of Osh1 and Nvj1 is reduced after mutating the binding site of Osh1

(A) Osh1-Nvj1 interaction was analysed using the GFP-Trap method. *NVJ1* was chromosomally tagged with HA (cNVJ1-6xHA). GFP-Osh1 or GFP-Osh1_A159V were expressed from a plasmid under a *TEF1* promotor. Cells were grown to late stationary phase, lysed and immunoblotted. GFP was detected using an anti-GFP antibody, HA was detected with an anti-HA antibody.
(B) Localization of GFP-Osh1_A159V was analysed in *osh1*Δ cells and compared to GFP-Osh1 and GFP. The cells were grown to stationary phase, starved in SD(-N) medium for 2 h and then analysed using the Delta Vision microscope.

4.3.3 GFP-Osh1_A159V is degraded in equal amounts as GFP-Osh1

The mutated construct GFP-Osh1_A159V and Nvj1 were demonstrated not to interact (Chapter 4.3.1). Additionally, GFP-Osh1_A159V was shown not to be localized to the NVJs (Chapter 4.3.2). Within this study, the degradation of GFP-Osh1_A159V was measured in comparison to the degradation of GFP-Osh1. Therefore, the breakdown of GFP-Osh1_A159V was measured in different knockout strains and was compared to the breakdown of GFP-Osh1 in wild type cells. For this reason, the amount of free GFP after 24 h starvation in SD(-N) medium in the wild type strain expressing GFP-Osh1 was set to 100%.

Compared to wild type cells expressing GFP-Osh1, GFP-Osh1_A159V was degraded to the same amount in wild type cells, namely 94,25 % ± 14,94%. The degradation of GFP-Osh1_A159V was blocked in *atg1*Δ and *vac8*Δ cells (*atg1*Δ: 15,25% ± 6,3%; *vac8*Δ: 22,75% ± 10,78%) and slightly reduced in *nvj1*Δ cells (66,75% ± 11,06%). But it was not significantly reduced in *atg39*Δ, *atg40*Δ and *atg39*Δ *atg40*Δ cells (*atg39*Δ: 114% ± 18.04%; *atg40*Δ: 131,3% ± 72,47%; *atg39*Δ *atg40*Δ: 62% ± 18,55%) (Figure 4.13 A, B). Direct comparison of GFP-Osh1 and GFP-Osh1_A159V degradation in the respective knockout strains, showed no differences between these two marker proteins (Figure 4.13 C). These results were surprising, as a reduced degradation of GFP-Osh1_A159V in comparison to GFP-Osh1 was expected. This outcome could be explained by the assumption, that Osh1 isn't exclusively degraded via PMN, but dependent on Atg1 and Vac8. This in turn would lead to the conclusion, that GFP-Osh1 is no bona fide marker for the measurement of PMN. Probably, Nop1-GFP or Nvj1-GFP are more suitable marker proteins for measurement of PMN.

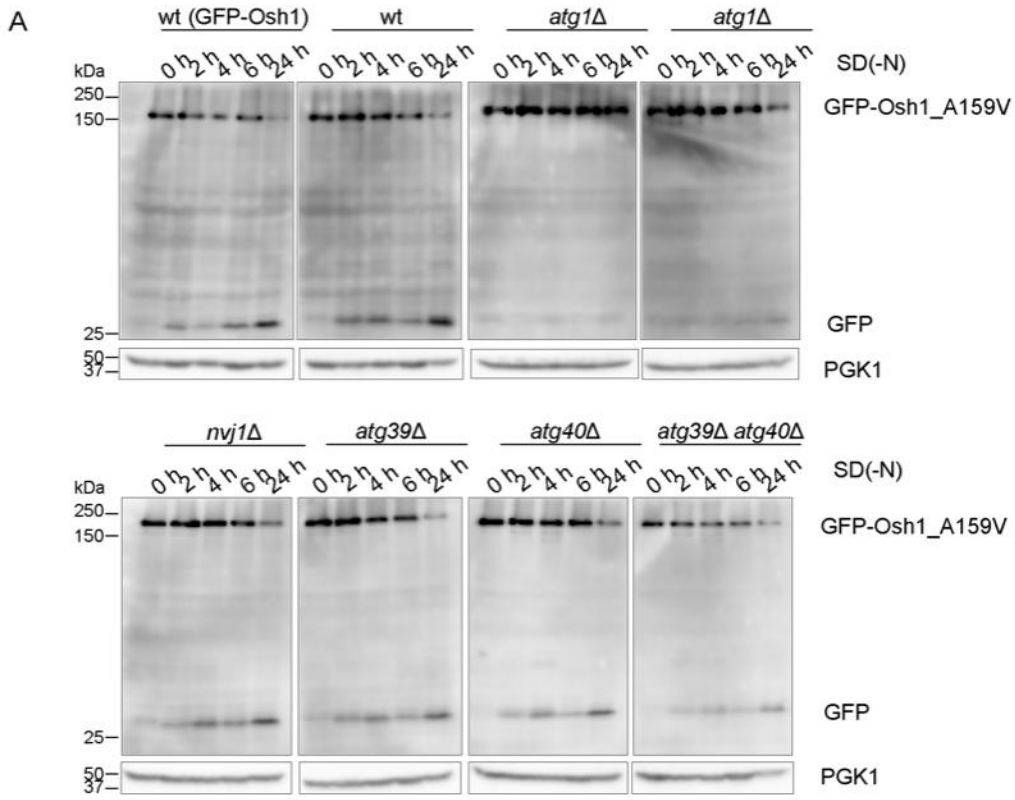
A
wt (GFP-Osh1)
wt
atg1Δ
atg1Δ
kDa
0 h 2 h 4 h 6 h 24 h
SD(-N)
250
150
GFP-Osh1_A159V
25
GFP
50
37
PGK1
nvj1Δ
atg39Δ
atg40Δ
atg39Δ atg40Δ
kDa
0 h 2 h 4 h 6 h 24 h
SD(-N)
250
150
GFP-Osh1_A159V
25
GFP
50
37
PGK1

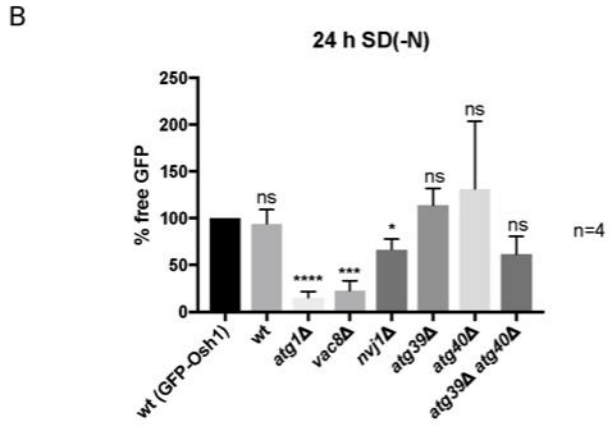
B
24 h SD(-N)
% free GFP
250
200
150
100
50
0
ns
ns
ns
ns
****
***
*
n=4
wt (GFP-Osh1)
wt
atg1Δ
vac8Δ
nvj1Δ
atg39Δ
atg40Δ
atg39Δ atg40Δ

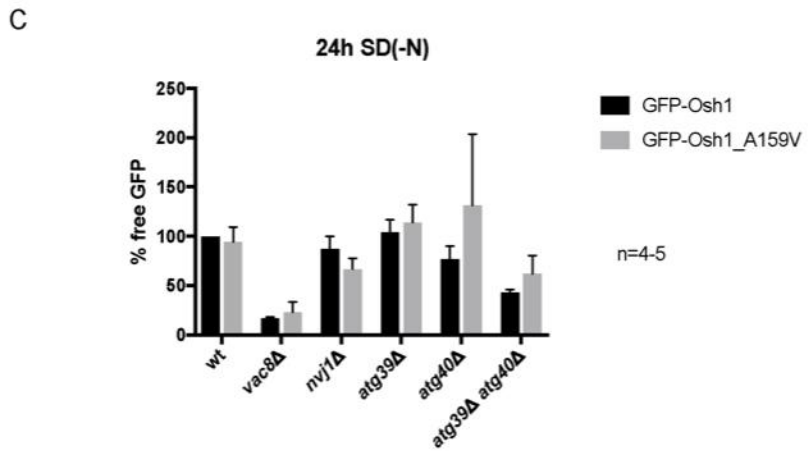
C
24h SD(-N)
% free GFP
250
200
150
100
50
0
GFP-Osh1
GFP-Osh1_A159V
n=4-5
wt
vac8Δ
nvj1Δ
atg39Δ
atg40Δ
atg39Δ atg40Δ

Figure 4.13: GFP-Osh1_A159V and GFP-Osh1 show no differences in regard to their degradation

(A) The indicated yeast strains expressing GFP-Osh1 or GFP-Osh1_A159V were starved in SD(-N) medium. Samples were taken at 0 h, 2 h, 4 h, 6 h and 24 h, were alkaline lysed and immunoblotted. Free GFP was detected using an anti-GFP antibody. Pgk1 was used as a loading control and was stained with an anti-Pgk1 antibody.
(B) Quantification of four independent experiments showed, that degradation of GFP-Osh1_A159 was wild type like in *atg39*Δ, *atg40*Δ and *atg39*Δ *atg40*Δ cells. The amount of free GFP was reduced in *atg1*Δ, *vac8*Δ and *nvj1*Δ cells. The amount of free GFP after 24 h starvation in SD(-N) medium in the wild type strain expressing GFP-Osh1 was set to 100%. Statistics were performed using the one sample t-test. Error bars represent SEM and asterisks represent p-values.
(C) Direct comparison of degradation of GFP-Osh1 and GFP-Osh1_A159V in different deletion strains showed no differences in regard of free GFP between both marker proteins.

4.4 Role of Atg39 and Atg40 in PMN

Recently, two new Atg-proteins were described: Atg39 and Atg40 (Mochida *et al.*, 2015). Atg39 was described to be localized to the perinuclear ER and to be involved in the degradation of parts of the nucleus and the perinuclear ER. Atg40 is localized to the cortical and cytoplasmic ER and is involved in loading of ER subdomains into autophagosomes (Mochida *et al.*, 2015). It was of great interest, to get to know how Atg39 and Atg40 are involved in PMN. Therefore, the degradation of different marker proteins was measured in the respective deletion strains.

4.4.1 Degradation of GFP-Osh1 suggests crosstalk between Atg39 and Atg40

In order to determine the role of Atg39 and Atg40 during PMN, degradation of GFP-Osh1 was measured, even though this marker protein might not be the ideal marker for the measurement of PMN (Chapter 4.3.3). Deletion strains expressing GFP-Osh1 from a plasmid under a *TEF1* promotor were grown to late stationary phase and then starved in SD(-N) medium. Samples were taken after 0 h, 2 h, 4 h, 6 h and 24 h starvation, were alkaline lysed and immunoblotted. The free GFP on the western blots was detected using an anti-GFP antibody.

The amount of free GFP was wild type like in *atg39*Δ and *atg40*Δ cells and reduced in *atg39*Δ *atg40*Δ cells (Figure 4.14 A). Quantification showed wild type like amounts of free GFP in *atg39*Δ (104% ± 12,65%) *atg40*Δ cells (77,06% ± 12,8%) and *nvj1*Δ cells (87,16% ± 12,7%) (Figure 4.14 B). Degradation of GFP-Osh1 was reduced in *atg39*Δ *atg40*Δ cells (43,22% ± 2,74%) and blocked in *vac8*Δ cells (16,76% ± 1,42%). A single knockout of either *ATG39* or *ATG40* didn't affect degradation of GFP-Osh1. However, knockout of both Atg-proteins resulted in a lower amount of free GFP, what indicated a crosstalk between these two proteins. However, these results have to be handled with care, since GFP-Osh1 was used as a marker protein, that was previously described as not ideally suitable for PMN measurement (Chapter 4.3.3).

Therefore, the role of Atg39 and Atg40 in nucleophagy was studied in more detail by using Nop1-GFP (Chapter 4.4.2) and Nvj1-GFP (Chapter 4.4.3) as additional nucleophagy marker proteins.

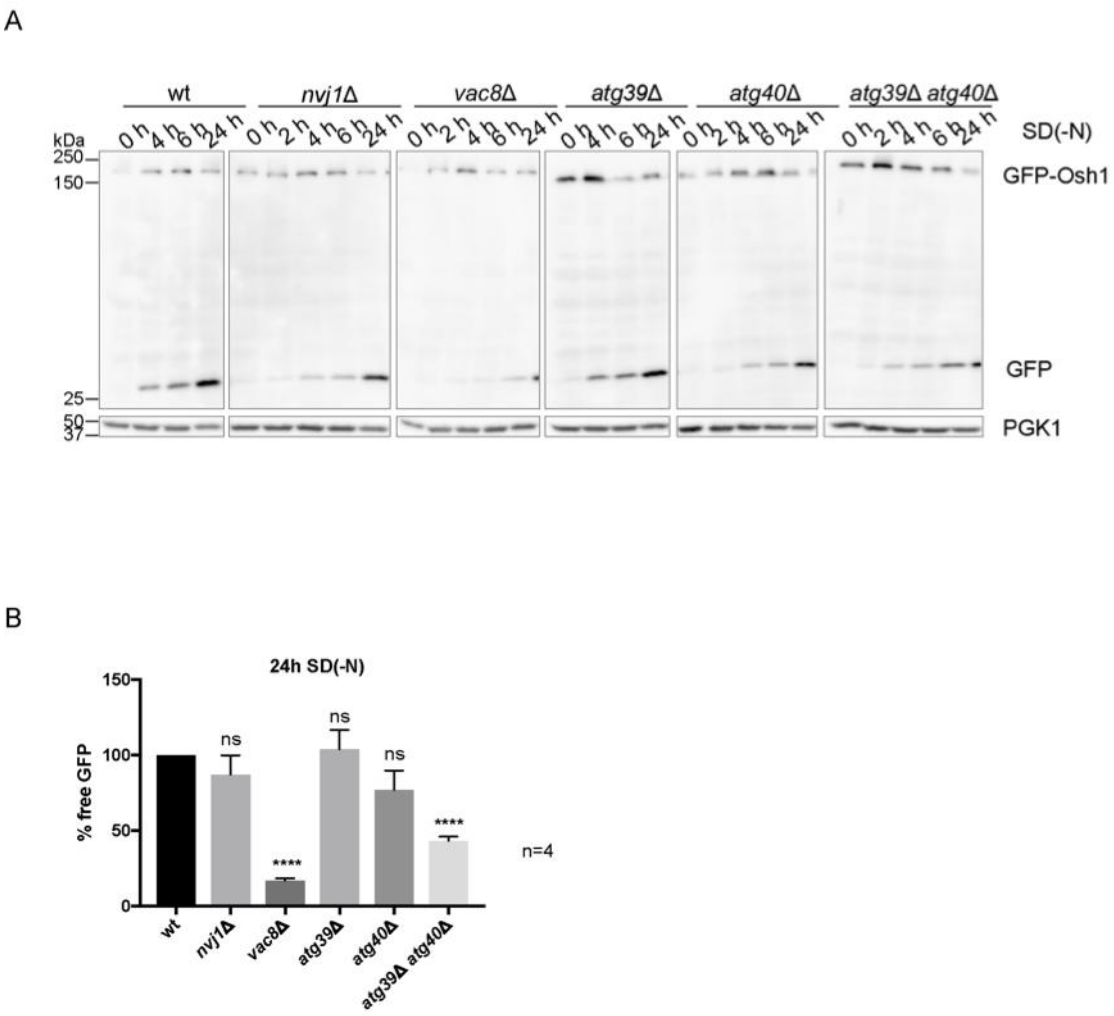

Figure 4.14: Degradation of GFP-Osh1 is reduced in *atg39*Δ *atg40*Δ cells

(A) The indicated deletion strains expressing GFP-Osh1 were starved in SD(-N) medium. Samples were taken at 0 h, 2 h, 4 h, 6 h and 24 h, were alkaline lysed and immunoblotted. Free GFP was detected using an anti-GFP antibody. Pgk1 was used as a loading control and was stained with anti-Pgk1 antibody.

(B) Quantification of four independent experiments showed that degradation of GFP-Osh1 was wild type like in *nvj1*Δ, *atg39*Δ and *atg40*Δ cells. The amount of free GFP was reduced in *vac8*Δ and *atg39*Δ *atg40*Δ cells. Statistics were performed using the one sample t-test. Error bars represent SEM and asterisks represent p-values.

4.4.2 Degradation of Nop1-GFP is dependent on Atg39 and Atg40

To further analyse the role of Atg39 and Atg40 in nucleophagy, the degradation of Nop1-GFP was measured. Previous results regarding these two Atg-proteins in this study were based on the breakdown of GFP-Osh1 (Chapter 4.3.3). Thus, different deletion strains expressing Nop1-GFP from a plasmid under a *MET25* promotor were grown to late stationary phase in CM-medium containing 0,3 mM methionine. The cells were starved in SD(-N) medium and samples were taken after 0 h, 2 h, 4 h, 6 h and 24 h starvation. The samples were alkaline lysed and immunoblotted. Free GFP on western blots was detected using an anti-GFP antibody.

In comparison to the wild type, the amount of free GFP was reduced in *nvj1*Δ and *atg40*Δ cells (Figure 4.15 A). However, no free GFP was visible in *vac8*Δ, *atg39*Δ and *atg39*Δ *atg40*Δ cells. This was confirmed by quantification of the western blots (Figure 4.15 B). Compared to the wild type, the *nvj1*Δ deletion strain was reduced to 56,36% ± 13,61% and the *atg40*Δ deletion strain to 30,48% ± 3,26%. All additionally tested deletion strains showed a complete block of Nop1-GFP degradation (*vac8*Δ: 3,12% ± 1,28%; *atg39*Δ: 9,02% ± 1,03%; *atg39*Δ *atg40*Δ: 4,1% ± 0,94%). This suggested that degradation of Nop1-GFP was dependent on primarily Atg39, but also on Atg40, as it was reported recently (Mochida *et al.*, 2015).

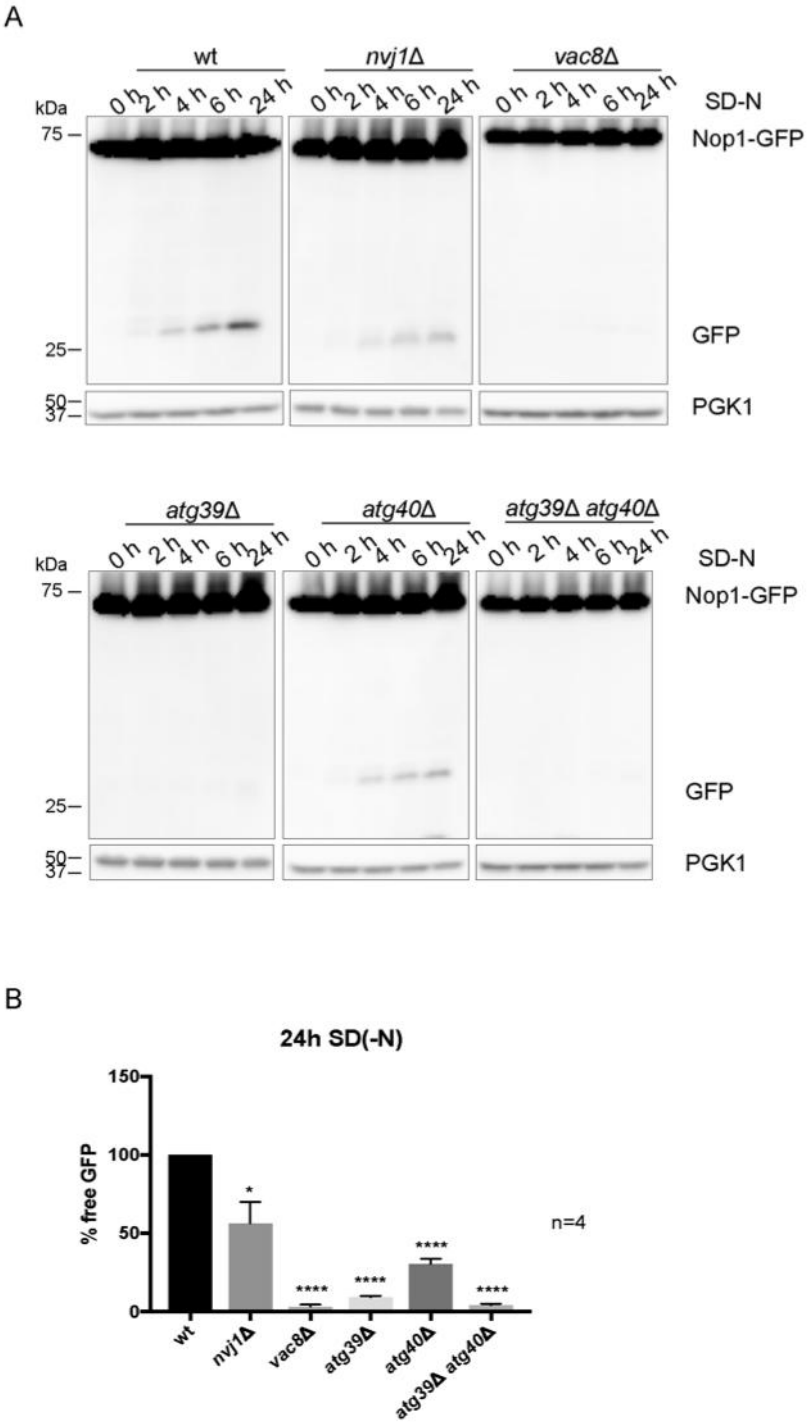

Figure 4.15: Degradation of Nop1-GFP is dependent on Atg39

(A) The indicated deletion strains expressing Nop1-GFP were starved in SD(-N) medium. Samples were taken at 0 h, 2 h, 4 h, 6 h and 24 h, were alkaline lysed and immunoblotted. Free GFP was detected using an anti-GFP antibody. Pgk1 was used as a loading control and was stained with an anti-Pgk1 antibody.

(B) Quantification of four independent experiments showed, that degradation of Nop1-GFP was reduced in *nvj1*Δ and *atg40*Δ cells and was blocked in *vac8*Δ, *atg39*Δ and *atg39*Δ *atg40*Δ cells. Statistics were performed using the one sample t-test. Error bars represent SEM and asterisks represent p-values.

4.4.3 Atg39 and Atg40 are necessary of degradation of Nvj1-GFP

As previously shown (Chapter 4.3), GFP-Osh1 is not the best choice for the measurement of PMN. Instead, Nvj1-GFP might be the more suitable marker protein, in order to determine the roles of Atg39 and Atg40 during PMN. Different deletion strains expressing Nvj1-GFP from a plasmid under a *MET25* promotor were grown to late stationary phase in CM-medium containing 0,3 mM methionine. Cells were starved in SD(-N) medium and samples were taken after 0 h, 2 h, 4 h, 6 h and 24 h starvation. The samples were alkaline lysed and immunoblotted. Free GFP was detected on western blots using anti-GFP antibody.

In comparison to the wild type and *nvj1*Δ cells, less free GFP was detectable in *atg40*Δ cells (Figure 4.16 A). No free GFP could be seen in *atg1*Δ, *vac8*Δ, *atg39*Δ and *atg39*Δ *atg40*Δ cells. Quantification of four independent experiments showed wild type like degradation of Nvj1-GFP in *nvj1*Δ cells (109% ± 38,78%) and therewith that deletion of *NVJ1* could be rescued using Nvj1-GFP from a plasmid under a *MET25* promotor. The degradation of Nvj1-GFP was reduced in *atg40*Δ cells (62,25% ± 15,01%) (Figure 4.16 B) and was blocked in all remaining deletion strains (*atg1*Δ: 15% ± 2,16%; *vac8*Δ: 28,5% ± 3,79%; *atg39*Δ: 21,5% ± 4,37%; *atg39*Δ *atg40*Δ:16,75% ± 3,75%). Therefore it can be concluded, that degradation of Nvj1-GFP is dependent of Atg39, but also on Atg40, as it was the case for Nop1-GFP (Chapter 4.4.2).

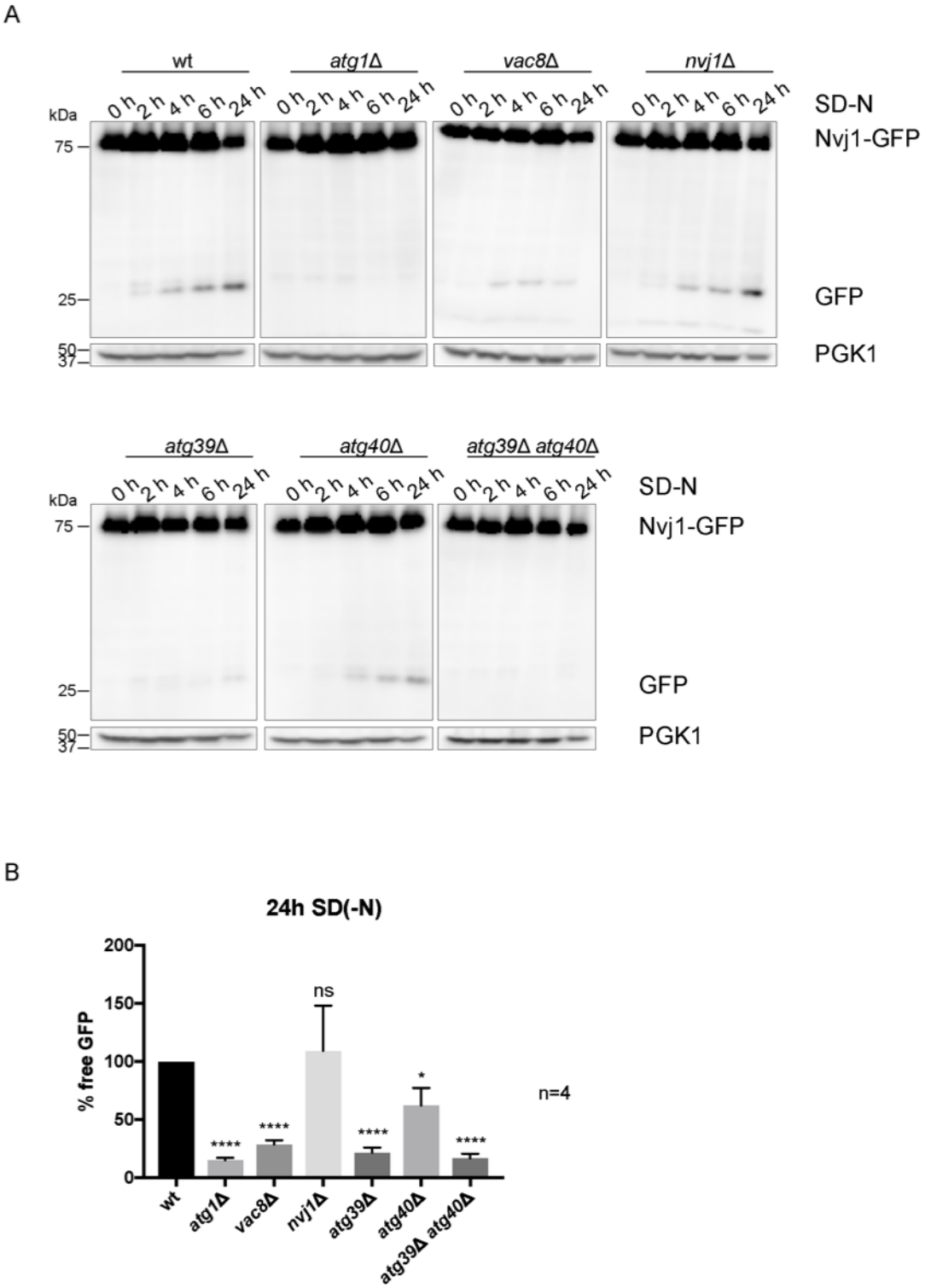

Figure 4.16: Degradation of Nvj1-GFP is dependent on Atg39 and Atg40.

(A) The indicated deletion strains expressing Nvj1-GFP were starved in SD(-N) medium. Samples were taken at 0 h, 2 h, 4 h, 6 h and 24 h, were alkaline lysed and immunoblotted. Free GFP was detected using an anti-GFP antibody. Pgk1 was used as a loading control and was stained with an anti-Pgk1 antibody.

(B) Quantification of four independent experiments showed, that degradation of Nvj1-GFP was reduced in *atg40*Δ cells and was blocked in *vac8*Δ,

*atg39*Δ and *atg39*Δ *atg40*Δ cells. Statistics were performed using the one sample t-test. Error bars represent SEM and asterisks represent p-values.

4.5 New insights into the role of Nvj1 during PMN

4.5.1 The hydrophobic core of Nvj1 is essential for its function in PMN

Nvj1 contains a hydrophobic core, that is essential for strictly perinuclear localization (Millen *et al.*, 2008). Mutation of the region, e.g. the introduction of charged residues to L20E_V23E, leads to mislocalization of Nvj1. In order to get a better insight into the role of Nvj1 during PMN, the question came up, if interaction of Nvj1 and Vac8 was sufficient for Nvj1 degradation, or if the perinuclear localization or the hydrophobic core of Nvj1, respectively, had an impact on PMN.

4.5.1.1 Perinuclear localization is disrupted for Nvj1_V20E_V23E-GFP

Before measuring the degradation of Nvj1_V20E_V23E-GFP, the localization of this construct was tested in order to confirm the findings of previous studies (Millen *et al.*, 2008). Therefore, vacuoles of wild type cells or *vac8*Δ cells expressing Nvj1-GFP or Nvj1_V20E_V23E-GFP were stained with FM4-64. The cells were starved for 2 h in SD(-N) medium and then analysed using the Delta Vision microscope.

Nvj1-GFP and Nvj1_V20E_V23E-GFP in wild type cells were localized to the NVJs (Figure 4.17). In *vac8*Δ cells Nvj1-GFP is localized to the perinuclear ER, in contrast to that, Nvj1_V20E_V23E-GFP localization was deranged. This was in congruency with the findings of Millen *et al.* (2008), who postulated, that the hydrophobic sequence next to the N-terminus is necessary for correct localization of Nvj1. Following, the degradation of Nvj1_V20E_V23E-GFP was measured (Chapter 4.5.1.2).

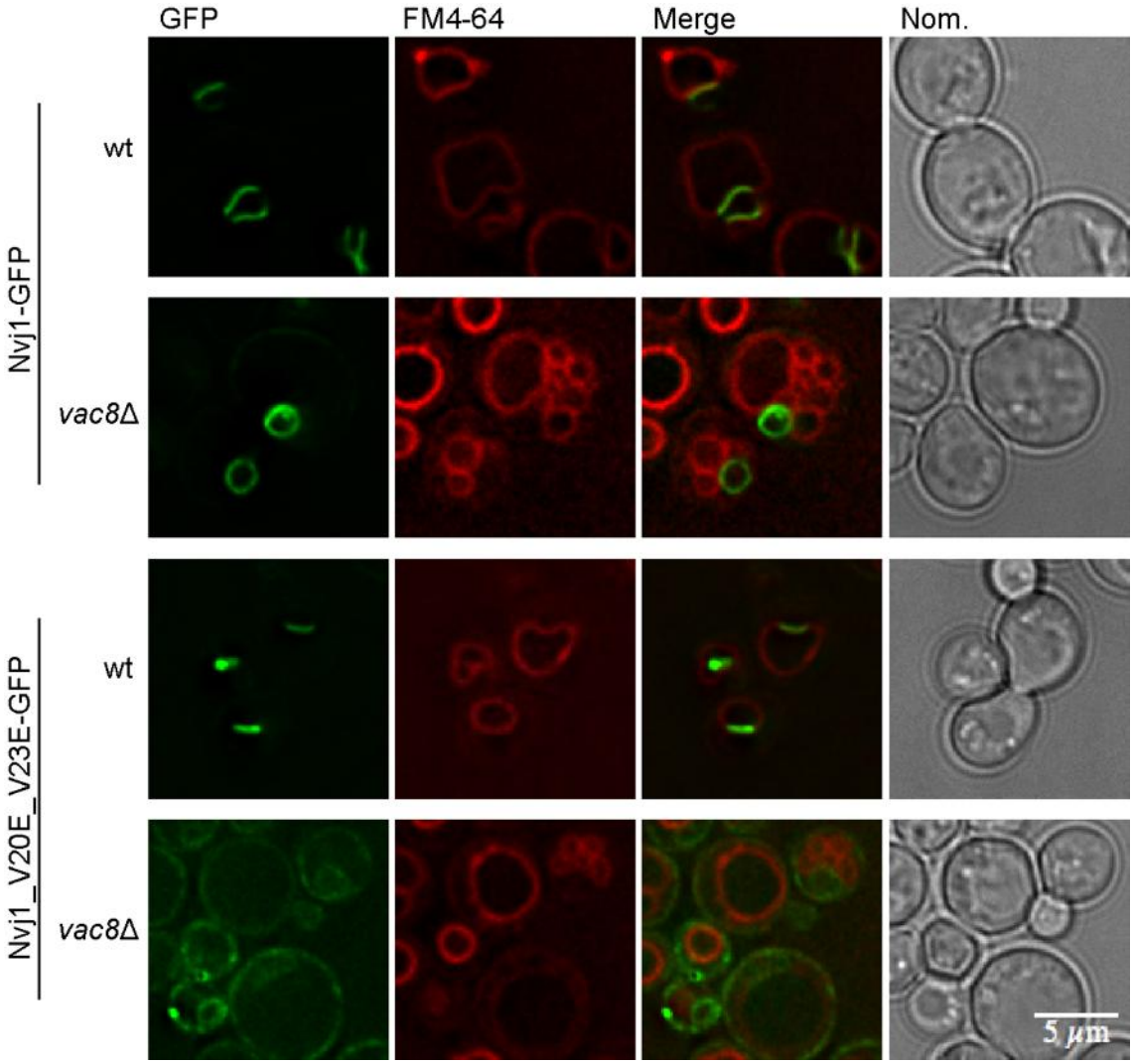

Figure 4.17: Microscopic evaluation of Nvj1_V20E_V23E-GFP

Vacuoles were stained with FM4-64 in wild type or *vac8*Δ cells expressing either Nvj1-GFP or Nvj1_V20E_V23E-GFP. The cells were starved for 2 h in SD(-N) medium. Finally, the deletion strains were analysed using fluorescence microscopy.

4.5.1.2 The hydrophobic ER-anchor is necessary for degradation of Nvj1-GFP

It was shown, that a hydrophobic sequence at the N-terminus is necessary for localization of Nvj1 to the nER (this study) (Millen *et al.*, 2008). But it is unknown, if this sequence is important for the degradation of Nvj1. Thus, cells expressing Nvj1_V20E_V23E-GFP from a plasmid under a *MET25* promotor were grown in CM medium containing 0,3 mM methionine to late stationary phase. The cells were starved in SD(-N) medium and samples were taken after 0 h, 2 h, 4 h, 6 h and 24 h starvation. The samples were alkaline lysed and immunoblotted. Free GFP was detected using an anti-GFP antibody. The

amount of free GFP after 24 h starvation in wild type cells expressing Nvj1-GFP was set 100%.

In wild type cells, as well as in all tested deletion strains, free GFP was barely visible (Figure 4.18 A). Quantification of the experiment underlined this impression: wt: 21% ± 3,11%; *atg1*Δ: 4,75% ± 2,49%; *vac8*Δ: 15% ± 4,34%; *nvj1*Δ: 22,25% ± 3,43%; *atg39*Δ: 21,75% ± 3,9%; *atg40*Δ: 15,25% ± 4,25%; *atg39*Δ *atg40*Δ: 9,25% ± 4,87%. This showed, that degradation of Nvj1_V20E_V23E-GFP is blocked even in the wild type, when compared to the degradation of Nvj1-GFP. This means, that the perinuclear localization of Nvj1, or more likely, the hydrophobic core of the N-terminus, is crucial for its degradation.

A

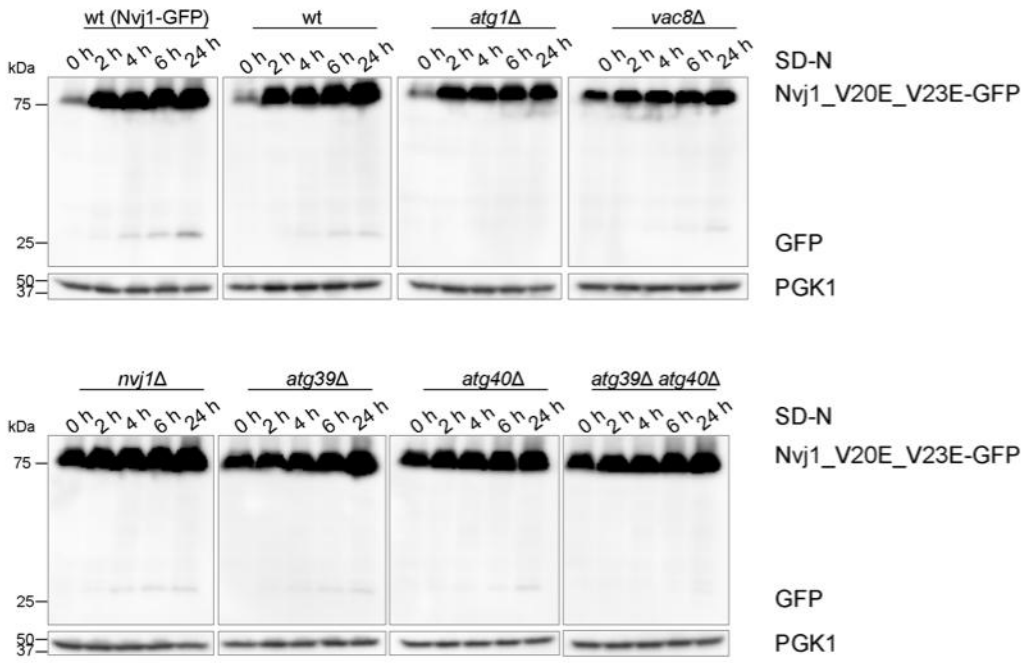

B

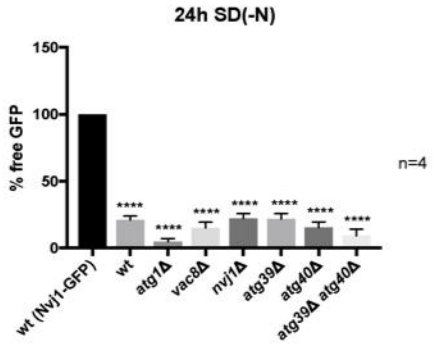

Figure 4.18: Degradation of Nvj1_V20E_V23E-GFP is blocked

(A) The indicated deletion strains expressing Nvj1_V20E_V23E-GFP were starved in SD(-N) medium. Samples were taken at 0 h, 2 h, 4 h, 6 h and 24 h, were alkaline lysed and immunoblotted. Free GFP was detected using an anti-GFP antibody. Pgk1 was used as a loading control and was stained with an anti-Pgk1 antibody.
(B) Quantification of four independent experiments showed, that degradation of Nvj1_V20E_V23E-GFP was reduced in *atg40*Δ cells and was blocked in *vac8*Δ, *atg39*Δ and *atg39*Δ *atg40*Δ cells. Statistics were performed using the one sample t-test. Error bars represent SEM and asterisks represent p-values.

4.5.2 Nvj1 degradation is independent of Vac8 dimerization

It is known, that a truncated version of Nvj1, Nvj1$^{\Delta 318\text{-}321}$, is able to bind to Vac8, but fails to induce Vac8 dimerization (Jeong *et al.*, 2017). This led to the question, whether Vac8 dimerization induced by Nvj1 was essential for degradation of Nvj1$^{\Delta 318\text{-}321}$-GFP and therewith PMN.

4.5.2.1 Nvj1$^{\Delta 318\text{-}321}$-GFP is not exclusively localized to nucleus-vacuole junctions

In order to verify the correct localization of Nvj1$^{\Delta 318\text{-}321}$-GFP, vacuoles of wild type and *vac8*Δ cells expressing Nvj1-GFP or Nvj1$^{\Delta 318\text{-}321}$-GFP from a plasmid were stained with FM4-64. The cells were starved for 2 h in SD(-N) medium and then analysed using the Delta Vision microscope.

In wild type cells Nvj1-GFP is exclusively localized to NVJs, whereas Nvj1$^{\Delta 318\text{-}321}$-GFP was localized to the perinuclear ER (Figure 4.19). The localization to the perinuclear ER also could be observed in *vac8*Δ cells expressing either Nvj1-GFP or Nvj1$^{\Delta 318\text{-}321}$-GFP, since here Nvj1 wasn't retained to the NVJs by interaction with Vac8. These findings were in congruency with Jeong *et al.* (2017) and therefore, degradation of Nvj1$^{\Delta 318\text{-}321}$-GFP could be measured (Chapter 4.5.2.2).

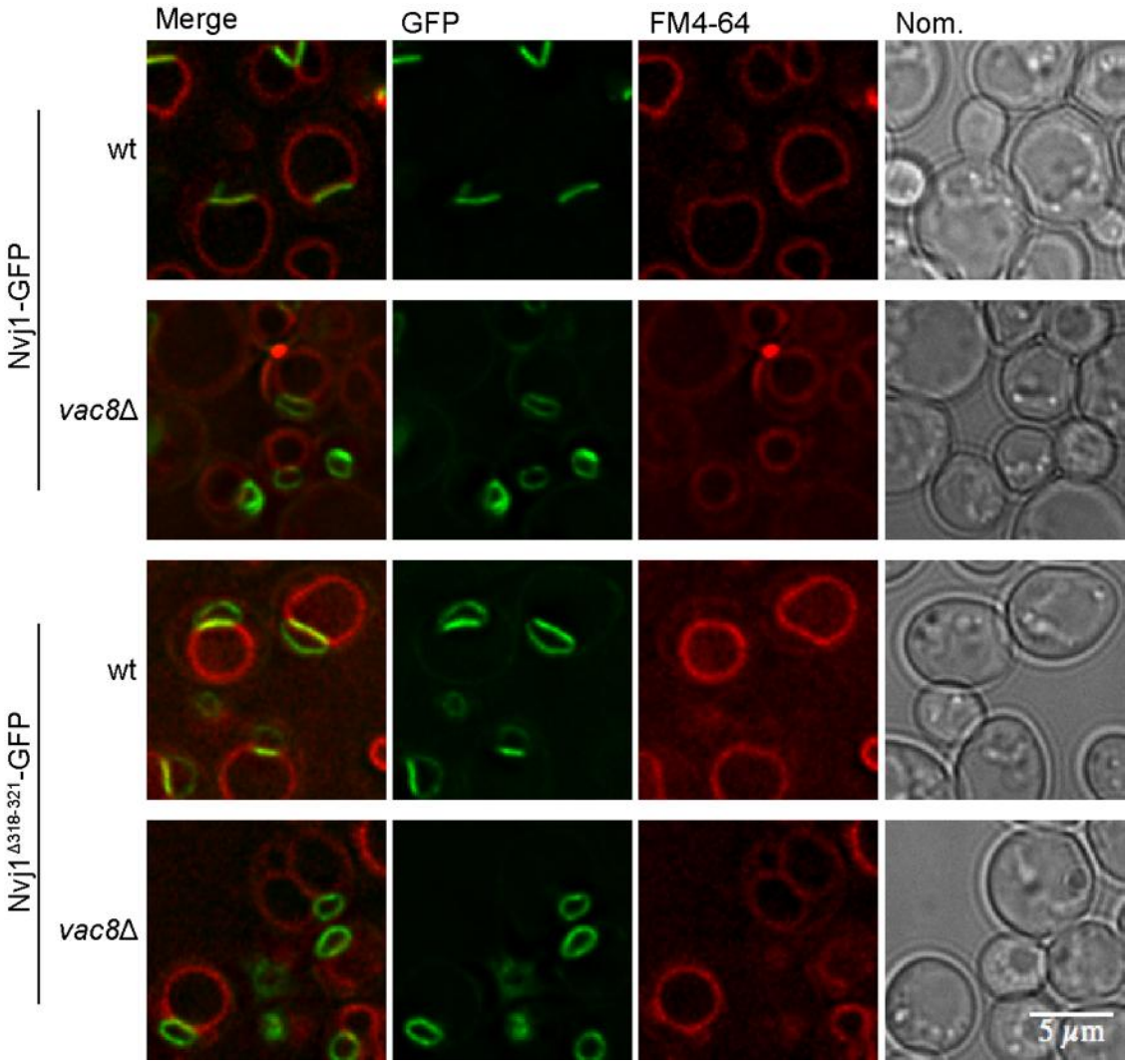

Figure 4.19: Microscopic evaluation of Nvj1$^{\Delta 318\text{-}321}$-GFP

Vacuoles were stained with FM4-64 and wild type or *vac8*Δ cells expressing either Nvj1-GFP or Nvj1$^{\Delta 318\text{-}321}$-GFP were starved for 2 h in SD(-N) medium. Finally, the cells were analysed using fluorescence microscopy.

4.5.2.2 Vac8 dimerization is not essential for Nvj1 degradation

In order to determine, if degradation of Nvj1 is dependent on Nvj1 induced Vac8 dimerization, the degradation of Nvj1$^{\Delta 318\text{-}321}$-GFP was measured. This truncated version of Nvj1 is still able to bind to Vac8, but is unable to induce Vac8 dimerization (Jeong *et al.*, 2017).

Therefore, diverse deletion strains expressing Nvj1$^{\Delta 318\text{-}321}$-GFP from a plasmid under a *MET25* promotor were grown to late stationary phase in CM medium containing 0,3 mM methionine. Wild type cells expressing Nvj1-GFP were used as a reference for the amount of degraded Nvj1$^{\Delta 318\text{-}321}$-GFP. The cells were starved in SD(-N) medium and samples were taken after 0 h, 2 h, 4 h, 6 h and

24 h starvation. The samples were alkaline lysed and immunoblotted. Free GFP was detected on western blots using anti-GFP antibody. The amount of free GFP in wild type cells expressing Nvj1-GFP after 24 h starvation was set to 100%.

No free GFP or reduced amounts were seen in *atg1*Δ (3,25% ± 1,11%), *vac8*Δ (27,75% ± 7,59%), *atg39*Δ *nvj1*Δ (30% ± 5,61%) and *atg39*Δ *atg40*Δ *nvj1*Δ cells (11,5% ± 2,9%) (Figure 4.20 A, B). The degradation of Nvj1$^{\Delta 318\text{-}321}$-GFP in *atg40*Δ *nvj1*Δ cells was comparable to the control (132,5% ± 38,79%). Surprisingly, in wild type cells and *nvj1*Δ expressing Nvj1$^{\Delta 318\text{-}321}$-GFP, significantly more free GFP was detected when compared to wild type cells expressing Nvj1-GFP (wt: 221% ± 10,64%; *nvj1*Δ: 279,8% ± 64,53%). There was no significant difference in the amount of free GFP in wild type cells and *nvj1*Δ expressing Nvj1$^{\Delta 318\text{-}321}$-GFP. Possibly, the disrupted localization of the truncated Nvj1 is the reason, why in wild type and *nvj1*Δ cells expressing Nvj1$^{\Delta 318\text{-}321}$-GFP more free GFP was detectable, than in wild type cells expressing Nvj1-GFP. It is thinkable, that this degradation occurs in an Atg39 dependent manner. Vac8 dimerization seems not to have any impact on Nvj1 degradation, as the obtained results, except for wild type and *nvj1*Δ cells, were comparable to those obtained for Nvj-GFP degradation (Chapter 4.4.3).

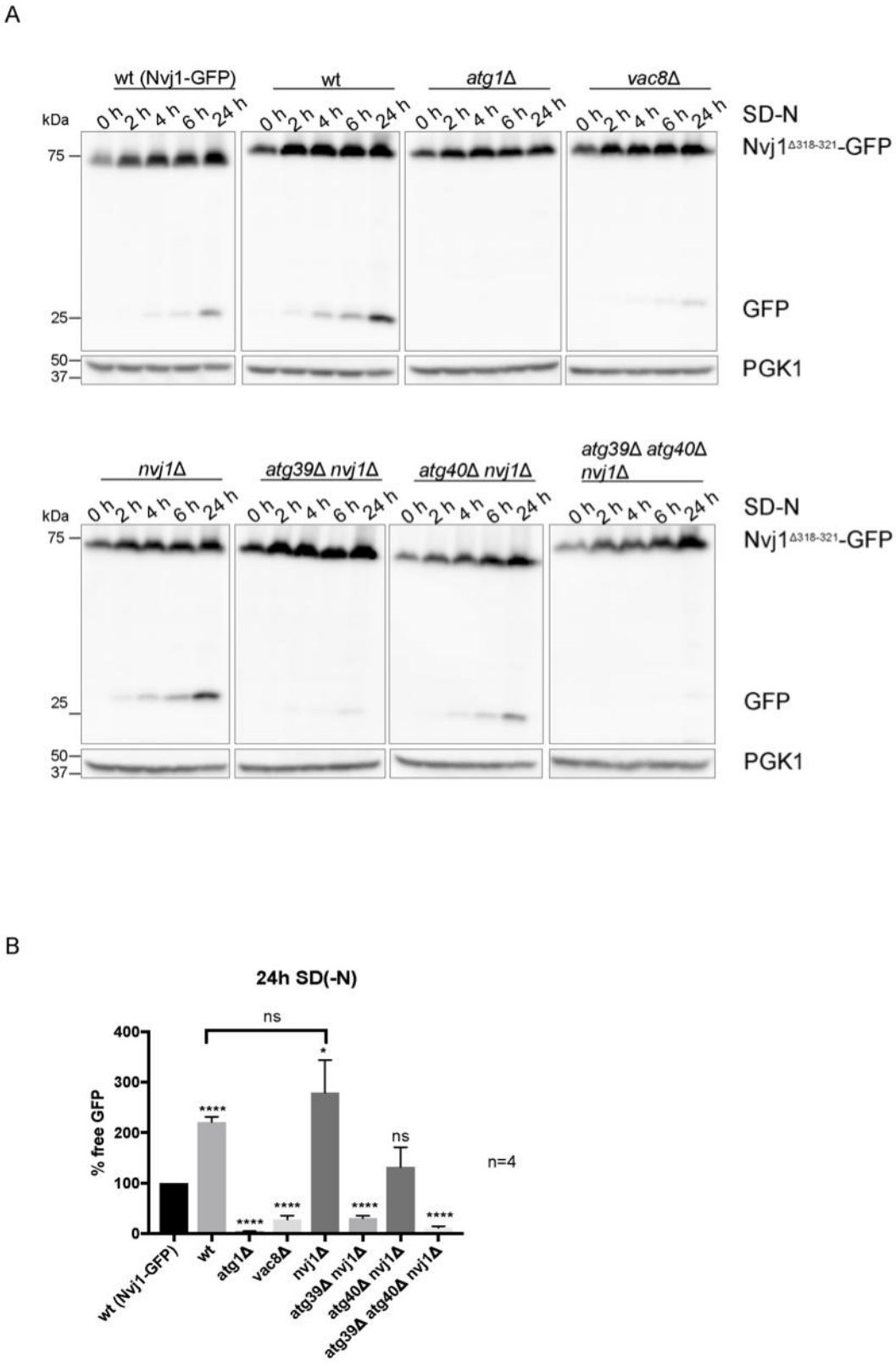

Figure 4.20: Degradation of Nvj1$^{\Delta 318-321}$-GFP is increased in wild type and *nvj1*Δ cells

(A) The indicated deletion strains expressing Nvj1-GFP or Nvj1$^{\Delta 318-321}$-GFP were starved in SD(-N) medium. Samples were taken at 0 h, 2 h, 4 h, 6 h and 24 h, were alkaline lysed and immunoblotted. Free GFP was

detected using an anti-GFP antibody. Pgk1 was used as a loading control and was stained with an anti-Pgk1 antibody.
(B) Quantification of four independent experiments showed, that degradation of Nvj1$^{\Delta 318\text{-}321}$-GFP was reduced in *atg1*Δ, *vac8*Δ, *atg39*Δ*nvj1*Δ and *atg39*Δ *atg40*Δ *nvj1*Δ cells. Significantly increased amounts of free GFP were seen in wild type and *nvj1*Δ cells. *atg40*Δ *nvj1*Δ deletion cells showed wild type like amounts of free GFP. The amount of free GFP in wild type cells expressing Nvj1-GFP after 24 h starvation was set to 100%. Statistics were performed using the one sample t-test. Error bars represent SEM and asterisks represent p-values.

4.6 Pho8-GFP is no suitable marker for differentiation between micro- and macroautophagy in western blots

Recently it was described, that nucleophagy not only occurs as microautophagy (or micronucleophagy/ PMN), but also as macroautophagy (or macronucleophagy) (Mochida *et al.*, 2015). However, so far it is not possible to easily distinguish between these two types of autophagy. Pho8 is a vacuolar protein (Klionsky and Emr, 1989), that was thought to be a suitable marker protein for the differentiation between micro- and macroautophagy. During macroautophagy, the outer autophagosomal membrane fuses with the vacuolar membrane (Darsow *et al.*, 1997; Sato *et al.*, 1998) and the content is released into the vacuole, therefore, no degradation of Pho8-GFP was to be expected. In contrast to that, PMN vesicles that are released into the vacuole are surrounded a vacuolar membrane and two ER membranes (Krick *et al.*, 2009b; Elbaz and Schuldiner, 2011) and so Pho8-GFP might be degraded.

4.6.1 Pho8-GFP is localized to the vacuolar membrane

Using the Delta Vision microscope, it was determined, if the Pho8-GFP construct was localized to the vacuolar membrane. In wild type cells expressing Pho8-GFP from a plasmid under an endogenous promotor, the vacuoles of wild type cells were stained with FM4-64 and then starved for 2 h in SD(-N) medium. Fluorescence microscopy showed very faint expression of Pho8-GFP. Nevertheless, colocalisation of Pho8-GFP and the vacuolar marker FM4-64 was clearly visible (Figure 4.21). Therefore, Pho8-GFP could be tested as a marker protein in order to being able to distinguish between micro- and macroautophagy (Chapter 4.6.2).

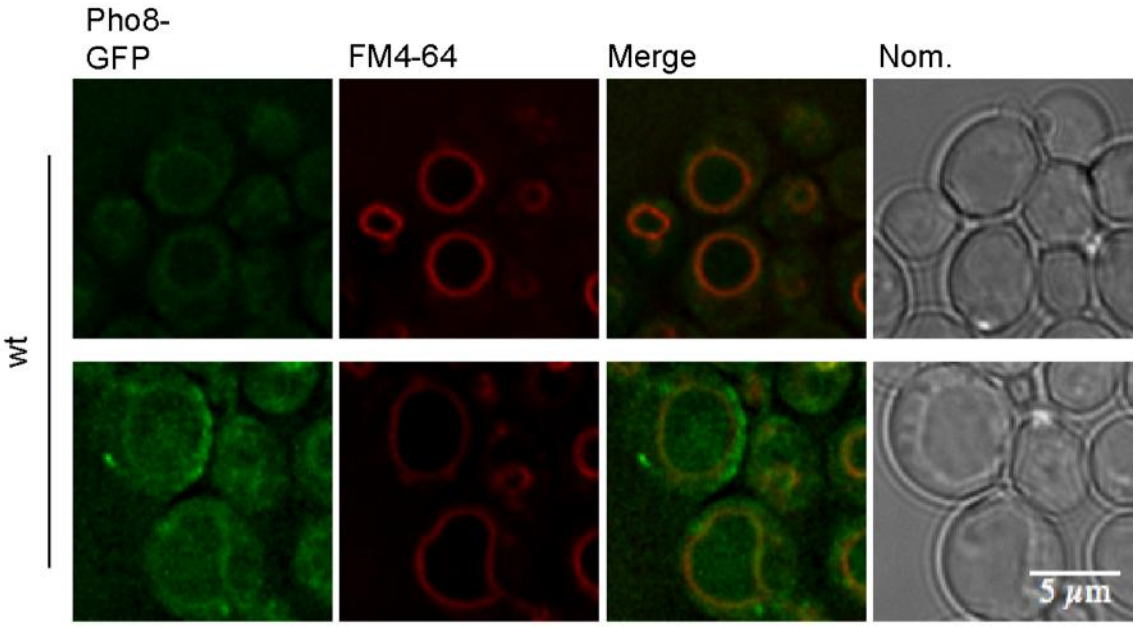

Figure 4.21: Pho8-GFP is localized to the vacuole

Vacuoles of wild type cells expressing Pho8-GFP were stained with FM4-64 and then starved for 2 h in SD(-N) medium. Finally, the cells were examined using the Delta Vision microscope.

4.6.2 Pho8-GFP is degraded independent of Nvj1, Atg39 and Atg40

In order to being able to distinguish between microautophagy and macroautophagy, the degradation of the potential marker protein Pho8-GFP was measured. Different deletion strains expressing Pho8-GFP from a plasmid under an endogenous promotor, were grown to late stationary phase and then starved in SD(-N) medium. Samples were taken after 0 h, 2 h, 4 h, 6 h and 24 h starvation. The samples were alkaline lysed and immunoblotted. Free GFP on western blots was detected using an anti-GFP antibody.

Degradation of Pho8-GFP was blocked in *atg1*Δ and *vac8*Δ cells (Figure 4.22 A). Degradation of Pho8-GFP was observed in *nvj1*Δ, *atg39*Δ, *atg40*Δ, *atg39*Δ *atg40*Δ and *atg39*Δ *atg40*Δ *nvj1*Δ cells. Quantification showed no degradation of Pho8-GFP in *ATG1* and *VAC8* deletion strains (*atg1*Δ: 13,5% ± 5,91%; *vac8*Δ: 25% ± 7,56%) (Figure 4.22 B). Wild type like degradation was seen in *nvj1*Δ (106% ± 21,74%) *atg39*Δ (179,3% ± 54,75%), *atg40*Δ (212% ± 70,85%), *atg39*Δ a*tg40*Δ (137% ± 38,75%) and *atg39*Δ *atg40*Δ *nvj1*Δ cells (74% ± 11,94%). Atg40 is not thought to be directly involved in PMN and therefore was expected to be blocked in regard of Pho8-GFP degradation. Also, Atg39 was considered to be blocked, since this Atg-protein is thought to be

mainly involved in macronucleophagy. Surprisingly this wasn't the case and free GFP was visible in these two deletion strains, as well as in all additionally tested deletion strains, except for the negative controls *ATG1* and *VAC8*. This leads to the conclusion, that Pho8-GFP possibly is degraded via an another autophagic pathway, dependent on Atg1 and Vac8.

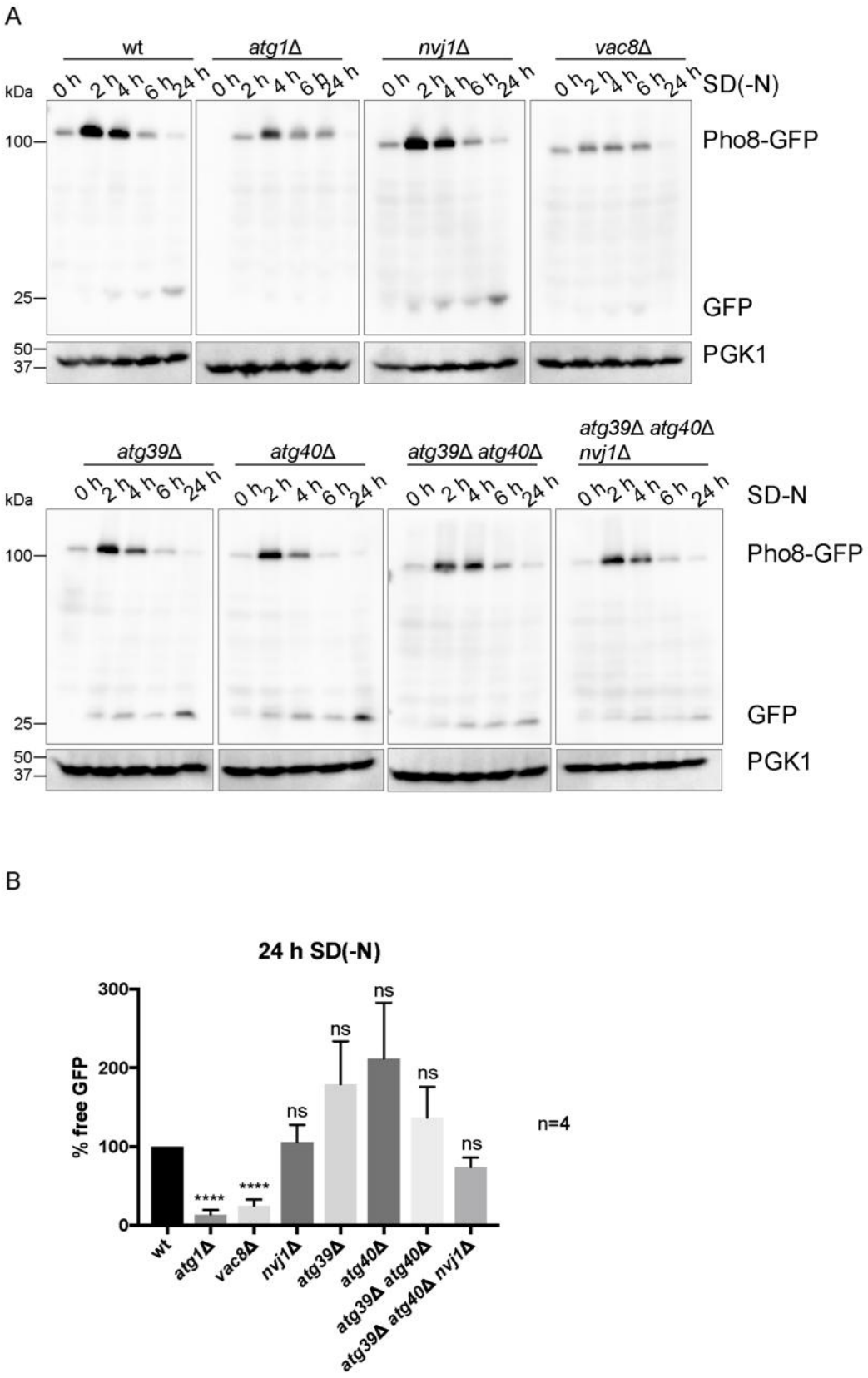

Figure 4.22: Pho8-GFP is degraded dependent on Atg1 and Vac8

(A) The indicated deletion strains expressing Pho8-GFP were starved in SD(-N) medium. Samples were taken at 0 h, 2 h, 4 h, 6 h and 24 h, were alkaline lysed and immunoblotted. Free GFP was detected using an anti-

GFP antibody. Pgk1 was used as a loading control and was stained with an anti-Pgk1 antibody.
(B) Quantification of four independent experiments showed that degradation of Pho8-GFP was wild type like in *nvj1*Δ, *atg39*Δ, *atg40*Δ, *atg39*Δ *atg40*Δ and *atg39*Δ *atg40*Δ *nvj1*Δ cells. Degradation of Pho8-GFP was blocked in *atg1*Δ and *vac8*Δ cells. Statistics were performed using the one sample t-test. Error bars represent SEM and asterisks represent p-values.

4.7 Screen for selective substrates of PMN

In cooperation with the group of Prof. Blanche Schwappach, a screen for selective substrates of PMN was performed. Therefore, GFP-Osh1 was expressed from a plasmid under a *TEF1* promotor and Nop1 was chromosomally tagged with mCherry in a BY4741 deletion library and a DAmP library. Microscopic pictures were then taken with an automated microscope system. Evaluation of the obtained data was performed using the MATLAB software in cooperation with Prof. Dr. Silvio Rizzoli. Here, the distance between the weighted average of the NVJ and the mass centre of the nucleolus was calculated. The data then was ordered according to the nucleolus NVJ distance (

Figure 4.23). The mean distance between NVJ and nucleolus was 0,96 µm. In deletion cells with a great gap between nucleolus and NVJ a distance of 1,3 and 1,46 µm was measured. In deletion cells with a small gap between nucleolus and NVJ a distance of 0,6 and 0,75 µm was measured. A further in-depth analysis of the obtained hits is under progress.

Great Distance (Nucleolus NVJ)	
ORF	Gene
YLR182W	SWI6
YHR184W	SSP1
YKL074C	MUD2
YAL011W	SWC3
YDR195W	REF2
YGL041C	YGL041C
YBR058C-A	TSC3
YEL036C	ANP1
YLR357W	RSC2
YER120W	SCS2
YJL090C	DPB11
YPL058C	PDR12
YIL086C	YIL086C
YDR150W	NUM1
YMR277W	FCP1
YPR185W	ATG13
YPR042C	PUF2
YPL052W	OAZ1
YGL154C	LYS5

Small Distance (Nucleolus NVJ)	
ORF	Gene
YGL124C	MON1
YNR030W	ALG12
YPL253C	VIK1
YNL039W	BDP1
YER010C	YER010C
YBL092W	RPL32
YGL188C-A	YGL188C-A
YGL091C	NBP35
YNL099C	OCA1
YAL055W	PEX22
YGL007C-A	YGL007C-A
YML001W	YPT7
YKLO72W	YKLO72W
YNL173C	MDG1
YIL141W	YIL141W
YDL077C	VAM6
YLL034C	RIX7
YEL007W	MIT1
YCR053W	THR4

Deletion Library
DAmP Library

Figure 4.23: Potential hits of selective substrates of PMN

Cells from a BY4741 deletion library or DAmP library expressing chromosomal Nop1-mCherry and GFP-Osh1 from a plasmid were microscopically analysed and ordered in regard to the nucleolus NVJ distance. Represented here are hits with the greatest or smallest measured nucleolus NVJ distance.

5 Discussion

Autophagy is a catabolic process for the degradation of superfluous or damaged organelles, but also occurs under normal conditions at a basal level. This process is conserved among all eukaryotes (Reggiori and Klionsky, 2002). Autophagy appears in two forms, macroautophagy and microautophagy. Initiation of macroautophagy, or short autophagy, starts with the formation of a cup-shaped isolation membrane, the phagophore. This structure finally evolves into a double membrane vesicle, the autophagosome, that sequesters the respective cargo (Klionsky and Ohsumi, 1999). The autophagosome then fuses with the vacuole and the autophagic body is released into the vacuole, where it is degraded. The biogenesis of the autophagosome is located at the PAS (Suzuki *et al.*, 2001; Noda *et al.*, 2002), here the core Atg-machinery, consisting of 18 Atg-proteins is localized (Ariosa and Klionsky, 2016). Autophagy can take place either as bulk autophagy or selective autophagy, depending on the way, how the cargo is loaded into the autophagosomes.

Nucleophagy is defined as the autophagic degradation of non-essential parts of the nucleus including parts of the nuclear ER and is therefore a selective form of autophagy. It can occur via two distinct mechanisms: PMN (also called micronucleophagy) (Roberts *et al.*, 2003) and the recently described macronucleophagy (Mochida *et al.*, 2015). Until now, both processes are poorly understood.

Macronucleophagy and ER-phagy have been shown to be dependent on Atg39 and Atg40 (Mochida *et al.*, 2015). Atg39 is localized to the pnER and is important for macronucleophagy combined with pnER-phagy. During macronucleophagy non-essential parts of the nucleus are sequestered in autophagosomes in a Atg39 dependent manner, the vesicles then fuses with the vacuole, the content is released and finally degraded in the vacuole (Mochida *et al.*, 2015). The degradation of cortical ER is dependent on Atg40, a protein localized to cytoplasmic and cortical ER (Nakatogawa and Mochida, 2015). Both above mentioned Atg-proteins contain AIMs, that can interact with Atg8 on forming autophagosomal membranes (Mochida *et al.*, 2015).

PMN is a microautophagic type of autophagy and takes place at the NVJ, a contact site between nucleus and vacuole (Roberts *et al.*, 2003). The NVJ consists of at least four proteins: Nvj1, Vac8, Osh1 and Tsc13 (Pan *et al.*, 2000a; Kohlwein *et al.*, 2001; Levine and Munro, 2001). The backbone of this contact site is formed by the interaction of Nvj1 and Vac8. Absence of one of these two proteins results in the loss or at least significant reduced formation of the NVJs (Pan *et al.*, 2000a). Starvation leads to bulging of the NVJs into the vacuole and formation of a teardrop-like bleb, that buds off. Finally, the vacuolar extensions fuse and the vesicle is released into the vacuole, where it is degraded (Kvam and Goldfarb, 2007).

It has been proposed, that PMN is dependent on the core Atg-machinery and furthermore, it was shown, that degradation of GFP-Osh1, a marker protein for PMN, is blocked in a *NVJ1* deletion strain (Krick *et al.*, 2008). However, Mochida *et al.* (2015) reported, that degradation of Nop1-GFP, also a marker protein for microautophagy, isn't blocked in a *NVJ1* deletion strain. This discrepancy was used as a starting point for this study.
Results of this study suggest, that PMN should be renamed into NVJ-phagy (Chapter 5.2.3). When appropriate, in the following discussion PMN will be referred to as PMN/ NVJ-phagy.

5.1 GFP-Osh1 can be degraded in a Nvj1 independent manner

Under nutrient rich conditions, Osh1 is localized to the late Golgi, cytoplasm and the NVJs, whereas during starving conditions Osh1 is only localized to the cytoplasm and for the main part to the NVJs (Levine and Munro, 2001). The localization of Osh1 to the NVJs is based on physical interaction with Nvj1 (Kvam and Goldfarb, 2004). These characteristics suggest, that Osh1 is almost exclusively degraded via the mechanism known as PMN/ NVJ-phagy. Therefore, GFP-Osh1 was used as a marker protein to measure the PMN/ NVJ-phagy rate (Krick *et al.*, 2008; Millen *et al.*, 2009). Surprisingly, within this study it was shown, that degradation of GFP-Osh1 can also take place independent of Nvj1 (Chapter 4.1.1). The assumption, that GFP-Osh1 is exclusively degraded via PMN/ NVJ-phagy, was based on a *NVJ1* knockout that was proven to be wrong (Chapter 4.1).

Even in the absence of the NVJs, GFP-Osh1 can be degraded in a wild type like amount (Figure 4.1 A, B). This shows, that GFP-Osh1 is not exclusively degraded via PMN/ NVJ-phagy and can be degraded in a Nvj1 independent manner. In cells missing the NVJs, GFP-Osh1 can also be degraded, however, this most likely occurs via an alternative autophagic pathway. How exactly GFP-Osh1 is degraded in *nvj1*Δ cells remains to be clarified.

Manik *et al.* (2017) were able to partially solve the structure of Osh1 and also showed that a mutated version of Osh1, Osh1_A159V isn't interacting with Nvj1. This knowledge was used for the better characterization of GFP-Osh1 as a marker protein. First of all, the interaction of Osh1_A159V and Nvj1 was analysed *in vivo* using the GFP-trap approach. Indeed, the interaction of GFP-Osh1_A159V and Nvj1-6xHA was impeded (Figure 4.12 A). Also, visualization of GFP-Osh1_A159V showed patch-like localization in the cells, when compared to GFP-Osh1, that is localized to the NVJs (Figure 4.12 B). Osh1 is known to be localized to the Golgi under non-starving conditions (Levine and Munro, 2001). Possibly, the patches observed for GFP-Osh1_A159V represent the Golgi apparatus. However, the pictures were taken under starving conditions and a cytosolic localization of GFP-Osh1_A159V would be more likely. Therefore, it still remains to be clarified, if this mutated Osh1 construct is located to the Golgi, appears as protein aggregates in the cytoplasm or is localized to a different cellular structure.
Degradation of GFP-Osh1_A159V occurred to the same amount as GFP-Osh1 and was comparable in the respective tested knockout strains (Figure 4.13). This was in congruency with the above-mentioned results. In the absence of the NVJs or impeded interaction of Osh1 and Nvj1, Osh1 can be degraded via an alternative autophagic pathway independent of PMN/ NVJ-phagy. The amount of degraded GFP-Osh1 is comparable in both pathways.
Within this study it was shown, that up to date no genetic knockout is available, that selectively blocks PMN/ NVJ-phagy (Chapter 4.1 and 5.4). This in turn means, that no final conclusion can be drawn how GFP-Osh1 is degraded in a respective knockout. Therefore, GFP-Osh1 shouldn't be the first choice, when one wants to measure PMN/ NVJ-phagy. In that case, Nvj1-GFP would probably be the better choice.

5.2 Nvj1-GFP – a superior marker protein for PMN/ NVJ-phagy measurement

As PMN/ NVJ-phagy is defined as the degradation of Nvj1 and this protein is exclusively located to the perinuclear ER (Pan *et al.*, 2000a), Nvj1-GFP represents a better possibility for measurement of this process. However, as a genetic knockout, that selectively blocks PMN/ NVJ-phagy is not available, two mutated versions of Nvj1 were taken into account as a negative control, Nvj1$^{\Delta 318\text{-}321}$-GFP and Nvj1_V20E_V23E-GFP.

5.2.1 Nvj1$^{\Delta 318\text{-}321}$-GFP is not suitable as negative control for PMN/ NVJ-phagy measurement

Nvj1 induces Vac8 dimerization and recently it was shown, that a truncated version of Nvj1 missing the last four amino acids impedes this dimerization, but is still able to bind to Vac8 (Jeong *et al.*, 2017). The almost exclusive localization to the NVJ of Nvj1 in wild type cells is impeded in the truncated version Nvj1$^{\Delta 318\text{-}321}$-GFP, which is located in the perinuclear ER, not only in *vac8*Δ cells, but also in wild type cells (Figure 4.19). This shows, that the last four amino acids of Nvj1 are not only essential for Vac8 dimerization, but are also important for proper formation of NVJs. These results were in congruency with data recently described Jeong *et al.* (2017). Surprisingly, degradation of Nvj1$^{\Delta 318\text{-}321}$-GFP was significantly increased in wild type and in *nvj1*Δ cells when compared to the degradation of Nvj1-GFP in wild type cells (Figure 4.20 A, B). This shows, that mislocalization of Nvj1$^{\Delta 318\text{-}321}$-GFP leads to an increased degradation of this protein. Potentially, this overcompensated degradation of Nvj1$^{\Delta 318\text{-}321}$-GFP is mediated by Atg39 dependent ER-phagy, what can take place in larger amounts than PMN/ NVJ-phagy. Therefore, this mutant can't be used as negative control for PMN/ NVJ-phagy measurement.

5.2.2 The hydrophobic core of Nvj1 is crucial for PMN/ NVJ-phagy

It is known, that introduction of charged residues in the hydrophobic core of Nvj1, impedes its strict localization to the perinuclear ER (Millen *et al.*, 2008). A mutated version of Nvj1-GFP, Nvj1_V20E_V23E-GFP, was examined in regard of its localization. Indeed, its localization was disrupted in *vac8*Δ cells (Figure

4.17) (Millen *et al.*, 2008). In wild type cells, Nvj1_V20E_V23E-GFP was localized to the NVJs, based on the physical interaction of Vac8 and Nvj1.
Degradation of Nvj1_V20E_V23E-GFP was blocked in all tested deletion strains, as well as in the wild type, when compared to the wild type expressing Nvj1-GFP, (Figure 4.18). Obviously, for the degradation of Nvj1, the perinuclear localization or an activity mediated by the N-terminus of Nvj1 is crucial, whereas its interaction with Vac8 and therewith localization to the NVJ seems to be irrelevant. Nvj1 is considered to be responsible for the bending of the whole NVJ during PMN/ NVJ-phagy (Millen *et al.*, 2008). Possibly, this function is mediated by the hydrophobic core of Nvj1. Mutation of this hydrophobic core leads to a loss of this function and therefore the bending of the structure is impeded. In conclusion this suggests, that Nvj1 mediated bending of the NVJ is crucial for PMN/ NVJ-phagy. Furthermore, this means, that Nvj1_V20E_V23E-GFP can serve as negative control for PMN/ NVJ-phagy measurement.

5.2.3 PMN – a process for the degradation of the nucleus-vacuole junction?

PMN is described as a process for the specific degradation of the nucleus and nucleolus (Roberts *et al.*, 2003; Dawaliby and Mayer, 2010). PMN was not only observed visually (Roberts *et al.*, 2003; Kvam and Goldfarb, 2007; Krick *et al.*, 2009a), but was also measured quantitatively (Krick *et al.*, 2008; Millen *et al.*, 2009). The new analyses presented here showed, that degradation of nucleolar proteins, as well as nuclear proteins aren't blocked in *nvj1*Δ cells (this study, Chapter 4.1.6) (Mijaljica *et al.*, 2012; Mochida *et al.*, 2015). Though, results of this study showed, that degradation of Nop1-GFP is reduced to about 56% in the respective *NVJ1* deletion strain (Figure 4.15 B). This indicates, that only a part of the nucleolar proteins is degraded via PMN. If degradation of nuclear components via PMN is unselective, or possesses selectivity is under investigation (Chapter 4.7). Also, unknown intranuclear parts of the NVJ could be degraded via this mechanism. However, it is reported, that degradation of Nop1-GFP in different genetic backgrounds is wild type like in the absence of Nvj1 (Mochida *et al.*, 2015; Mostofa *et al.*, 2018). Nevertheless, this underlines the new theory, that degradation of nucleolar and nuclear proteins can take place in the absence of NVJs and therewith PMN. Furthermore, the obtained

results led to the conclusion, that degradation of nuclear components is mainly based on Atg39 and, to a smaller amount, on Atg40 dependent macronucleophagy (Mochida *et al.*, 2015) and that PMN only plays a partial role in this degradation pathway.
However, it is undeniable, that nuclear material is degraded during PMN. Roberts *et al.* (2003) were able to visualize, that portions of the nucleolus are sequestered into PMN vesicles. Also, electron microscopy showed bulging of nucleolar material into a PMN vesicle (Kvam and Goldfarb, 2007). Additionally, PMN vesicles with a diameter of about 1,5 µm were observed in wild type cells using Nvj1-GFP as a marker for the NVJ and FM4-64 as a marker for the vacuolar membrane (Kvam *et al.*, 2005). Finally, in wild type cells, expressing Nvj1-GFP as a marker for the NVJ and Nab-NLS-mCherry as a nuclear marker, PMN vesicles containing nuclear material were observed (Florian Otto, unpublished data).

If the main goal of PMN is not the degradation of nuclear material, the question comes up, what is PMN needed for? Most likely, the purpose of this process is the removal of the NVJs. Proteins involved in lipid biosynthesis and trafficking are localized to the NVJs. Tsc13 and Osh1 both interact with Nvj1 and are known to play a role in lipid biosynthesis (Elbaz and Schuldiner, 2011). Osh1 belongs to the family of oxysterol-binding proteins. These are lipid-binding proteins, that are involved in diverse cellular processes. They are considered to function in signalling, vesicular trafficking, lipid transfer and lipid metabolism (Raychaudhuri and Prinz, 2010). Upon starvation, Osh1 is almost exclusively localized to the NVJs (Levine and Munro, 2001). Knockout of all seven Osh proteins in *S. cerevisiae* results in an inhibition of PMN (Kvam and Goldfarb, 2004).Tsc13 is an essential enoyl-CoA reductase and catalyses the very last step of very-long-chain fatty acid biosynthesis (Kohlwein *et al.*, 2001). Under starving conditions Tsc13 is degraded via PMN vesicles in a Nvj1 dependent manner. It was shown, that mutants impaired in elongation of very-long-chain fatty acid biosynthesis exhibit smaller PMN vesicles than wild type cells. The same effect was observed for cells treated with cerulenin and therefore, Tsc13 metabolites can be considered to play an important role during PMN (Kvam *et al.*, 2005). It was shown, that lack of the acyl-CoA-binding protein Acb1 in

S. cerevisiae, impedes protein trafficking, ceramide levels, vacuole fusion and structure (Faergeman *et al.*, 2004). Also, the PI3P binding protein Mdm1, that was shown to be an interorganelle tethering protein, is degraded like Nvj1 under nitrogen starvation conditions (Henne *et al.*, 2015). Furthermore, it is known, that under starvation conditions, the NVJs serve as sites for production of lipid droplets (Hariri *et al.*, 2018). This is reasonable, as the NVJs contain several proteins involved in lipid synthesis (Schuldiner and Bohnert, 2017). During stationary phase, the lipid droplets move away from the NVJ and surround the vacuole (Schuldiner and Bohnert, 2017). Approximately at the same time, PMN and therewith the degradation of the NVJs starts.
Since the main goal of the process known as PMN possibly isn't the autophagic degradation of nuclear material, but the degradation of the NVJ and associated components, PMN should be renamed into NVJ-phagy.

5.3 Atg39 is pivotal for PMN/ NVJ-phagy and macronucleophagy

Degradation of Nvj1-GFP was completely blocked in *atg39*Δ and reduced in *atg40*Δ cells (Figure 4.16). Therewith, this study showed for the first time, that Atg39 is not only essential for degradation of the perinuclear ER and macronucleophagy (Mochida *et al.*, 2015), but is also crucial for PMN/ NVJ-phagy. This suggests, that PMN/ NVJ-phagy is a specific Atg39 dependent type of ER-phagy, aiming specifically for the NVJs and associated proteins. This leads to the conclusion, that Atg39 is a pivotal regulator of macronucleophagy and PMN/ NVJ-phagy. Therewith, also in the absence of Nvj1 the residuals of the NVJ can be removed.
As expected, Atg39 dependent degradation of Nvj1 isn't limited to the NVJs, but occurs at the whole perinuclear ER. Degradation of a truncated version of Nvj1, Nvj1$^{\Delta 318\text{-}321}$-GFP, which localization is not limited to the NVJs, but is found in the perinuclear ER, was even overcompensated (Chapter 4.5.2.2).
However, degradation of GFP-Osh1 was not dependent on Atg39. Possibly, this maker protein is degraded via an alternative autophagic mechanism.

The present study shows, that PMN/ NVJ-phagy and macronucleophagy are linked via Atg39. This poses the question, if there is also a crosstalk between these two degradation pathways. Degradation of Nop1-GFP is reduced in *nvj1*Δ

cells (Figure 4.15) and completely blocked in *atg39*Δ cells (this study) (Mochida *et al.*, 2015). This shows, that Nop1-GFP can be degraded via both nucleophagic pathways. Cells deficient for *NVJ1* are incapable of micronucleophagic degradation of nuclear material via PMN/ NVJ-phagy (Mostofa *et al.*, 2018). However, degradation of Nop1-GFP is only reduced in *nvj1*Δ cells (Figure 4.15). This shows, that in the absence of Nvj1, PMN/ NVJ-phagy can be compensated by Atg39 dependent macronucleophagy. If macronucleophagy can be compensated by PMN/ NVJ-phagy is unknown, but as Atg39 is crucial for both nucleophagic processes, a compensation seems to be unlikely.

5.4 A knockout strain selectively inhibited for PMN/ NVJ-phagy is not available

5.4.1 Nvj2, Glc8 and Ymr310c play no direct role in PMN/ NVJ-phagy

Degradation of GFP-Osh1, as well as nuclear and nucleolar marker proteins were shown not to be dependent on Nvj1 (Chapter 4.1) (Mijaljica *et al.*, 2012; Mochida *et al.*, 2015). Therefore, it was of interest, if other proteins alone or in combination with Nvj1 were involved in PMN/ NVJ-phagy.

Since Nvj2 is enriched in NVJs (Toulmay and Prinz, 2012), this protein was considered to be involved in PMN/ NVJ-phagy. Degradation of GFP-Osh1 and Nop1-GFP was neither blocked in the *nvj2*Δ cells nor in *nvj1*Δ *nvj2*Δ cells (Figure 4.6 A-D). Microscopic evaluation showed intact NVJs in a *NVJ2* deletion strain. In *nvj1*Δ *nvj2*Δ cells no NVJs were visible (Figure 4.7). This was to be expected, because the knockout of *NVJ1* leads to the loss of NVJs (Pan *et al.*, 2000a). Also Toulmay and Prinz (2012) postulated that Nvj2 is localized to the NVJs, but is not necessary for the formation of this contact site. Degradation of Nop1-GFP in *nvj1*Δ *nvj2*Δ cells potentially is mediated by Atg39 and to lesser extend by Atg40 in a macronucleophagic manner (Mochida *et al.*, 2015). If Nop1-GFP in *nvj2*Δ cells is degraded via PMN/ NVJ-phagy or via Atg39 dependent macronucleophagy is unknown. Results obtained for experiments based on the degradation of GFP-Osh1 have to be evaluated cautiously, because this marker protein can also be degraded independent of PMN/ NVJ-phagy (Chapter 4.3.3 and 5.1). Therefore, degradation of GFP-Osh1 in *nvj1*Δ

*nvj2*Δ cells results most likely from ER-phagy, since it is dispersed under these conditions.

The already existing *nvj1*Δ::*HIS3* strain was shown to be an otherwise affected knockout, nevertheless, this knockout strain showed a very interesting phenotype, since it was blocked for the degradation of GFP-Osh1 and Nop1-GFP (Figure 4.1 A-D, Chapter 4.1). In order to identify the gene, that might have been knocked out by chance, a PCR approach was used. Two potential hits were obtained: *GLC8* and the putative methyltransferase *YMR310C*. *GLC8* was considered to be a reasonable hit, since it is the activator of *GLC7* (Nigavekar *et al.*, 2002), the catalytic subunit of protein phosphatase 1 (Ramaswamy *et al.*, 1998). *GLC8* and *YMR310C* were knocked out and the respective knockout strains were evaluated using the Delta Vision microscope. Both knockout strains showed intact NVJs (Figure 4.11). This was to be expected, since the *nvj1*Δ::*HIS3* strain also showed intact NVJs (Figure 4.3). Following, these strains were tested in regard of their ability for degradation of GFP-Osh1 and Nop1-GFP. The degradation of both marker proteins was wild type like in *glc8*Δ and in *ymr310c*Δ cells (Figure 4.10 A-D). This led to the conclusion, that neither *GLC8* nor *YMR310C* were the gene(s) knocked out or were affected in the *nvj1*Δ::*HIS3* strain. Probably, the obtained PCR product resulted from unspecific binding of the used primers. The final analysis of the gene knockout out in the *nvj1*Δ::*HIS3* strain via genomic sequencing is still outstanding.

5.4.2 Scs2 is required for the intactness of the nucleus-vacuole junction and is not directly involved in autophagic degradation of nucleolar proteins

Microscopic evaluation of *nvj1*Δ *scs2*Δ cells showed disrupted NVJs, when using GFP-Osh1 as junction marker (Figure 4.9). This was to be expected, as knockout of *NVJ1* leads to this phenotype (Pan *et al.*, 2000a). Surprisingly, in *scs2*Δ cells the NVJs were only partially visible. Possibly, this can be explained by the fact, that Scs2, like Nvj1 also interacts with Osh1 (Loewen *et al.*, 2003). Is Scs2 missing, less GFP-Osh1 can be recruited to the NVJs, so that the NVJs are only partially or less clearly visible. However, it is also thinkable, that the

disruption of the NVJ is a problem of the visualization and that a different marker protein, e.g. Nvj1-GFP, shows intact NVJs. On the other hand, the disrupted appearance of the NVJs in *scs2*Δ cells can also be caused by a functional or structural disruption of this contact site. This has to be determined in future studies.

Scs2 together with six other proteins is involved in tethering endoplasmic reticulum-plasma membrane (ER-PM) junctions (Manford *et al.*, 2012). So, it wouldn't be surprising, if Scs2 is also part of the NVJ, even though it plays no essential role. Additionally, it is known, that not only Nvj1, Vac8, Osh1 and Tsc13 (Pan *et al.*, 2000a; Kohlwein *et al.*, 2001; Levine and Munro, 2001) are located at the contact site between nucleus and vacuole, but also different proteins, like Nvj2, Nvj3, Lam5, Lam6, Mdm1 and Vps13 (Toulmay and Prinz, 2011; Elbaz-Alon *et al.*, 2015b; Gatta *et al.*, 2015; Henne *et al.*, 2015; Murley *et al.*, 2015; Lang *et al.*, 2015b). There are also hints that the tethering of vacuole and ER can take place in the absence of Nvj1 (Henne *et al.*, 2015). Lam6 is an integral ER membrane protein and is not only localized to the NVJs via its interaction with Vac8, but is also found at two other contact sites, the ERMES and the vCLAMP. Lam6 mediates crosstalk between these two cellular contact sites (Murley *et al.*, 2015; Elbaz-Alon *et al.*, 2015b). Also Mdm1 and its paralogue Nvj3 were shown to be interorganellar tethering proteins, that are localized to the NVJ independent of Nvj1 (Henne *et al.*, 2015). It is unclear, to what extent the afore mentioned proteins are involved in the formation of the NVJs or if this contact site represents an interaction possibility for the respective proteins. Since the most relevant backbone of the NVJ is formed by Nvj1 and Vac8, the absence of one of these two proteins leads to reduced formation of NVJs (Pan *et al.*, 2000a). Nevertheless, this means, that the NVJ is more complex than initially thought.

To examine the role of Scs2 in PMN/ NVJ-phagy, the degradation of GFP-Osh1 as well as Nop1-GFP was measured in the respective knockout strains (Chapter 4.2.2). The degradation of GFP-Osh1 was slightly increased in *scs2*Δ cells in comparison to *nvj1*Δ and *nvj1*Δ *scs2*Δ cells (Figure 4.8 A, B). The impaired NVJ in the *SCS2* knockout strain seemed to not have any impact on the degradation of GFP-Osh1. Although it is known, that Scs2 as well as Nvj1

are interaction partners of Osh1 (Loewen *et al.*, 2003; Kvam and Goldfarb, 2004). However, the results obtained for GFP-Osh1 have to be handled with care, since also degradation of GFP-Osh1 independent of PMN/ NVJ-phagy is possible (Chapter 5.1). Therefore, it is considered, that GFP-Osh1 might be degraded via an alternative autophagic pathway in the respective knockout strains. But it can't be ruled out, that the interaction with Scs2 and Nvj1 somehow effects the degradation of GFP-Osh1.

The degradation of Nop1-GFP was wild type like in *scs2*Δ, *nvj1*Δ and in *nvj1*Δ *scs2*Δ cells (Figure 4.8 C, D). As PMN/ NVJ-phagy is blocked in *nvj1*Δ cells, degradation of Nop1-GFP in *nvj1*Δ *scs2*Δ cells can take place via Atg39 dependent macronucleophagy. How degradation of the nucleolar marker takes place in *scs2*Δ cells is unclear. It could take place via PMN/ NVJ-phagy, although, this mechanism now is considered to primarily degrade the NVJ and not nuclear content as initially thought (Chapter 5.2.3*).* It is also unknown, if the partially disrupted NVJ had an impact on degradation of Nop1-GFP via this micronucleophagic pathway. However, it is more probable, that also in *scs2*Δ cells, degradation of Nop1-GFP takes place in a Atg39 dependent macronucleophagic manner, as recently described (Mochida *et al.*, 2015).

Mdm1 and Nvj3 have been shown to be located at the NVJs. In the absence of Mdm1 and Nvj3 PMN vesicles are formed, indicating, that both proteins aren't required for PMN/ NVJ-phagy. Furthermore, Mdm1-GFP was observed to be incorporated in protrusions into the vacuole. Meaning, that Mdm1 is degraded in a manner comparable to Nvj1 during PMN/ NVJ-phagy (Henne *et al.*, 2015). This implicates, that even though Scs2 isn't involved in PMN/ NVJ-phagy at the first glance, it still can play a role.

5.4.3 A multiple knockout as negative control for PMN/ NVJ-phagy

Mostofa *et al.* (2018) suggested, that *nvj1*Δ cells are deficient for PMN/ NVJ-phagy and *atg39*Δ*atg40*Δ cells are deficient for macronucleophagy. This seems to be reasonable, since they observed a reduction of Nop1-GFP degradation to about 50% in *atg39*Δ*atg40*Δ cells, whereas degradation of Nop1-GFP was wild type like in *nvj1*Δ cells. In fact, in *atg39*Δ *atg40*Δ *nvj1*Δ cells, deficient for micro- and macronucleophagy, degradation of Nop1-GFP was blocked (Rahman *et al.*,

2018). This shows, that the respective knockouts could represent reasonable negative controls for PMN/ NVJ-phagy or macronucleophagy.

Though within this present study, degradation of Nop1-GFP was shown to be completely blocked in *atg39*Δ *atg40*Δ cells (Figure 4.15). This was also observed by Mochida *et al.* (2015). They also observed wild type like degradation of Nop1-GFP in *nvj1*Δ cells, whereas within this study a reduction to about 50% was seen. Possibly, the diverse results of the different studies are caused by the different genetic yeast backgrounds.

Based on these diverse results it is unclear, if the respective knockout strains would represent suitable negative controls for PMN/ NVJ-phagy or macronucleophagy.

5.5 Pho8-GFP and Nab-NLS-mCherry are no suitable marker proteins

5.5.1 A differentiation between macro- and microautophagy via the degradation of Pho8-GFP is not possible

A differentiation between micro- and macroautophagy via the degradation of the so far used marker proteins is not possible. Therefore, the vacuolar protein Pho8 (Klionsky and Emr, 1989) was considered to be a possibility to get an insight into these two mechanisms. Macroautophagy is based on the fusion of the autophagosomal membrane and the disposal of the content into the vacuole. This leads to the assumption, that Pho8-GFP isn't degraded during macroautophagy. In contrast to that, during PMN/ NVJ-phagy, the vesicles are surrounded by a vacuolar membrane before the release into the vacuole and therefore, Pho8-GFP was expected to be degraded. Unfortunately, degradation of Pho8-GFP was only blocked in *atg1*Δ and *vac8*Δ cells, but appeared to be wild type like in *nvj1*Δ, *atg39*Δ, *atg40*Δ, *atg39*Δ *atg40*Δ and *atg39*Δ *atg40*Δ *nvj1*Δ cells (Figure 4.22). Microscopic evaluation of Pho8-GFP showed only very faint signals at the vacuolar membrane, hardly more intense than cytoplasmic signals (Figure 4.21).

Unfortunately, the obtained results show, that Pho8-GFP was degraded unspecifically. Finally, it can be said, that measurement of Pho8-GFP degradation is not suitable for differentiation of micro- and macroautophagy.

5.5.2 Nab-NLS-mCherry is degraded via unspecific nucleophagy

Nab-NLS-mCherry is a nuclear marker protein (Ryan *et al.*, 2007), that was tested in regard to be an alternative marker protein for measurement of nucleophagy. Surprisingly, degradation of Nab-NLS-mCherry was only blocked in *atg1*Δ cells, but not in all other tested deletion stains, including *vac8*Δ cells (Figure 4.4). This shows, that Nab-NLS-mCherry is not degraded via PMN/ NVJ-phagy, nor the Atg39/ Atg40 dependent macronucleophagy (data not shown), but via an alternative autophagic pathway. Therefore, this marker protein doesn't represent a new possibility to measure nucleophagy.

5.6 Conclusion

This study predicts, that the main goal of PMN is not the degradation of nucleoplasm, but the degradation of the NVJ. Therefore, this process should be renamed into NVJ-phagy. Furthermore, it was shown, that Atg39 is not only involved in macronucleophagy, but also plays a crucial role in PMN/ NVJ-phagy.

6 Bibliography

Abeliovich, H., and Klionsky, D. J. (2001). Autophagy in yeast: mechanistic insights and physiological function. Microbiol Mol Biol Rev *65*, 463–79–tableofcontents.

Agarraberes, F. A., and Dice, J. F. (2001). A molecular chaperone complex at the lysosomal membrane is required for protein translocation. J Cell Sci *114*, 2491–2499.

Ano, Y., Hattori, T., Oku, M., Mukaiyama, H., Baba, M., Ohsumi, Y., Kato, N., and Sakai, Y. (2005). A sorting nexin PpAtg24 regulates vacuolar membrane dynamics during pexophagy via binding to phosphatidylinositol-3-phosphate. Mol Biol Cell *16*, 446–457.

Arias, E., and Cuervo, A. M. (2011). Chaperone-mediated autophagy in protein quality control. Curr Opin Cell Biol *23*, 184–189.

Ariosa, A. R., and Klionsky, D. J. (2016). Autophagy core machinery: overcoming spatial barriers in neurons. J Mol Med (Berl) *94*, 1217–1227.

Baba, M., Osumi, M., Scott, S. V., Klionsky, D. J., and Ohsumi, Y. (1997). Two distinct pathways for targeting proteins from the cytoplasm to the vacuole/lysosome. J Cell Biol *139*, 1687–1695.

Backues, S. K., Orban, D. P., Bernard, A., Singh, K., Cao, Y., and Klionsky, D. J. (2015). Atg23 and Atg27 Act at the Early Stages of Atg9 Trafficking in S. cerevisiae. Traffic *16*, 172–190.

Balderhaar, H. J. K., Arlt, H., Ostrowicz, C., Bröcker, C., Sündermann, F., Brandt, R., Babst, M., and Ungermann, C. (2010). The Rab GTPase Ypt7 is linked to retromer-mediated receptor recycling and fusion at the yeast late endosome. J Cell Sci *123*, 4085–4094.

Bandyopadhyay, U., Kaushik, S., Varticovski, L., and Cuervo, A. M. (2008). The chaperone-mediated autophagy receptor organizes in dynamic protein complexes at the lysosomal membrane. Mol Cell Biol *28*, 5747–5763.

Bas, L., Papinski, D., Licheva, M., Torggler, R., Rohringer, S., Schuschnig, M., and Kraft, C. (2018). Reconstitution reveals Ykt6 as the autophagosomal SNARE in autophagosome-vacuole fusion. J. Cell Biol. *217*, 3656–3669.

Baudin, A., Ozier-Kalogeropoulos, O., Denouel, A., Lacroute, F., and Cullin, C. (1993). A simple and efficient method for direct gene deletion in Saccharomyces cerevisiae. Nucleic Acids Res *21*, 3329–3330.

Cao, Y., and Klionsky, D. J. (2007). Atg26 is not involved in autophagy-related pathways in Saccharomyces cerevisiae. Autophagy *3*, 17–20.

Cao, Y., Cheong, H., Song, H., and Klionsky, D. J. (2008). In vivo reconstitution of autophagy in Saccharomyces cerevisiae. J Cell Biol *182*, 703–713.

Cebollero, E., der Vaart, van, A., Zhao, M., Rieter, E., Klionsky, D. J., Helms, J. B., and Reggiori, F. (2012). Phosphatidylinositol-3-phosphate clearance plays a key role in autophagosome completion. Curr Biol *22*, 1545–1553.

Chang, T., Schroder, L., Thomson, J., Klocman, A., Tomasini, A., Stromhaug, P., and Dunn, W. (2005). PpATG9 encodes a novel membrane protein that traffics to vacuolar membranes, which sequester peroxisomes during pexophagy in Pichia pastoris. Mol Biol Cell *16*, 4941–4953.

Cheong, H., Nair, U., Geng, J., and Klionsky, D. J. (2008). The Atg1 kinase complex is involved in the regulation of protein recruitment to initiate sequestering vesicle formation for nonspecific autophagy in Saccharomyces cerevisiae. Mol Biol Cell *19*, 668–681.

Darsow, T., Rieder, S., and Emr, S. (1997). A multispecificity syntaxin homologue, Vam3p, essential for autophagic and biosynthetic protein transport to the vacuole. J Cell Biol *138*, 517–529.

Davies, C. W., Stjepanovic, G., and Hurley, J. H. (2015). How the Atg1 complex assembles to initiate autophagy. Autophagy *11*, 185–186.

Dawaliby, R., and Mayer, A. (2010). Microautophagy of the nucleus coincides with a vacuolar diffusion barrier at nuclear-vacuolar junctions. Mol Biol Cell *21*, 4173–4183.

Delorme-Axford, E., Guimaraes, R. S., Reggiori, F., and Klionsky, D. J. (2014). The yeast Saccharomyces cerevisiae: An overview of methods to study autophagy progression. Methods.

Dietrich, L. E. P., Gurezka, R., Veit, M., and Ungermann, C. (2004). The SNARE Ykt6 mediates protein palmitoylation during an early stage of homotypic vacuole fusion. Embo J *23*, 45–53.

Duina, A. A., Miller, M. E., and Keeney, J. B. (2014). Budding yeast for budding geneticists: a primer on the Saccharomyces cerevisiae model system. Genetics *197*, 33–48.

Dunn, W., Cregg, J., Kiel, J., Der Klei, Van, I., Oku, M., Sakai, Y., Sibirny, A., Stasyk, O., and Veenhuis, M. (2005). Pexophagy: the selective autophagy of peroxisomes. Autophagy *1*, 75–83.

Elbaz, Y., and Schuldiner, M. (2011). Staying in touch: the molecular era of organelle contact sites. Trends in Biochemical Sciences *36*, 616–623.

Elbaz-Alon, Y., Eisenberg-Bord, M., Shinder, V., Stiller, S. B., Shimoni, E., Wiedemann, N., Geiger, T., and Schuldiner, M. (2015a). Lam6 Regulates the Extent of Contacts between Organelles. Cell Rep *12*, 7–14.

Elbaz-Alon, Y., Eisenberg-Bord, M., Shinder, V., Stiller, S. B., Shimoni, E., Wiedemann, N., Geiger, T., and Schuldiner, M. (2015b). Lam6 Regulates the Extent of Contacts between Organelles. Cell Rep *12*, 7–14.

Epple, U. D., Suriapranata, I., Eskelinen, E.-L., and Thumm, M. (2001).

Aut5/Cvt17p, a putative lipase essential for disintegration of autophagic bodies inside the vacuole. J Bacteriol *183*, 5942–5955.

Faergeman, N. J., Feddersen, S., Christiansen, J. K., Larsen, M. K., Schneiter, R., Ungermann, C., Mutenda, K., Roepstorff, P., and Knudsen, J. (2004). Acyl-CoA-binding protein, Acb1p, is required for normal vacuole function and ceramide synthesis in Saccharomyces cerevisiae. Biochem J *380*, 907–918.

Farré, J.-C., and Subramani, S. (2004). Peroxisome turnover by micropexophagy: an autophagy-related process. Trends Cell Biol *14*, 515–523.

Farré, J.-C., and Subramani, S. (2016). Mechanistic insights into selective autophagy pathways: lessons from yeast. Nat Rev Mol Cell Biol *17*, 537–552.

Farré, J.-C., Krick, R., Subramani, S., and Thumm, M. (2009). Turnover of organelles by autophagy in yeast. Curr Opin Cell Biol *21*, 522–530.

Farré, J.-C., Manjithaya, R., Mathewson, R. D., and Subramani, S. (2008). PpAtg30 tags peroxisomes for turnover by selective autophagy. Dev Cell *14*, 365–376.

Feng, Y., He, D., Yao, Z., and Klionsky, D. J. (2013). The machinery of macroautophagy. Cell Res *24*, 24–41.

Fleckenstein, D., Rohde, M., Klionsky, D., and Rudiger, M. (1998). Yel013p (Vac8p), an armadillo repeat protein related to plakoglobin and importin alpha is associated with the yeast vacuole membrane. J Cell Sci *111 (Pt 20)*, 3109–3118.

Fry, M. R., Thomson, J. M., Tomasini, A. J., and Dunn, W. A. (2006). Early and late molecular events of glucose-induced pexophagy in Pichia pastoris require Vac8. Autophagy *2*, 280–288.

Fujioka, Y., Suzuki, S. W., Yamamoto, H., Kondo-Kakuta, C., Kimura, Y., Hirano, H., Akada, R., Inagaki, F., Ohsumi, Y., and Noda, N. N. (2014). Structural basis of starvation-induced assembly of the autophagy initiation complex. Nat Struct Mol Biol, 1–12.

Fukui, S., Kawamoto, S., Yasuhara, S., Tanaka, A., and Osumi, M. (1975a). Microbody of methanol-grown yeasts. Localization of catalase and flavin-dependent alcohol oxidase in the isolated microbody. Eur J Biochem *59*, 561–566.

Fukui, S., Tanaka, A., Kawamoto, S., Yasuhara, S., Teranishi, Y., and Osumi, M. (1975b). Ultrastructure of methanol-utilizing yeast cells: appearance of microbodies in relation to high catalase activity. J Bacteriol *123*, 317–328.

Gable, K., Garton, S., Napier, J. A., and Dunn, T. M. (2004). Functional characterization of the Arabidopsis thaliana orthologue of Tsc13p, the enoyl reductase of the yeast microsomal fatty acid elongating system. J Exp Bot *55*, 543–545.

Galluzzi, L., Pedro, J. M. B.-S., Levine, B., Green, D. R., and Kroemer, G.

(2017). Pharmacological modulation of autophagy: therapeutic potential and persisting obstacles. Nature Publishing Group *16*, 1–25.

Gatta, A. T., Wong, L. H., Sere, Y. Y., Calderón-Noreña, D. M., Cockcroft, S., Menon, A. K., and Levine, T. P. (2015). A new family of StART domain proteins at membrane contact sites has a role in ER-PM sterol transport. Elife *4*, 400.

Geng, J., and Klionsky, D. J. (2008). The Atg8 and Atg12 ubiquitin-like conjugation systems in macroautophagy. “Protein modifications: beyond the usual suspects” review series. EMBO Rep *9*, 859–864.

Goffeau, A. *et al.* (1996). Life with 6000 genes. Science *274*, 546.

Hanada, T., Noda, N. N., Satomi, Y., Ichimura, Y., Fujioka, Y., Takao, T., Inagaki, F., and Ohsumi, Y. (2007). The Atg12-Atg5 conjugate has a novel E3-like activity for protein lipidation in autophagy. J Biol Chem *282*, 37298–37302.

Hanson, S. J., and Wolfe, K. H. (2017). An Evolutionary Perspective on Yeast Mating-Type Switching. Genetics *206*, 9–32.

Hariri, H., Rogers, S., Ugrankar, R., Liu, Y. L., Feathers, J. R., and Henne, W. M. (2018). Lipid droplet biogenesis is spatially coordinated at ER-vacuole contacts under nutritional stress. EMBO Rep *19*, 57–72.

He, C., Song, H., Yorimitsu, T., Monastyrska, I., Yen, W.-L., Legakis, J. E., and Klionsky, D. J. (2006). Recruitment of Atg9 to the preautophagosomal structure by Atg11 is essential for selective autophagy in budding yeast. J Cell Biol *175*, 925–935.

Henne, W. M., Zhu, L., Balogi, Z., Stefan, C., Pleiss, J. A., and Emr, S. D. (2015). Mdm1/Snx13 is a novel ER-endolysosomal interorganelle tethering protein. J Cell Biol *210*, 541–551.

Hofer, S., Kainz, K., Zimmermann, A., Bauer, M. A., Pendl, T., Poglitsch, M., Madeo, F., and Carmona-Gutierrez, D. (2018). Studying Huntington's Disease in Yeast: From Mechanisms to Pharmacological Approaches. Front Mol Neurosci *11*, 318.

Huang, W. P., Scott, S. V., Kim, J., and Klionsky, D. J. (2000). The itinerary of a vesicle component, Aut7p/Cvt5p, terminates in the yeast vacuole via the autophagy/Cvt pathways. J Biol Chem *275*, 5845–5851.

Hurley, J. H. (2010). The ESCRT complexes. Critical Reviews in Biochemistry and Molecular Biology *45*, 463–487.

Hurley, J. H., and Hanson, P. I. (2010). Membrane budding and scission by the ESCRT machinery: it's all in the neck. Nat Rev Mol Cell Biol *11*, 556–566.

Hutchins, M., Veenhuis, M., and Klionsky, D. (1999). Peroxisome degradation in Saccharomyces cerevisiae is dependent on machinery of macroautophagy and the Cvt pathway. J Cell Sci *112*, 4079–4087.

Ichimura, Y. *et al.* (2000). A ubiquitin-like system mediates protein lipidation.

Nature *408*, 488–492.

Janke, C. *et al.* (2004). A versatile toolbox for PCR-based tagging of yeast genes: new fluorescent proteins, more markers and promoter substitution cassettes. Yeast *21*, 947–962.

Jao, C. C., Ragusa, M. J., Stanley, R. E., and Hurley, J. H. (2013). What the N-terminal domain of Atg13 looks like and what it does: A HORMA fold required for PtdIns 3-kinase recruitment. Autophagy *9*.

Jeong, H., Park, J., Kim, H.-I., Lee, M., Ko, Y.-J., Lee, S., Jun, Y., and Lee, C. (2017). Mechanistic insight into the nucleus-vacuole junction based on the Vac8p-Nvj1p crystal structure. Proc Natl Acad Sci U S A *114*, E4539–E4548.

Kabeya, Y., Noda, N. N., Fujioka, Y., Suzuki, K., Inagaki, F., and Ohsumi, Y. (2009). Characterization of the Atg17-Atg29-Atg31 complex specifically required for starvation-induced autophagy in Saccharomyces cerevisiae. Biochem Biophys Res Commun *389*, 612–615.

Kagiwada, S., Hosaka, K., Murata, M., Nikawa, J., and Takatsuki, A. (1998). The Saccharomyces cerevisiae SCS2 gene product, a homolog of a synaptobrevin-associated protein, is an integral membrane protein of the endoplasmic reticulum and is required for inositol metabolism. J Bacteriol *180*, 1700–1708.

Kamada, Y., Funakoshi, T., Shintani, T., Nagano, K., Ohsumi, M., and Ohsumi, Y. (2000). Tor-mediated induction of autophagy via an Apg1 protein kinase complex. J Cell Biol *150*, 1507–1513.

Kaufmann, A., Beier, V., Franquelim, H. G., and Wollert, T. (2014). Molecular mechanism of autophagic membrane-scaffold assembly and disassembly. Cell *156*, 469–481.

Kawamata, T., Kamada, Y., Kabeya, Y., Sekito, T., and Ohsumi, Y. (2008). Organization of the pre-autophagosomal structure responsible for autophagosome formation. Mol Biol Cell *19*, 2039–2050.

Kihara, A., Noda, T., Ishihara, N., and Ohsumi, Y. (2001). Two distinct Vps34 phosphatidylinositol 3-kinase complexes function in autophagy and carboxypeptidase Y sorting in Saccharomyces cerevisiae. J Cell Biol *152*, 519–530.

Kim, J., and Klionsky, D. J. (2000). Autophagy, cytoplasm-to-vacuole targeting pathway, and pexophagy in yeast and mammalian cells. Annu Rev Biochem *69*, 303–342.

Kim, J., Huang, W., and Klionsky, D. (2001a). Membrane recruitment of Aut7p in the autophagy and cytoplasm to vacuole targeting pathways requires Aut1p, Aut2p, and the autophagy conjugation complex. J Cell Biol *152*, 51–64.

Kim, J., Kamada, Y., Stromhaug, P. E., Guan, J., Hefner-Gravink, A., Baba, M., Scott, S. V., Ohsumi, Y., Dunn, W. A., and Klionsky, D. J. (2001b). Cvt9/Gsa9 functions in sequestering selective cytosolic cargo destined for the vacuole. J

Cell Biol *153*, 381–396.

Kim, J., Scott, S., Oda, M., and Klionsky, D. (1997). Transport of a large oligomeric protein by the cytoplasm to vacuole protein targeting pathway. J Cell Biol *137*, 609–618.

Kirisako, T., Ichimura, Y., Okada, H., Kabeya, Y., Mizushima, N., Yoshimori, T., Ohsumi, M., Takao, T., Noda, T., and Ohsumi, Y. (2000). The reversible modification regulates the membrane-binding state of Apg8/Aut7 essential for autophagy and the cytoplasm to vacuole targeting pathway. J Cell Biol *151*, 263–276.

Klionsky, D., and Emr, S. (1989). Membrane protein sorting: biosynthesis, transport and processing of yeast vacuolar alkaline phosphatase. Embo J *8*, 2241–2250.

Klionsky, D., and Ohsumi, Y. (1999). Vacuolar import of proteins and organelles from the cytoplasm. Annu Rev Cell Dev Biol *15*, 1–32.

Klionsky, D., Cueva, R., and Yaver, D. (1992). Aminopeptidase I of Saccharomyces cerevisiae is localized to the vacuole independent of the secretory pathway. J Cell Biol *119*, 287–299.

Knop M, Siegers, K., Pereira, G., Zachariae, W., Winsor, B., Nasmyth, K., and Schiebel, E. (1999). Epitope tagging of yeast genes using a PCR-based strategy: more tags and improved practical routines. Yeast *15*, 963–972.

Kohlwein, S. D., Eder, S., Oh, C. S., Martin, C. E., Gable, K., Bacikova, D., and Dunn, T. (2001). Tsc13p is required for fatty acid elongation and localizes to a novel structure at the nuclear-vacuolar interface in Saccharomyces cerevisiae. Mol Cell Biol *21*, 109–125.

Kondo-Okamoto, N., Noda, N. N., Suzuki, S. W., Nakatogawa, H., Takahashi, I., Matsunami, M., Hashimoto, A., Inagaki, F., Ohsumi, Y., and Okamoto, K. (2012). Autophagy-related Protein 32 Acts as Autophagic Degron and Directly Initiates Mitophagy. Journal of Biological Chemistry *287*, 10631–10638.

Kraft, C., Reggiori, F., and Peter, M. (2009). Selective types of autophagy in yeast. BBA - Molecular Cell Research *1793*, 1404–1412.

Krick, R., Muehe, Y., Prick, T., Bremer, S., Schlotterhose, P., Eskelinen, E.-L., Millen, J., Goldfarb, D. S., and Thumm, M. (2008). Piecemeal microautophagy of the nucleus requires the core macroautophagy genes. Mol Biol Cell *19*, 4492–4505.

Krick, R., Mühe, Y., Prick, T., Bredschneider, M., Bremer, S., Wenzel, D., Eskelinen, E.-L., and Thumm, M. (2009a). Piecemeal microautophagy of the nucleus: genetic and morphological traits. Autophagy *5*, 270–272.

Krick, R., Mühe, Y., Prick, T., Bredschneider, M., Bremer, S., Wenzel, D., Eskelinen, E.-L., and Thumm, M. (2009b). Piecemeal microautophagy of the nucleus: genetic and morphological traits. Autophagy *5*, 270–272.

Krick, R., Tolstrup, J., Appelles, A., Henke, S., and Thumm, M. (2006). The relevance of the phosphatidylinositolphosphat-binding motif FRRGT of Atg18 and Atg21 for the Cvt pathway and autophagy. FEBS Letters *580*, 4632–4638.

Kuma, A., Mizushima, N., Ishihara, N., and Ohsumi, Y. (2002). Formation of the approximately 350-kDa Apg12-Apg5.Apg16 multimeric complex, mediated by Apg16 oligomerization, is essential for autophagy in yeast. J Biol Chem *277*, 18619–18625.

Kvam, E., and Goldfarb, D. (2007). Nucleus-vacuole junctions and piecemeal microautophagy of the nucleus in S. cerevisiae. Autophagy *3*, 85–92.

Kvam, E., and Goldfarb, D. S. (2004). Nvj1p is the outer-nuclear-membrane receptor for oxysterol-binding protein homolog Osh1p in Saccharomyces cerevisiae. J Cell Sci *117*, 4959–4968.

Kvam, E., and Goldfarb, D. S. (2006). Structure and function of nucleus-vacuole junctions: outer-nuclear-membrane targeting of Nvj1p and a role in tryptophan uptake. J Cell Sci *119*, 3622–3633.

Kvam, E., Gable, K., Dunn, T. M., and Goldfarb, D. S. (2005). Targeting of Tsc13p to nucleus-vacuole junctions: a role for very-long-chain fatty acids in the biogenesis of microautophagic vesicles. Mol Biol Cell *16*, 3987–3998.

Lang, A. B., John Peter, A. T., Walter, P., and Kornmann, B. (2015a). ER-mitochondrial junctions can be bypassed by dominant mutations in the endosomal protein Vps13. J. Cell Biol. *210*, 883–890.

Lang, A. B., Peter, A. T. J., Walter, P., and Kornmann, B. (2015b). ER–mitochondrial junctions can be bypassed by dominant mutations in the endosomal protein Vps13. J Cell Biol *210*, 883–890.

Levine, T., and Munro, S. (2001). Dual targeting of Osh1p, a yeast homologue of oxysterol-binding protein, to both the Golgi and the nucleus-vacuole junction. Mol Biol Cell *12*, 1633–1644.

Li, W.-W., Li, J., and Bao, J.-K. (2012). Microautophagy: lesser-known self-eating. Cell Mol Life Sci *69*, 1125–1136.

Loewen, C. J. R., Roy, A., and Levine, T. P. (2003). A conserved ER targeting motif in three families of lipid binding proteins and in Opi1p binds VAP. Embo J *22*, 2025–2035.

Longtine, M. S., McKenzie, A., Demarini, D. J., Shah, N. G., Wach, A., Brachat, A., Philippsen, P., and Pringle, J. R. (1998). Additional modules for versatile and economical PCR-based gene deletion and modification in Saccharomyces cerevisiae. Yeast *14*, 953–961.

Luo, M., Zhao, X., Song, Y., Cheng, H., and Zhou, R. (2016). Nuclear autophagy: An evolutionarily conserved mechanism of nuclear degradation in the cytoplasm. Autophagy *12*, 1973–1983.

Manford, A. G., Stefan, C. J., Yuan, H. L., Macgurn, J. A., and Emr, S. D.

(2012). ER-to-plasma membrane tethering proteins regulate cell signaling and ER morphology. Dev Cell *23*, 1129–1140.

Manik, M. K., Yang, H., Tong, J., and Im, Y. J. (2017). Structure of Yeast OSBP-Related Protein Osh1 Reveals Key Determinants for Lipid Transport and Protein Targeting at the Nucleus-Vacuole Junction. Structure *25*, 617–629.e3.

Mao, K., Chew, L. H., Inoue-Aono, Y., Cheong, H., Nair, U., Popelka, H., Yip, C. K., and Klionsky, D. J. (2013a). Atg29 phosphorylation regulates coordination of the Atg17-Atg31-Atg29 complex with the Atg11 scaffold during autophagy initiation. Proc Natl Acad Sci U S A *110*, E2875–E2884.

Mao, K., Wang, K., Liu, X., and Klionsky, D. J. (2013b). The Scaffold Protein Atg11 Recruits Fission Machinery to Drive Selective Mitochondria Degradation by Autophagy. Developmental Cell *26*, 9–18.

Mari, M., Griffith, J., Rieter, E., Krishnappa, L., Klionsky, D. J., and Reggiori, F. (2010). An Atg9-containing compartment that functions in the early steps of autophagosome biogenesis. J Cell Biol *190*, 1005–1022.

Matsuura, A., Tsukada, M., Wada, Y., and Ohsumi, Y. (1997). Apg1p, a novel protein kinase required for the autophagic process in Saccharomyces cerevisiae. Gene *192*, 245–250.

Mayer, A., and Wickner, W. (1997). Docking of yeast vacuoles is catalyzed by the Ras-like GTPase Ypt7p after symmetric priming by Sec18p (NSF). J. Cell Biol. *136*, 307–317.

Mekhail, K., Seebacher, J., Gygi, S. P., and Moazed, D. (2008). Role for perinuclear chromosome tethering in maintenance of genome stability. Nature *456*, 667–670.

Menzies, F. M. *et al.* (2017). Autophagy and Neurodegeneration: Pathogenic Mechanisms and Therapeutic Opportunities. Neuron *93*, 1015–1034.

Mesmin, B., and Antonny, B. (2016). The counterflow transport of sterols and PI4P. Biochim Biophys Acta *1861*, 940–951.

Mijaljica, D., Prescott, M., and Devenish, R. J. (2012). A late form of nucleophagy in Saccharomyces cerevisiae. PLoS ONE *7*, e40013.

Millen, J. I., Krick, R., Prick, T., Thumm, M., and Goldfarb, D. S. (2009). Measuring piecemeal microautophagy of the nucleus in Saccharomyces cerevisiae. Autophagy *5*, 75–81.

Millen, J. I., Pierson, J., Kvam, E., Olsen, L. J., and Goldfarb, D. S. (2008). The luminal N-terminus of yeast Nvj1 is an inner nuclear membrane anchor. Traffic *9*, 1653–1664.

Miller, S. B. M., Mogk, A., and Bukau, B. (2015). Spatially Organized Aggregation of Misfolded Proteins as Cellular Stress Defense Strategy. J Mol Biol, 1–11.

Mizushima, N. (2010). The role of the Atg1/ULK1 complex in autophagy regulation. Curr Opin Cell Biol *22*, 132–139.

Mizushima, N., and Komatsu, M. (2011). Autophagy: renovation of cells and tissues. Cell *147*, 728–741.

Mizushima, N., Kuma, A., Kobayashi, Y., Yamamoto, A., Matsubae, M., Takao, T., Natsume, T., Ohsumi, Y., and Yoshimori, T. (2003). Mouse Apg16L, a novel WD-repeat protein, targets to the autophagic isolation membrane with the Apg12-Apg5 conjugate. J Cell Sci *116*, 1679–1688.

Mizushima, N., Noda, T., and Ohsumi, Y. (1999). Apg16p is required for the function of the Apg12p-Apg5p conjugate in the yeast autophagy pathway. Embo J *18*, 3888–3896.

Mizushima, N., Sugita, H., Yoshimori, T., and Ohsumi, Y. (1998). A new protein conjugation system in human. The counterpart of the yeast Apg12p conjugation system essential for autophagy. J Biol Chem *273*, 33889–33892.

Mizushima, N., Yamamoto, A., Hatano, M., Kobayashi, Y., Kabeya, Y., Suzuki, K., Tokuhisa, T., Ohsumi, Y., and Yoshimori, T. (2001). Dissection of autophagosome formation using Apg5-deficient mouse embryonic stem cells. J Cell Biol *152*, 657–668.

Mochida, K., Oikawa, Y., Kimura, Y., Kirisako, H., Hirano, H., Ohsumi, Y., and Nakatogawa, H. (2015). Receptor-mediated selective autophagy degrades the endoplasmic reticulum and the nucleus. Nature *522*, 359–362.

Monastyrska, I., Kiel, J., Krikken, A., Komduur, J., Veenhuis, M., and Der Klei, Van, I. (2005). The Hansenula polymorpha ATG25 gene encodes a novel coiled-coil protein that is required for macropexophagy. Autophagy *1*, 92–100.

Mostofa, M. G. *et al.* (2018). CLIP and cohibin separate rDNA from nucleolar proteins destined for degradation by nucleophagy. J. Cell Biol. *217*, 2675–2690.

Motley, A. M., Nuttall, J. M., and Hettema, E. H. (2012). Pex3-anchored Atg36 tags peroxisomes for degradation in Saccharomyces cerevisiae. Embo J *31*, 2852–2868.

Mukaiyama, H., Baba, M., Osumi, M., Aoyagi, S., Kato, N., Ohsumi, Y., and Sakai, Y. (2004). Modification of a ubiquitin-like protein Paz2 conducted micropexophagy through formation of a novel membrane structure. Mol Biol Cell *15*, 58–70.

Mukaiyama, H., Oku, M., Baba, M., Samizo, T., Hammond, A. T., Glick, B. S., Kato, N., and Sakai, Y. (2002). Paz2 and 13 other PAZ gene products regulate vacuolar engulfment of peroxisomes during micropexophagy. Genes Cells *7*, 75–90.

Murley, A., Sarsam, R. D., Toulmay, A., Yamada, J., Prinz, W. A., and Nunnari, J. (2015). Ltc1 is an ER-localized sterol transporter and a component of ER-mitochondria and ER-vacuole contacts. J Cell Biol *209*, 539–548.

Nair, U., Cao, Y., Xie, Z., and Klionsky, D. J. (2010). Roles of the lipid-binding motifs of Atg18 and Atg21 in the cytoplasm to vacuole targeting pathway and autophagy. Journal of Biological Chemistry *285*, 11476–11488.

Nakatogawa, H., and Mochida, K. (2015). Reticulophagy and nucleophagy: New findings and unsolved issues. Autophagy *11*, 2377–2378.

Nakatogawa, H., Ichimura, Y., and Ohsumi, Y. (2007). Atg8, a ubiquitin-like protein required for autophagosome formation, mediates membrane tethering and hemifusion. Cell *130*, 165–178.

Nakatogawa, H., Suzuki, K., Kamada, Y., and Ohsumi, Y. (2009). Dynamics and diversity in autophagy mechanisms: lessons from yeast. Nat Rev Mol Cell Biol *10*, 458–467.

Nazarko, T. Y., Farré, J.-C., and Subramani, S. (2009). Peroxisome size provides insights into the function of autophagy-related proteins. Mol Biol Cell *20*, 3828–3839.

Nazarko, T. Y., Polupanov, A. S., Manjithaya, R. R., Subramani, S., and Sibirny, A. A. (2007). The requirement of sterol glucoside for pexophagy in yeast is dependent on the species and nature of peroxisome inducers. Mol Biol Cell *18*, 106–118.

Nazarko, V. Y., Nazarko, T. Y., Farré, J.-C., Stasyk, O. V., Warnecke, D., Ulaszewski, S., Cregg, J. M., Sibirny, A. A., and Subramani, S. (2011). Atg35, a micropexophagy-specific protein that regulates micropexophagic apparatus formation in Pichia pastoris. Autophagy *7*, 375–385.

Nigavekar, S. S., Tan, Y. S. H., and Cannon, J. F. (2002). Glc8 is a glucose-repressible activator of Glc7 protein phosphatase-1. Archives of Biochemistry and Biophysics *404*, 71–79.

Noda, T., and Ohsumi, Y. (1998). Tor, a phosphatidylinositol kinase homologue, controls autophagy in yeast. J Biol Chem *273*, 3963–3966.

Noda, T., Kim, J., Huang, W. P., Baba, M., Tokunaga, C., Ohsumi, Y., and Klionsky, D. J. (2000). Apg9p/Cvt7p is an integral membrane protein required for transport vesicle formation in the Cvt and autophagy pathways. J Cell Biol *148*, 465–480.

Noda, T., Suzuki, K., and Ohsumi, Y. (2002). Yeast autophagosomes: de novo formation of a membrane structure. Trends Cell Biol *12*, 231–235.

Obara, K., Sekito, T., and Ohsumi, Y. (2006). Assortment of phosphatidylinositol 3-kinase complexes--Atg14p directs association of complex I to the pre-autophagosomal structure in Saccharomyces cerevisiae. Mol Biol Cell *17*, 1527–1539.

Oda, M. N., Scott, S. V., Hefner-Gravink, A., Caffarelli, A. D., and Klionsky, D. J. (1996). Identification of a cytoplasm to vacuole targeting determinant in aminopeptidase I. J Cell Biol *132*, 999–1010.

Ohashi, Y. *et al.* (2016). Characterization of Atg38 and NRBF2, a fifth subunit of the autophagic Vps34/PIK3C3 complex. Autophagy *12*, 2129–2144.

Ohashi, Y., and Munro, S. (2010). Membrane delivery to the yeast autophagosome from the Golgi-endosomal system. Mol Biol Cell *21*, 3998–4008.

Oku, M., Warnecke, D., Noda, T., Müller, F., Heinz, E., Mukaiyama, H., Kato, N., and Sakai, Y. (2003). Peroxisome degradation requires catalytically active sterol glucosyltransferase with a GRAM domain. Embo J *22*, 3231–3241.

Pan, X., and Goldfarb, D. S. (1998). YEB3/VAC8 encodes a myristylated armadillo protein of the Saccharomyces cerevisiae vacuolar membrane that functions in vacuole fusion and inheritance. J Cell Sci *111 (Pt 15)*, 2137–2147.

Pan, X., Roberts, P., Chen, Y., Kvam, E., Shulga, N., Huang, K., Lemmon, S., and Goldfarb, D. S. (2000a). Nucleus-vacuole junctions in Saccharomyces cerevisiae are formed through the direct interaction of Vac8p with Nvj1p. Mol Biol Cell *11*, 2445–2457.

Pan, X., Roberts, P., Chen, Y., Kvam, E., Shulga, N., Huang, K., Lemmon, S., and Goldfarb, D. S. (2000b). Nucleus-vacuole junctions in Saccharomyces cerevisiae are formed through the direct interaction of Vac8p with Nvj1p. Mol Biol Cell *11*, 2445–2457.

Park, Y.-E., Hayashi, Y. K., Bonne, G., Arimura, T., Noguchi, S., Nonaka, I., and Nishino, I. (2009). Autophagic degradation of nuclear components in mammalian cells. Autophagy *5*, 795–804.

Parzych, K. R., Ariosa, A., Mari, M., and Klionsky, D. J. (2018). A newly characterized vacuolar serine carboxypeptidase, Atg42/Ybr139w, is required for normal vacuole function and the terminal steps of autophagy in the yeast Saccharomyces cerevisiae. Mol Biol Cell *29*, 1089–1099.

Ragusa, M. J., Stanley, R. E., and Hurley, J. H. (2012). Architecture of the Atg17 Complex as a Scaffold for Autophagosome Biogenesis. Cell *151*, 1501–1512.

Rahman, M. A., Mostofa, M. G., and Ushimaru, T. (2018). The Nem1/Spo7-Pah1/lipin axis is required for autophagy induction after TORC1 inactivation. Febs J *285*, 1840–1860.

Ramaswamy, N. T., Li, L., Khalil, M., and Cannon, J. F. (1998). Regulation of yeast glycogen metabolism and sporulation by Glc7p protein phosphatase. Genetics *149*, 57–72.

Raychaudhuri, S., and Prinz, W. A. (2010). The diverse functions of oxysterol-binding proteins. Annu Rev Cell Dev Biol *26*, 157–177.

Reggiori, F., and Klionsky, D. (2002). Autophagy in the eukaryotic cell. Eukaryot Cell *1*, 11–21.

Reggiori, F., Tucker, K., Stromhaug, P., and Klionsky, D. (2004). The Atg1-

Atg13 complex regulates Atg9 and Atg23 retrieval transport from the pre-autophagosomal structure. Dev Cell *6*, 79–90.

Roberts, P., Moshitch-Moshkovitz, S., Kvam, E., O'Toole, E., Winey, M., and Goldfarb, D. (2003). Piecemeal microautophagy of nucleus in Saccharomyces cerevisiae. Mol Biol Cell *14*, 129–141.

Romanov, J., Walczak, M., Ibiricu, I., Schüchner, S., Ogris, E., Kraft, C., and Martens, S. (2012). Mechanism and functions of membrane binding by the Atg5-Atg12/Atg16 complex during autophagosome formation. Embo J *31*, 4304–4317.

Ryan, K. J., Zhou, Y., and Wente, S. R. (2007). The karyopherin Kap95 regulates nuclear pore complex assembly into intact nuclear envelopes in vivo. Mol Biol Cell *18*, 886–898.

Sakai, Y., Koller, A., Rangell, L. K., Keller, G. A., and Subramani, S. (1998). Peroxisome degradation by microautophagy in Pichia pastoris: identification of specific steps and morphological intermediates. J Cell Biol *141*, 625–636.

Sato, T., Darsow, T., and Emr, S. (1998). Vam7p, a SNAP-25-like molecule, and Vam3p, a syntaxin homolog, function together in yeast vacuolar protein trafficking. Mol Cell Biol *18*, 5308–5319.

Schmalix, W. A., and Bandlow, W. (1994). SWH1 from yeast encodes a candidate nuclear factor containing ankyrin repeats and showing homology to mammalian oxysterol-binding protein. Biochim Biophys Acta *1219*, 205–210.

Schneider, B. L., Seufert, W., Steiner, B., Yang, Q. H., and Futcher, A. B. (1995). Use of polymerase chain reaction epitope tagging for protein tagging in Saccharomyces cerevisiae. Yeast *11*, 1265–1274.

Schuck, S., Gallagher, C. M., and Walter, P. (2014). ER-phagy mediates selective degradation of endoplasmic reticulum independently of the core autophagy machinery. J Cell Sci *127*, 4078–4088.

Schuldiner, M., and Bohnert, M. (2017). A different kind of love - lipid droplet contact sites. Biochim Biophys Acta *1862*, 1188–1196.

Scott, S. V., Nice, D. C., Nau, J. J., Weisman, L. S., Kamada, Y., Keizer-Gunnink, I., Funakoshi, T., Veenhuis, M., Ohsumi, Y., and Klionsky, D. J. (2000). Apg13p and Vac8p are part of a complex of phosphoproteins that are required for cytoplasm to vacuole targeting. J Biol Chem *275*, 25840–25849.

Scott, S., Baba, M., Ohsumi, Y., and Klionsky, D. (1997). Aminopeptidase I is targeted to the vacuole by a nonclassical vesicular mechanism. J Cell Biol *138*, 37–44.

Scott, S., Guan, J., Hutchins, M., Kim, J., and Klionsky, D. (2001). Cvt19 is a receptor for the cytoplasm-to-vacuole targeting pathway. Mol Cell *7*, 1131–1141.

Scott, S., Hefner-Gravink, A., Morano, K., Noda, T., Ohsumi, Y., and Klionsky,

D. (1996). Cytoplasm-to-vacuole targeting and autophagy employ the same machinery to deliver proteins to the yeast vacuole. Proceed. Nat. Acad. Sci. USA *93*, 12304–12308.

Shintani, T., Huang, W., Stromhaug, P., and Klionsky, D. (2002). Mechanism of cargo selection in the cytoplasm to vacuole targeting pathway. Dev Cell *3*, 825–837.

Shintani, T., Mizushima, N., Ogawa, Y., Matsuura, A., Noda, T., and Ohsumi, Y. (1999). Apg10p, a novel protein-conjugating enzyme essential for autophagy in yeast. Embo J *18*, 5234–5241.

Shintani, T., Suzuki, K., Kamada, Y., Noda, T., and Ohsumi, Y. (2001). Apg2p functions in autophagosome formation on the perivacuolar structure. J Biol Chem *276*, 30452–30460.

Spitzer, C., Li, F., Buono, R., Roschzttardtz, H., Chung, T., Zhang, M., Osteryoung, K. W., Vierstra, R. D., and Otegui, M. S. (2015). The endosomal protein CHARGED MULTIVESICULAR BODY PROTEIN1 regulates the autophagic turnover of plastids in Arabidopsis. Plant Cell *27*, 391–402.

Stephan, J. S., Yeh, Y.-Y., Ramachandran, V., Deminoff, S. J., and Herman, P. K. (2009). The Tor and PKA signaling pathways independently target the Atg1/Atg13 protein kinase complex to control autophagy. Proc Natl Acad Sci USA *106*, 17049–17054.

Straub, M., Bredschneider, M., and Thumm, M. (1997). AUT3, a serine/threonine kinase gene, is essential for autophagocytosis in Saccharomyces cerevisiae. J Bacteriol *179*, 3875–3883.

Su, M.-Y., Peng, W.-H., Ho, M.-R., Su, S.-C., Chang, Y.-C., Chen, G.-C., and Chang, C.-I. (2015). Structure of yeast Ape1 and its role in autophagic vesicle formation. Autophagy, 0.

Suzuki, H., Osawa, T., Fujioka, Y., and Noda, N. N. (2016). Structural biology of the core autophagy machinery. Current Opinion in Structural Biology *43*, 10–17.

Suzuki, K., Akioka, M., Kondo-Kakuta, C., Yamamoto, H., and Ohsumi, Y. (2013). Fine mapping of autophagy-related proteins during autophagosome formation in Saccharomyces cerevisiae. J Cell Sci *126*, 2534–2544.

Suzuki, K., and Ohsumi, Y. (2010). Current knowledge of the pre-autophagosomal structure (PAS). FEBS Letters *584*, 1280–1286.

Suzuki, K., Kamada, Y., and Ohsumi, Y. (2002). Studies of cargo delivery to the vacuole mediated by autophagosomes in Saccharomyces cerevisiae. Developmental Cell *3*, 815–824.

Suzuki, K., Kirisako, T., Kamada, Y., Mizushima, N., Noda, T., and Ohsumi, Y. (2001). The pre-autophagosomal structure organized by concerted functions of APG genes is essential for autophagosome formation. Embo J *20*, 5971–5981.

Suzuki, K., Kubota, Y., Sekito, T., and Ohsumi, Y. (2007). Hierarchy of Atg

proteins in pre-autophagosomal structure organization. Genes Cells *12*, 209–218.

Tang, F., Peng, Y., Nau, J., Kauffman, E., and Weisman, L. (2006). Vac8p, an armadillo repeat protein, coordinates vacuole inheritance with multiple vacuolar processes. Traffic *7*, 1368–1377.

Tenreiro, S., Franssens, V., Winderickx, J., and Outeiro, T. F. (2017). Yeast models of Parkinson's disease-associated molecular pathologies. Curr. Opin. Genet. Dev. *44*, 74–83.

Tewari, R., Bailes, E., Bunting, K. A., and Coates, J. C. (2010). Armadillo-repeat protein functions: questions for little creatures. Trends Cell Biol *20*, 470–481.

Thumm, M., Egner, R., Koch, B., Schlumpberger, M., Straub, M., Veenhuis, M., and Wolf, D. H. (1994). Isolation of autophagocytosis mutants of Saccharomyces cerevisiae. FEBS Letters *349*, 275–280.

Tong, A., and Boone, C. (2006). Synthetic genetic array analysis in Saccharomyces cerevisiae. Methods Mol Biol *313*, 171–192.

Toulmay, A., and Prinz, W. A. (2011). Lipid transfer and signaling at organelle contact sites: the tip of the iceberg. Curr Opin Cell Biol *23*, 458–463.

Toulmay, A., and Prinz, W. A. (2012). A conserved membrane-binding domain targets proteins to organelle contact sites. J Cell Sci *125*, 49–58.

Tuttle, D. L., and Dunn, W. A. (1995). Divergent modes of autophagy in the methylotrophic yeast Pichia pastoris. J Cell Sci *108 (Pt 1)*, 25–35.

Veenhuis, M., Douma, A., Harder, W., and Osumi, M. (1983). Degradation and turnover of peroxisomes in the yeast Hansenula polymorpha induced by selective inactivation of peroxisomal enzymes. Arch Microbiol *134*, 193–203.

Veenhuis, M., van der Klei, I. J., Titorenko, V., and Harder, W. (1992). Hansenula polymorpha: an attractive model organism for molecular studies of peroxisome biogenesis and function. Fems Microbiol Lett *100*, 393–403.

Vigié, P., Cougouilles, E., Bhatia-Kissova, I., Salin, B., Blancard, C., and Camougrand, N. (2019). The mitochondrial phosphatidylserine decarboxylase Psd1 is involved in nitrogen starvation-induced mitophagy in yeast. J Cell Sci *132*, jcs221655.

Wach, A., Brachat, A., Alberti-Segui, C., Rebischung, C., and Philippsen, P. (1997). Heterologous HIS3 marker and GFP reporter modules for PCR-targeting in Saccharomyces cerevisiae. Yeast *13*, 1065–1075.

Wach, A., Brachat, A., Pohlmann, R., and Philippsen, P. (1994). New heterologous modules for classical or PCR-based gene disruptions in Saccharomyces cerevisiae. Yeast *10*, 1793–1808.

Wang, W., and Subramani, S. (2017). Assays to Monitor Pexophagy in Yeast. Meth Enzymol *588*, 413–427.

Wang, Y., Catlett, N., and Weisman, L. (1998). Vac8p, a vacuolar protein with armadillo repeats, functions in both vacuole inheritance and protein targeting from the cytoplasm to vacuole. J Cell Biol *140*, 1063–1074.

Xie, Z., and Klionsky, D. J. (2007). Autophagosome formation: core machinery and adaptations. Nat Cell Biol *9*, 1102–1109.

Xie, Z., Nair, U., and Klionsky, D. J. (2008). Atg8 controls phagophore expansion during autophagosome formation. Mol Biol Cell *19*, 3290–3298.

Yamamoto, H., Kakuta, S., Watanabe, T. M., Kitamura, A., Sekito, T., Kondo-Kakuta, C., Ichikawa, R., Kinjo, M., and Ohsumi, Y. (2012). Atg9 vesicles are an important membrane source during early steps of autophagosome formation. J Cell Biol *198*, 219–233.

Yamashita, S.-I., Oku, M., Wasada, Y., Ano, Y., and Sakai, Y. (2006). PI4P-signaling pathway for the synthesis of a nascent membrane structure in selective autophagy. J Cell Biol *173*, 709–717.

Yao, Z., Delorme-Axford, E., Backues, S. K., and Klionsky, D. J. (2015). Atg41/Icy2 regulates autophagosome formation. Autophagy *11*, 2288–2299.

Yen, W.-L., Legakis, J. E., Nair, U., and Klionsky, D. J. (2007). Atg27 is required for autophagy-dependent cycling of Atg9. Mol Biol Cell *18*, 581–593.

Yorimitsu, T., and Klionsky, D. (2005). Atg11 links cargo to the vesicle-forming machinery in the cytoplasm to vacuole targeting pathway. Mol Biol Cell *16*, 1593–1605.

7 Acknowledgement

Mein besonderer Dank gilt Herrn Prof. Dr. Michael Thumm für die Überlassung des Themas für meine Doktorarbeit. Ich möchte mich auch für die fachliche Betreuung, die Ratschläge und die konstruktiven Diskussionen bedanken.

Für das Anfertigen des Zweitgutachten möchte Frau Prof. Dr. Blanche Schwappach danken.

Den drei Mitgliedern meines Thesis Committees Herrn Prof. Dr. Michael Thumm, Frau Prof. Dr. Blanche Schwappach und Prof. Dr. Stefan Jakob danke ich für die hilfreichen Diskussionen und Ratschläge.

Für die Zusammenarbeit beim mikroskopischen Screen möchte ich mich bei Àkos Farkas, Ariane Wolf und Anne Clancy aus der AG Schwappach, sowie bei Prof. Dr. Silvio Rizzoli bedanken.

Florian danke ich für den wissenschaftlichen Austausch über unser gemeinsames Projekt.

Für das angenehme Arbeitsklima bedanke ich mich bei meinen aktuellen und ehemaligen Arbeitskollegen Florian, Hussein, Lena, LiMa, LiMi, Matthew, Petra, Peter und Roswitha.

Ein großer Dank geht an meine Freunde, für die Unterstützung und schöne Erlebnisse während meiner Doktorandenzeit.

Mein allergrößter Dank geht an meine Familie, vor allem an meine Eltern, ohne die ich niemals so weit im Leben gekommen wäre.